FR-2616-101

NASA CR-115891

Final Report

DESIGN MODIFICATIONS TO A MARS ATMOSPHERIC WATER DETECTION SPECTROPHOTOMETER

By: B. D. Henderson

Contract No. 952871

November 1970

Prepared For:

CALIFORNIA INSTITUTE OF TECHNOLOGY
Jet Propulsion Laboratory
4800 Oak Grove Drive
Pasadena, California 91103

Beckman® INSTRUMENTS, INC.
ADVANCED TECHNOLOGY OPERATIONS
FULLERTON, CALIFORNIA • 92634

Final Report

DESIGN MODIFICATIONS TO A MARS ATMOSPHERIC WATER DETECTION SPECTROPHOTOMETER

By: B. D. Henderson

Contract No. 952871

November 1970

Prepared For:

CALIFORNIA INSTITUTE OF TECHNOLOGY
Jet Propulsion Laboratory
4800 Oak Grove Drive
Pasadena, California 91103

Beckman® INSTRUMENTS, INC.
ADVANCED TECHNOLOGY OPERATIONS
FULLERTON, CALIFORNIA • 92634

TABLE OF CONTENTS

SECTION		PAGE
1.0	INTRODUCTION	1-1
1.1	General Discussion	1-1
1.2	Final Performance Specifications	1-2
2.0	RAY-TRACE DESCRIPTION	2-1
3.0	MONOCHROMATOR DESIGN	3-1
3.1	Double-Pass Monochromators	3-1
3.2	Single-Pass Monochromators	3-40
3.3	Error Analysis for Monochromators H and J	3-47
3.4	Component Dimensions for Monochromator H	3-52
4.0	TELESCOPE	4-1
5.0	OPTICS FOR NEON CALIBRATION SOURCE	6-1
6.0	INTENSITY CALIBRATION SOURCE	7-1
7.0	SPECTRAL RADIANT FLUX TRANSFERS	7-1
8.0	CONSTRUCTION TECHNIQUES FOR COLLIMATING MIRROR AND GRATING	8-1
	BIBLIOGRAPHY	B-1

LIST OF TABLES

TABLE NO.		PAGE
1	Definitions for Ray-Trace Dimensional Parameters (2 sheets)	2-2
2	Definitions for Ray-Surface Intercepts and Their Image Terminology (2 sheets)	2-4
3	Definitions for Ray Direction Cosines and Their Image Terminology (2 sheets)	2-6
4	Description of Ray-Trace Axis Systems Used for Double-Pass Monochromators	3-5
5	Dimensional Parameters for MAWD Monochromator A	3-6
6	Dimensional Parameters for MAWD Monochromator B	3-7
7	Dimensional Parameters for MAWD Monochromator C	3-8
8	Dimensional Parameters for MAWD Monochromators D and F	3-10
9	Dimensional Parameters for MAWD Monochromators E and G	3-11
10	Dimensional Parameters for MAWD Monochromator H	3-12
11	Differences Between Double-Pass Monochromators A,B,C,D,E,F,G&H	3-13
12	Coordinates on Grating Surface Which Define Both Its Used Area and the Aperture Stop of the Double-Pass Monochromator	3-14
13	The Wavelengths and Their Frequency Equivalents	3-14
14	Spectral Image Characteristics for Monochromator A	3-16
15	Spectral Image Characteristics for Monochromator A	3-17
16	Spectral Image Characteristics for Monochromator B	3-18
17	Spectral Image Characteristics for Monochromator B	3-19
18	Spectral Image Characteristics for Monochromator C	3-20
19	Spectral Image Characteristics for Monochromator C	3-21
20	Spectral Image Characteristics for Monochromator D	3-22
21	Spectral Image Characteristics for Monochromator D	3-23
22	Spectral Image Characteristics for Monochromator E	3-24
23	Spectral Image Characteristics for Monochromator E	3-25
24	Spectral Image Characteristics for Monochromator F	3-26
25	Spectral Image Characteristics for Monochromator F	3-27
26	Spectral Image Characteristics for Monochromator G	3-28
27	Spectral Image Characteristics for Monochromator G	3-29
28	Spectral Image Characteristics for Final Double-Pass Monochromator H	3-30
29	Spectral Image Characteristics for Final Double-Pass Monochromator H	3-31
30	Spectral Image Characteristics for Final Double-Pass Monochromator H	3-32
31	Spectral Image Characteristics Without Computer Focus for Final Double-Pass Monochromator H	3-33
32	Spectral Image Characteristics Without Computer Focus for Final Double-Pass Monochromator H	3-34
33	Spectral Image Characteristics Without Computer Focus for Final Double-Pass Monochromator H	3-35
34	Ray Locations on First Corner Mirror	3-39
35	Description of Ray-Trace Axis Systems Used for Single-Pass Monochromator	3-42

LIST OF TABLES (continued)

TABLE NO.		PAGE
36	Dimensional Parameters for MAWD Single-Pass Monochromator J	3-43
37	Spectral Image Characteristics for Single-Pass Monochromator J	3-44
38	Spectral Image Characteristics for Single-Pass Monochromator J	3-45
39	Spectral Image Characteristics for Single-Pass Monochromator J	3-46
40	Spectral Image Characteristics Without Computer Focus for Single-Pass Monochromator J	3-48
41	Spectral Image Characteristics Without Computer Focus for Single Monochromator J	3-49
42	Spectral Image Characteristics Without Computer Focus for Single Monochromator J	3-50
43	Single Ray Error Analysis for Single- and Double-Pass Monochromators	3-54
44	Single Ray Error Analysis for Single- and Double-Pass Monochromators	3-55
45	Single Ray Error Analysis for Single- and Double-Pass Monochromators	3-56
46	Single Ray Error Analysis for Single- and Double-Pass Monochromators	3-57
47	Single Ray Error Analysis for Single- and Double-Pass Monochromators	3-58
48	Single Ray Error Analysis for Single- and Double-Pass Monochromators	3-59
49	Single Ray Error Analysis for Single- and Double-Pass Monochromators	3-60
50	Two-Ray Error Analysis for Single- and Double-Pass Monochromators	3-67
51	Two-Ray Error Analysis for Single- and Double-Pass Monochromators	3-68
52	Description of Special Ray-Trace Axis Systems Used to Define the Hole Size in the Grating for the Double-Pass Monochromator HA (2 sheets)	3-69
53	Dimensional Parameters for MAWD Monochromator HA	3-71
54	Description of Ray-Trace Axis Systems Used for Telescopes	4-3
55	Dimensional Parameters for MAWD Telescope with 45° Beam Deviation	4-4
56	Dimensional Parameters for MAWD Telescope with 67.5° Beam Deviation	4-5
57	Dimensional Parameters for MAWD Telescope with 90° Beam Deviation	4-6
58	Description of Ray-Trace Axis Systems Used for Neon Source Optical System	5-3
59	Dimensional Parameters for Neon Source Optical System	5-4

LIST OF TABLES (continued)

TABLE NO.		PAGE
60	Description of Ray-Trace Axis Systems Used for 45° Telescope and Calibration Source Optical Systems	6-3
61	Dimensional Parameters for MAWD 45° Telescope with Calibration Source Optical System	6-4

LIST OF ILLUSTRATIONS

FIGURE NO.		PAGE
1	MAWD Fixed Double-Pass Littrow Mono--F/5, 1000 MM TFL, Paraboloid 7213.57 H	3-1
2	MAWD Fixed Double-Pass Littrow Monochromator F/5, 1000 MM TFL, Paraboloid, 7213.57 H	3-3
3	MAWD Spectral Image Characteristics for Monochromators A, B, C, and D	3-36
4	MAWD Monochromator H Spectral Image Characteristics	3-37
5	Monochromator H--Centroid Z_{14} vs Frequency	3-38
6	MAWD Fixed Single-Pass Littrow Mono, F/5, 1000 MM TFL, Paraboloid 7193.81 J	3-41
7	Monochromator J--Centroid Z_7 vs Frequency	3-42
8	Result of Error Analyses from Tables 43 through 49	3-53
9	The Nine-Ray Starting Points Used to Define the Respective Entrance Slits for Monochromators H and J	3-61
10	MAWD Fixed Double-Pass Littrow Mono--F/5, 1000 mm TFL, Paraboloid--7213.57 H	3-62
11	MAWD Fixed Double-Pass Littrow Mono--F/5, 1000 mm TFL, Paraboloid--7238.54 H	3-63
12	MAWD Fixed Double-Pass Littrow Mono--F/5, 1000 mm TFL, Paraboloid--7 frequencies	3-64
13	MAWD Fixed Double-Pass Littrow Mono--F/5, 1000 mm TFL, Paraboloid--7213.57 H	3-65
14	MAWD Fixed Double-Pass Littrow Mono--F/5, 1000 mm TFL, Paraboloid--7213.57 HA	3-72
15	MAWD Grating Hole Size and Location for Double-Pass Monochromator HA	3-73
16	MAWD Grating Hole Projection	3-74
17	MAWD Collimating Mirror Hole Size and Location for Double-Pass Monochromator, H	3-75
18	MAWD Telescope--45° with Paraboloid Mirror and Scan Mirror	4-2
19	MAWD Telescope--45-Degree with Paraboloid Mirror	4-7
20	MAWD Telescope--67.50° with Paraboloid Mirror and Scan Mirror	4-8
21	MAWD Telescope--67.5-Degree with Paraboloid Mirror	4-9
22	MAWD Telescope--90° with Paraboloid Mirror and Scan Mirror	4-10
23	MAWD Telescope--90-Degree with Paraboloid Mirror	4-11
24	MAWD Telescope--90-Degree with Spherical Mirror	4-12
25	MAWD Neon Calibration Lens System	5-2
26	MAWD 45° Paraboloid Telescope Mirror, Scanning Mirror, and Paraboloid Intensity Calibration Mirror	6-2

1.0 INTRODUCTION

1.1 General Discussion

The Mars Atmospheric Water Detection (MAWD) Spectrophotometer is an instrument package planned for the Viking Orbiter Spacecraft. To perform its radiometric measurements properly, this spectrophotometer must have high wavelength resolution and accuracy, and high photometric accuracy while still being light in weight and having a relatively small volume.

An earlier optical design study of the MAWD Spectrophotometer was conducted by Beckman Instruments, Inc., under Contract No. 952552 to Jet Propulsion Laboratory. In that study, a number of candidate spectrophotometer designs were analyzed and are described in the Preliminary Report[1]. The final optical design resulting from that study is described in the Final Report[2]. A spectrophotometer based on the optical design of the Final Report has since been built and tested at JPL.

The present optical design study which is detailed in this report is a continuation of the MAWD Spectrophotometer optical design described in the Final Report[2], and has been necessitated by the following new requirements:

(1) The frequency range has been increased more than two-fold, and this requires new entrance slit and detection locations.

(2) The prismatic corner reflector of the early design is to be changed to two corner mirrors.

---

(1) (2) See Bibliography at the end of this report.

(3) The telescope is to be changed from the quartz singlet lens of the earlier design to a reflecting telescope.

(4) A scanning mirror is to be added.

(5) An optical system is to be added which projects neon wavelength calibration sources into the monochromator.

(6) An optical system is to be added which projects an intensity calibration source into the monochromator.

The final optical design described in the Contract No. 952552 Final Report[2] is a double-pass monochromator with a single paraboloid collimating mirror, and that design is essentially monochromator A of this report. The final double-pass monochromator design resulting from the present design study is monochromator H, with six other double-pass monochromator variations, B, C, D, E, F, and G, being studied also. The performance characteristics of all eight double-pass monochromators, A through H, are detailed in this report. It is felt that such data may be of aid if future design modifications are required. As an added task, JPL requested an optical analysis of the monochromator H configuration performance when it is used in single-pass operation. This single-pass monochromator is monochromator J.

This report contains most of the significant engineering information obtained from the computer ray-trace studies, and many tables and figures with specialized terminology are used to accomplish this. Most of this terminology is defined in Section 2, which is a description of the ray trace.

1.2 Final Performance Specifications

The goal of the optical study presented in this report is to arrive at an optical design for the MAWD Spectrophotometer which satisfies the following final instrument performance specifications. These specifications include those defined by JPL, both at the start and during the performance of the contract.

1. The design study is to be based on the optical design presented in the Final Report[2] for JPL, Contract No. 952552.

2. All optics shall be reflective where feasible.

3. The entrance-slit size shall be 0.25 mm wide x 3.0 mm high, and the center of the 3.0-mm height shall be located at Y_o = 3.5 mm, or 3.5-mm above the Z_o-axis.

4. Detector sensitive areas shall be 0.25-mm wide x 1.0-mm high, and the center of the 1.0-mm height shall be located at Y_o = 3.5 mm, or 3.5 mm above the Z_o-axis. The detectors are located at the following monochromator center frequencies:

   i. 7223.12 cm^{-1}
   ii. 7226.14 cm^{-1}
   iii. 7229.09 cm^{-1}
   iv. 7232.12 cm^{-1}
   v. 7234.85 cm^{-1}
   vi. 7238.54 cm^{-1}

5. A neon reference line whose center frequency is at 14427.14 cm^{-1} shall be used for frequency calibration. Its spectral image is to be surrounded by four calibration detectors which indicate any lateral or vertical movement of the spectral image.

6. The neon reference source shall have an optical system which fills both the grating and the entrance slit of the monochromator with its radiation. It is permissible to use an auxiliary entrance slit for this source.

7. The field-of-view defining telescope shall have a focal length of approximately 125.0 mm.

8. A telescope scanning mirror shall rotate through an angle which causes the field-of-view to scan ±1.5°. Nominal position of the field-of-view is defined as a line parallel to the monochromator optical center line.

9. The intensity calibration source shall rotate through as small an angle as possible, cutting off planet radiation, to reflect radiation from an intensity calibration source into the telescope.

10. The intensity calibration source shall have an optical system which uniformly fills both the grating and the entrance slit of the monochromator.

11. The monochromator collimating mirror shall contain a center hole sized to mask off the projected image of the grating entrance hole.

12. Determine the spectral image shift in the image plane due to displacements of each optical element.

13. Determine the effect of optical and mechanical tolerances of all optical elements to maintain image quality at the exit slit within aberrations as evaluated.

14. Perform an investigation of optical structural stability using light-weight grating and parabolic mirror assemblies.

15. Perform instrument radiant transfer calculations, taking into account losses at each optical surface.

16. Provide the formulae for wavelength/position in the focal plane.

2.0 RAY-TRACE DESCRIPTION

The many computer ray-trace analyses which have been performed for this study are purely mathematical model-building procedures, wherein exact mathematical equations are used to express each optical surface and each light ray. Each optical surface is mathematically defined in a separate three-dimensional axis-system which may have any linear or angular orientation to its previous axis-system, and the light rays may have any orientation to these axis-systems. All mathematical calculations are exact since no mathematical approximations are required. The ray-trace computations and the eventual mathematical analysis of the ray patterns at any optical surface are performed by an IBM 360 Model 50 computer in double precision. The computed coordinate accuracy for each ray-surface intercept in its three-dimensional axis-system is given to an accuracy of 10^{-8} mm, and the computed direction cosine accuracy for each ray in its three-dimensional axis-system is given to an accuracy of 10^{-8} directional cosine units.

Table 1 defines those dimensional parameters which are necessary to every ray trace, and which are used to transform axis systems, describe surface shapes, etc. Table 2 defines the coordinates for the ray-surface intercepts and gives the terminology used for an image analysis at any surface. Table 3 defines the ray-direction cosines, and gives the terminology used for an angular image analysis. The "mathematical axis systems" which are occasionally used, facilitate in defining the orientation and location of the next axis system.

The coefficients and terminology listed below are required to discretely define each optical surface in its own axis system, and to discretely define its axis system relative to all other axis systems.

I. Each successive optical surface in any optical system must be defined by a separate three-dimensional and right-handed axis system (X_n, Y_n, Z_n) which carries a progressive set of subscripts which run from 0 to n, where n is the number of the surface being ray-traced at a particular time. The following dimensional parameters define both the linear and the rotational axis transformations from the $(X_{n-1}, Y_{n-1}, Z_{n-1})$ axis system of the previous optical surface to the (X_n, Y_n, Z_n) axis system:

A_n The X_{n-1} coordinate for the origin of the (X_n, Y_n, Z_n) axis system measured in the $(X_{n-1}, Y_{n-1}, Z_{n-1})$ axis system.

B_n The Y_{n-1} coordinate for the origin of the (X_n, Y_n, Z_n) axis system measured in the $(X_{n-1}, Y_{n-1}, Z_{n-1})$ axis system.

C_n The Z_{n-1} coordinate for the origin of the (X_n, Y_n, Z_n) axis system measured in the $(X_{n-1}, Y_{n-1}, Z_{n-1})$ axis system.

α_n An angular displacement of the X_n-axis in the X_n-Z_n plane. This angular displacement is positive when the positive X_n-axis is moved toward the positive Z_n-axis, and negative when the positive X_n-axis is moved toward the negative Z_n-axis.

β_n An angular displacement of the X_n-axis in the X_n-Y_n plane. This angular displacement is positive when the positive X_n-axis is moved toward the positive Y_n-axis, and negative when the positive X_n-axis is moved toward the negative Y_n-axis.

Table 1 (Sheet 1 of 2). Definitions for Ray-Trace Dimensional Parameters

γ_n An angular displacement of the Z_n-axis in the Y_n-Z_n plane. This angular displacement is positive when the positive Z_n-axis is moved toward the positive Y_n-axis, and negative when the positive Z_n-axis is moved toward the negative Y_n-axis.

The three angular transformations, α_n, β_n, γ_n, are operative only after the linear transformations, A_n, B_n, C_n, have been completed. Each of the three angular transformations must be taken singly, but they may be taken in any order, and each of the three angular transformations must be completed before the next becomes operative. That is, the order of succession of the three angular transformations, α_n, β_n, and γ_n is an input to the computer.

II. The dimensional parameters F_n, D_n, E_n, and R_n are used to define any conic surface, since they are the coefficients of the following general conic equation:

$$F_n X^2_n + D_n Y^2_n + E_n Z^2_n - 2R_n X_n = 0$$

III. A plane surface is always the Y_n-Z_n plane, and requires no descriptive dimensional parameters.

IV. The index of refraction of the optical medium immediately following the optical surface which is defined in the (X_n, Y_n, Z_n) axis system is described by the dimensional parameter N_n.

Table 1 (Sheet 2 of 2). Definitions for Ray-Trace Dimensional Parameters

X_n	The X_n coordinate of a single ray intercept with the optical surface in the (X_n, Y_n, Z_n) axis system.
Y_n	The Y_n coordinate of a single ray intercept with the optical surface in the (X_n, Y_n, Z_n) axis system.
Z_n	The Z_n coordinate of a single ray intercept with the optical surface in the (X_n, Y_n, Z_n) axis system.
D_n	The optical distance a single ray travels from the previous surface to the surface being ray-traced. This is defined as the true distance between the ray-intercept value $(X_{n-1}, Y_{n-1}, Z_{n-1})$ and the ray-intercept value (X_n, Y_n, Z_n) for a single ray, multiplied by N_{n-1}.
Centroid X_n	The mathematical centroid for all X_n values for a single family of rays.
Centroid Y_n	The mathematical centroid for all Y_n values for a single family of rays.
Centroid Z_n	The mathematical centroid for all Z_n values for a single family of rays.
ΔX_n	The largest mathematical difference among all X_n values for a single family of rays.
ΔY_n	The largest mathematical difference among all Y_n values for a single family of rays.

Table 2 (Sheet 1 of 2). Definitions for Ray-Surface Intercepts and Their Image Terminology

ΔZn	The largest mathematical difference among all Z_n values for a single family of rays.
75% ΔX_n	The largest mathematical difference among that 75% of the X_n values remaining from a single family of rays after the computer has removed that 25% of the X_n values which are numerically furthest from the central grouping of X_n values. This 75% ΔX_n value is generally a good approximation for the true half-power spread for all the X_n values of the family of rays.
75% ΔY_n	The largest mathematical difference among that 75% of the Y_n values remaining from a single family of rays after the computer has removed that 25% of the Y_n values which are numerically furthest from the central grouping of Y_n values. This 75% ΔY_n value is generally a good approximation for the true half-power spread for all the Y_n values of the family of rays.
75% ΔZ_n	The largest mathematical difference among that 75% of the Z_n values remaining from a single family of rays after the computer has removed that 25% of the Z_n values which are numerically furthest from the central grouping of Z_n values. This 75% ΔZ_n value is generally a good approximation for the true half-power spread for all the Z_n values of the family of rays.

Table 2 (Sheet 2 of 2). Definitions for Ray-Surface Intercepts and Their Image Analysis Terminology

Xi_n	The direction cosine component on the X_n-axis for a ray emerging (after reflection, refraction, diffraction, or transmission) from the (X_n,Y_n,Z_n) point on the optical surface of the (X_n,Y_n,Z_n) axis system.
Eta_n	The direction cosine component on the Y_n-axis for a ray emerging (after reflection, refraction, diffraction, or transmission) from the (X_n,Y_n,Z_n) point on the optical surface of the (X_n,Y_n,Z_n) axis system.
$Zeta_n$	The direction cosine component on the Z_n-axis for a ray emerging (after reflection, refraction, diffraction, or transmission) from the (X_n,Y_n,Z_n) point on the optical surface of the (X_n,Y_n,Z_n) axis system.
Centroid Xi_n	The mathematical centroid for all Xi_n values for a single family of rays.
Centroid Eta_n	The mathematical centroid for all Eta_n values for a single family of rays.
Centroid $Zeta_n$	The mathematical centroid for all $Zeta_n$ values for a single family of rays.
ΔXi_n	The largest mathematical difference among all Xi_n values for a single family of rays.
ΔEta_n	The largest mathematical difference among all Eta_n values for a single family of rays.

Table 3 (Sheet 1 of 2). Definitions for Ray Direction Cosines and Their Image Terminology

$Zeta_n$	The largest mathematical difference among all $Zeta_n$ values for a single family of rays.
75% ΔXi_n	The largest mathematical difference among that 75% of the Xi_n values remaining from a single family of rays after the computer has removed that 25% of the Xi_n values which are numerically furthest from the central grouping of Xi_n values. This 75% ΔXi_n value is generally a good approximation of the true half-power spread for all the Xi_n values of the family of rays.
75% ΔEta_n	The largest mathematical difference among that 75% of the Eta_n values remaining from a single family of rays after the computer has removed that 25% of the Eta_n values which are numerically furthest from the central grouping of Eta_n values. This 75% ΔEta_n value is generally a good approximation of the true half-power spread for all the Eta_n values of the family of rays.
75% $\Delta Zeta_n$	The largest mathematical difference among the 75% of the $Zeta_n$ values remaining from a single family of rays after the computer has removed that 25% of the $Zeta_n$ values which are numerically furthest from the central grouping of $Zeta_n$ values. This 75% $\Delta Zeta_n$ value is generally a good approximation of the true half-power spread for all the $Zeta_n$ values of the family of rays.

NOTE: When the direction cosine values are sufficiently small, they may be directly dimensioned as radian values.

Table 3 (Sheet 2 of 2). Definitions for Ray Direction Cosines and Their Image Terminology

3.0 MONOCHROMATOR DESIGN

3.1 Double-Pass Monochromators

This section describes the detailed optical characteristics of the eight double-pass monochromators, A through H. Monochromator H is the final double-pass monochromator design of this study.

Figure 1 shows two views of the monochromator H optical system which are plotted directly by computer. The upper view is a ray trace using a family of ten rays with a single entrance-slit starting point (X_o = 0, Y_o = 5.0, Z_o = 3.88), which form a uniform line array on the grating face between points (X_3 = 0, Y_3 = 50.0, Z_3 = 0) and (X_3 = 0, Y_3 = -50.0, Z_3 = 0). This particular line array does not fill the full grating area which has been later outlined with phantom lines. The lower view uses a different family of ten rays which start from the same entrance slit point as for the upper view, but these ten rays form a uniform line array on the grating face between points (X_3 = 0, Y_3 = 0, Z_3 = 90.0), and (X_3 = 0, Y_3 = 0, Z_3 = -90.0). Both of these ray-trace plots are for a frequency of 7213.57 cm^{-1} for which the boundary rays have their greatest spread from the monochromator center line.

Figure 2 is a computer generated isometric plot of the monochromator H optical system. This plot is also for a frequency of 7213.57 cm^{-1}; however, two families of nine rays each have been used. One family of nine rays which are printed in red starts from entrance-slit starting point (X_o = 0, Y_o = 2.0, Z_o = 4.0), and the other family of nine rays which are printed in black start from entrance-slit starting point (X_o = 0, Y_o = 5.0, Z_o = 3.880). Both families of nine rays intercept the grating in the same rectangular array which fills the full 100 x 180 used area of the grating.

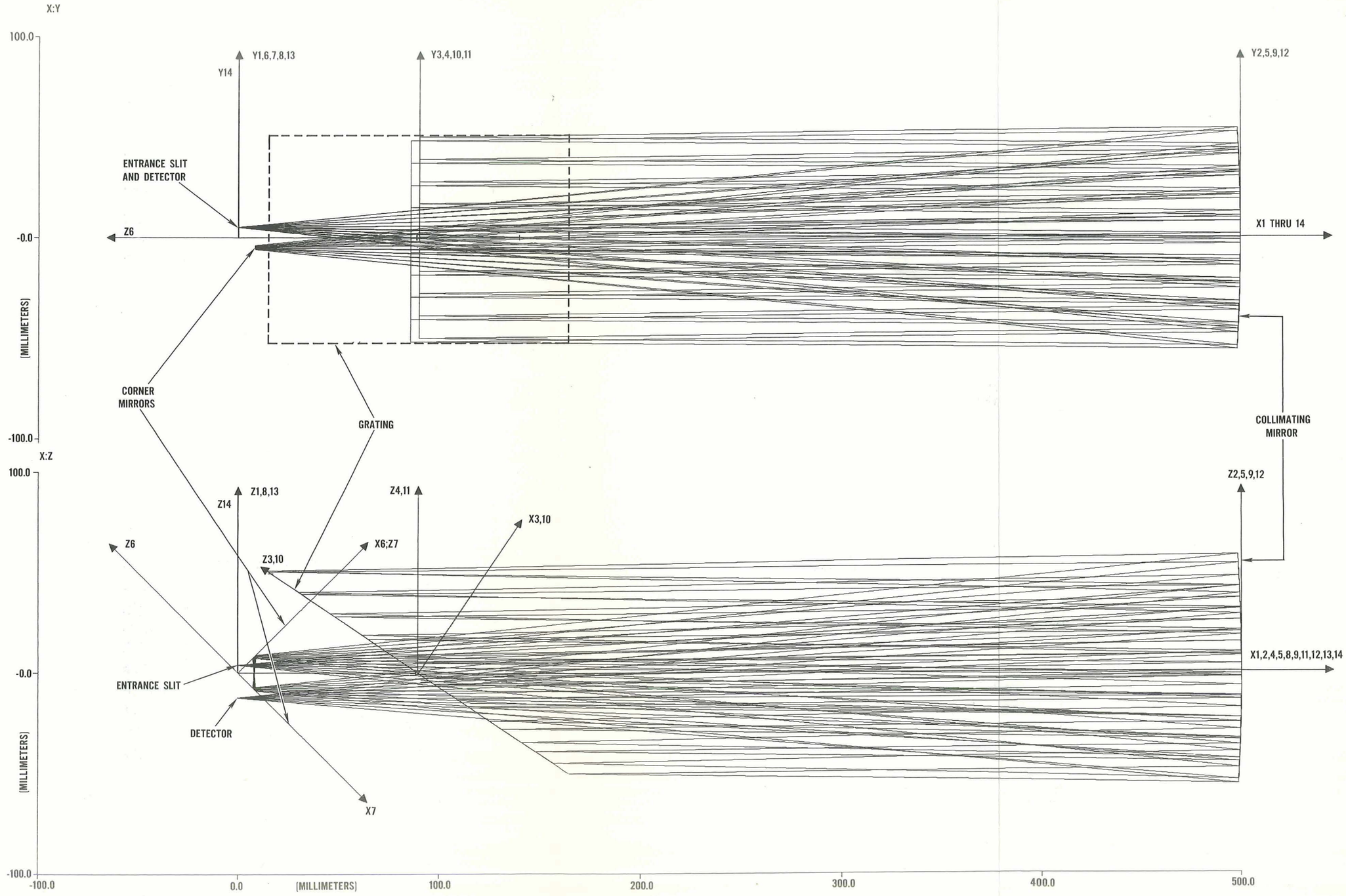

Figure 1. MAWD Fixed Double-Pass Littrow Mono--F/5, 1000 MM TFL, Paraboloid 7213.57 H

MAWD FIXED DOUBLE PASS LITTROW MONO-F/5-1000 MM TFL-PARABOLOID--7213.57 H 6-3-70
X:Y 0.03940 :1

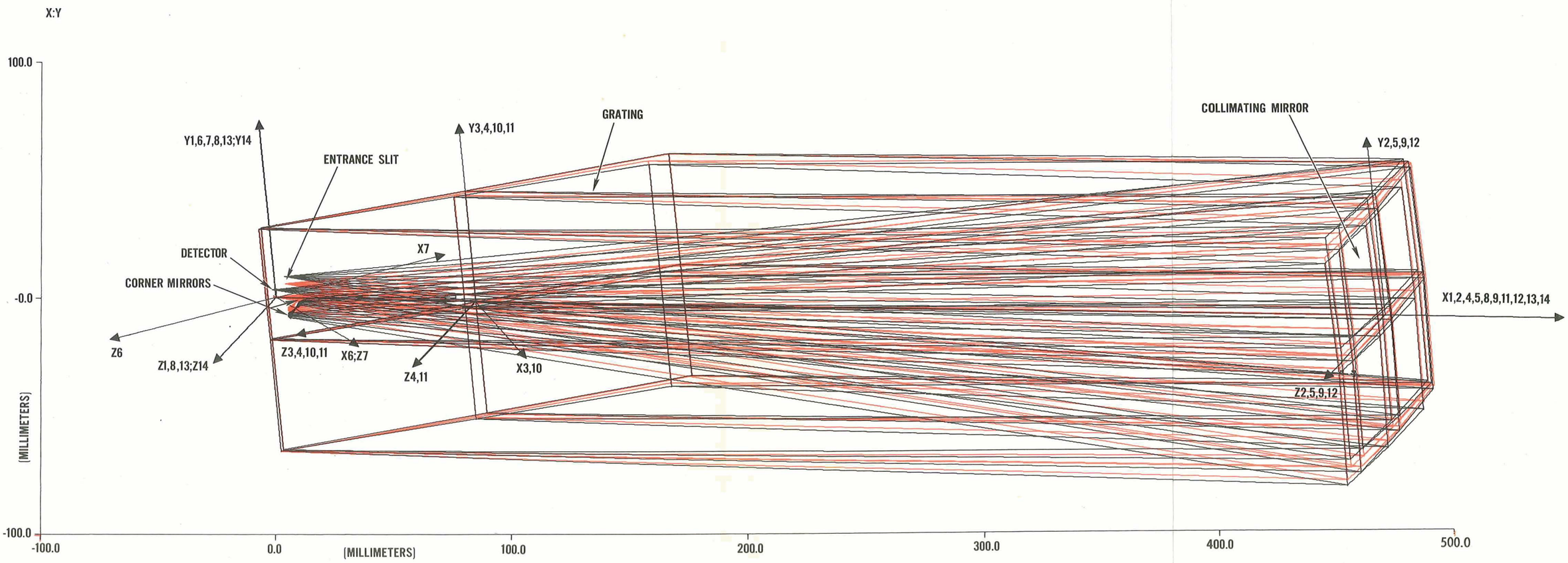

Figure 2. MAWD Fixed Double-Pass Littrow Monochromator F/5, 1000 MM TFL, Paraboloid, 7213.57 H

The axis systems shown in Figures 1 and 2 are applicable to all the double-pass monochromators A through H, and these axis systems are defined in Table 4. Figures 1 and 2 do not show the (X_o, Y_o, Z_o) axis system which has its Y_o-axis offset 1.160° from the Y_1-axis only for monochromator H. The (X_o, Y_o, Z_o) and (X_1, Y_1, Z_1) axis systems are identical for all the other double monochromators, A through G.

Monochromator A is essentially the same as the final monochromator design presented in the JPL Contract No. 952552 Final Report.[2] It differs only in the following ways:

(1) The entrance-slit plane has not been given the corrective tip and the entrance slit itself has not been given the corrective lateral tilt in its plane as used in the Final Report[2] monochromator design.

(2) The corner prism is replaced by two corner mirrors.

(3) A cover plate is not used in front of the detector sensitive area.

The dimensional parameters for monochromator A are given in Table 5.

Monochromator B differs from monochromator A in two ways:

(1) The grating angle $\alpha_{3,4,10,11}$ is changed from 56.055° to 56.115°.

(2) The entrance slit is moved laterally from Z_o=1.000 mm to Z_o=3.000 mm.

The dimensional parameters for monochromator B are given in Table 6.

In monochromator C, two new changes are added:

(1) The grating angle $\alpha_{3,4,10,11}$ is changed to 56.145°.

(2) The entrance slit is moved laterally to Z_o=4.000 mm.

The dimensional parameters for monochromator C are given in Table 7.

(X_o, Y_o, Z_o)	Entrance Slit--The entrance slit lies in the Y_o-Z_o plane, and each family of rays used to ray-trace the monochromator starts from a point on the entrance slit.
(X_1, Y_1, Z_1)	Mathematical Axis System
(X_2, Y_2, Z_2) (X_5, Y_5, Z_5) (X_9, Y_9, Z_9) (X_{12}, Y_{12}, Z_{12})	Paraboloid Collimating Mirror--These four axis systems are identical and may be referred to as the $(X_{2,5,9,12}, Y_{2,5,9,12}, Z_{2,5,9,12})$ axis system. The apex of this paraboloidal reflecting surface is at the origin of the $(X_{2,5,9,12}, Y_{2,5,9,12}, Z_{2,5,9,12})$ axis system, and the focus of the paraboloid is located on the negative $X_{2,5,9,12}$-axis.
(X_3, Y_3, Z_3) (X_{10}, Y_{10}, Z_{10})	Diffraction Grating--These two axis systems are identical and may be referred to as the $(X_{3,10}, Y_{3,10}, Z_{3,10})$ axis system. The ruled area of the grating is in the $Y_{3,10}$-$Z_{3,10}$ plane, and the grating rulings are parallel to the $Y_{3,10}$-axis.
(X_4, Y_4, Z_4) (X_{11}, Y_{11}, Z_{11})	Mathematical Axis Systems--These two axis systems are identical and may be referred to as the $(X_{4,11}, Y_{4,11}, Z_{4,11})$ axis system.
(X_6, Y_6, Z_6)	First Surface of Corner Mirrors--This is a plane-reflecting surface in the Y_6-Z_6 plane.
(X_7, Y_7, Z_7)	Second Surface of Corner Mirror--This is a plane-reflecting surface in the Y_7-Z_7 plane.
(X_8, Y_8, Z_8)	Mathematical Axis System.
(X_{13}, Y_{13}, Z_{13})	Front Face of Detector Cover Glass--This is a refracting surface in the Y_{13}-Z_{13} plane.
(X_{14}, Y_{14}, Z_{14})	Spectral Image Surface--The spectral images for the ray starting points on the entrance slit are formed on the Y_{14}-Z_{14} plane.

Table 4. Description of Ray-Trace Axis Systems Used for Double-Pass Monochromators

Axis Sub-Script (n)	A_n (mm)	B_n (mm)	C_n (mm)	α_n (deg)	β_n (deg)	γ_n (deg)	Surface Shape	Optical Function of Surface	D_n (mm)	E_n (mm)	F_n (mm)	R_n (mm)	N_n
1							Plane	Transmit					1.0000
2	500.000						Paraboloid	Reflect	1.000	1.000		-1000.000	1.0000
3	-420.000			56.055			Plane	Diffract					1.0000
4				-56.055			Plane	Transmit					1.0000
5	420.000						Paraboloid	Reflect	1.000	1.000		-1000.000	1.0000
6	-500.000			45.000			Plane	Reflect					1.0000
7				-90.000			Plane	Reflect					1.0000
8				45.000			Plane	Transmit					1.0000
9	500.000						Paraboloid	Reflect	1.000	1.000		-1000.000	1.0000
10	-420.000			56.055			Plane	Diffract					1.0000
11				-56.055			Plane	Transmit					1.0000
12	420.000						Paraboloid	Reflect	1.000	1.000		-1000.000	1.0000
13	-500.000						Plane	Refract					1.0000
14							Plane	Transmit					1.0000

Table 5. Dimensional Parameters for MAWD Monochromator A

Axis Sub-Script (n)	A_n (mm)	B_n (mm)	C_n (mm)	α_n (deg)	β_n (deg)	γ_n (deg)	Surface Shape	Optical Function of Surface	D_n (mm)	E_n (mm)	F_n (mm)	R_n (mm)	N_n
1							Plane	Transmit					1.0000
2	500.000						Paraboloid	Reflect	1.000	1.000		-1000.000	1.0000
3	-420.000			56.115			Plane	Diffract					1.0000
4				-56.115			Plane	Transmit					1.0000
5	420.000						Paraboloid	Reflect	1.000	1.000		-1000.000	1.0000
6	-500.000			45.000			Plane	Reflect					1.0000
7				-90.000			Plane	Reflect					1.0000
8				45.000			Plane	Transmit					1.0000
9	500.000						Paraboloid	Reflect	1.000	1.000		-1000.000	1.0000
10	-420.000			56.115			Plane	Diffract					1.0000
11				-56.115			Plane	Transmit					1.0000
12	420.000						Paraboloid	Reflect	1.000	1.000		-1000.000	1.0000
13	-500.000						Plane	Refract					1.0000
14							Plane	Transmit					1.0000

Table 6. Dimensional Parameters for MAWD Monochromator B

Axis Sub-Script (n)	A_n (mm)	B_n (mm)	C_n (mm)	α_n (deg)	β_n (deg)	γ_n (deg)	Surface Shape	Optical Function of Surface	D_n (mm)	E_n (mm)	F_n (mm)	R_n (mm)	N_n
1							Plane	Transmit					1.0000
2	500.000						Paraboloid	Reflect	1.000	1.000		-1000.000	1.0000
3	-420.000			56.145			Plane	Diffract					1.0000
4				-56.145			Plane	Transmit					1.0000
5	420.000						Paraboloid	Reflect	1.000	1.000		-1000.000	1.0000
6	-500.000			45.000			Plane	Reflect					1.0000
7				-90.000			Plane	Reflect					1.0000
8				45.000			Plane	Transmit					1.0000
9	500.000						Paraboloid	Reflect	1.000	1.000		-1000.000	1.0000
10	-420.000			56.145			Plane	Diffract					1.0000
11				-56.145			Plane	Transmit					1.0000
12	420.000						Paraboloid	Reflect	1.000	1.000		-1000.000	1.0000
13	-500.000						Plane	Refract					1.0000
14							Plane	Transmit					1.0000

Table 7. Dimensional Parameters for MAWD Monochromator C

In monochromator D, the grating angle $\alpha_{3,4,10,11}$ is returned to 56.055°, its value for monochromator A, and the entrance slit remains at Z_o=4.000, as in monochromator C. The dimensional parameters for monochromator D are given in Table 8.

Monochromator E is like monochromator D except the grating has been moved 10 mm further from the entrance slit. The dimensional parameters for monochromator E are given in Table 9.

Monochromator F is like monochromator D except it uses a 100-mm diameter aperture stop which is located at the grating but is normal to the monochromator axis. The dimensional parameters for monochromator F are given in Table 8.

Monochromator G is like monochromator E except it uses the same 100-mm-dia. aperture stop at the grating and normal to the monochromator axis, as in monochromator F. The dimensional parameters for monochromator G are given in Table 9.

Monochromator H, the final double-pass monochromator design, is very similar to monochromator E except for optimal shaping of the entrance slit, addition of a 0.250-mm-thick quartz cover plate in front of the detectors, and a slight change in the distance between the collimating mirror and the two corner mirrors. The dimensional parameters for monochromator H are given in Table 10.

Table 11 summarizes the dimensional differences between the eight double-pass monochromators A through H. Table 12 gives the four points on the grating surface which define the monochromator aperture stop for all double-pass monochromators except monochromators F and G. These two use a 100-mm-diameter circular aperture stop which is normal to the X_1-axis at the origin of the grating axis. Table 13 lists the seven frequencies which are used in the ray traces of each of the eight monochromators and gives their wavelength equivalents. Table 13 also lists the $\frac{N\lambda k}{1000}$ values used for each frequency. The 7213.57 cm^{-1} frequency value in Table 13 represents the grating second-order value for the neon center frequency of 14427.14 cm^{-1}.

Axis Sub-Script (n)	A_n (mm)	B_n (mm)	C_n (mm)	α_n (deg)	β_n (deg)	γ_n (deg)	Surface Shape	Optical Function of Surface	D_n (mm)	E_n (mm)	F_n (mm)	R_n (mm)	N_n
1							Plane	Transmit					
2	500.000						Paraboloid	Reflect	1.000	1.000		-1000.000	1.0000
3	-420.000			56.055			Plane	Diffract					1.0000
4				-56.055			Plane	Transmit					1.0000
5	420.000						Paraboloid	Reflect	1.000	1.000		-1000.000	1.0000
6	-500.000			45.000			Plane	Reflect					1.0000
7				-90.000			Plane	Reflect					1.0000
8				45.000			Plane	Transmit					1.0000
9	500.000						Paraboloid	Reflect	1.000	1.000		-1000.000	1.0000
10	-420.000			56.055			Plane	Diffract					1.0000
11				-56.055			Plane	Transmit					1.0000
12	420.000						Paraboloid	Reflect	1.000	1.000		-1000.000	1.0000
13	-500.000						Plane	Refract					1.0000
14							Plane	Transmit					1.0000

Table 8. Dimensional Parameters for MAWD Monochromators D and F

Axis Sub-Script (n)	A_n (mm)	B_n (mm)	C_n (mm)	α_n (deg)	β_n (deg)	γ_n (deg)	Surface Shape	Optical Function of Surface	D_n (mm)	E_n (mm)	F_n (mm)	R_n (mm)	N_n
1							Plane	Transmit					1.0000
2	500.000						Paraboloid	Reflect	1.000	1.000		-1000.000	1.0000
3	-410.000			56.055			Plane	Diffract					1.0000
4				-56.055			Plane	Transmit					1.0000
5	410.000						Paraboloid	Reflect	1.000	1.000		-1000.000	1.0000
6	-500.000			45.000			Plane	Reflect					1.0000
7				-90.000			Plane	Reflect					1.0000
8				45.000			Plane	Transmit					1.0000
9	500.000						Paraboloid	Reflect	1.000	1.000		-1000.000	1.0000
10	-410.000			56.055			Plane	Diffract					1.0000
11				-56.055			Plane	Transmit					1.0000
12	410.000						Paraboloid	Reflect	1.000	1.000		-1000.000	1.0000
13	-500.000						Plane	Refract					1.0000
14							Plane	Transmit					1.0000

Table 9. Dimensional Parameters for MAWD Monochromators E and G

Axis Sub-Script (n)	A_n (mm)	B_n (mm)	C_n (mm)	α_n (deg)	β_n (deg)	γ_n (deg)	Surface Shape	Optical Function of Surface	D_n (mm)	E_n (mm)	F_n (mm)	R_n (mm)	N_n
1					-1.160		Plane	Transmit					1.0000
2	500.000						Paraboloid	Reflect	1.000	1.000		-1000.000	1.0000
3	-410.000			56.055			Plane	Diffract					1.0000
4				-56.055			Plane	Transmit					1.0000
5	410.000						Paraboloid	Reflect	1.000	1.000		-1000.000	1.0000
6	-499.918			45.000			Plane	Reflect					1.0000
7				-90.000			Plane	Reflect					1.0000
8				45.000			Plane	Transmit					1.0000
9	499.918						Paraboloid	Reflect	1.000	1.000		-1000.000	1.0000
10	-410.000			56.055			Plane	Diffract					1.0000
11				-56.055			Plane	Transmit					1.0000
12	410.000						Paraboloid	Reflect	1.000	1.000		-1000.000	1.0000
13	-500.000						Plane	Refract					1.4460
14	-.250						Plane	Transmit					1.4460

Table 10. Dimensional Parameters for MAWD Monochromator H

Monochromator	$\lvert A_{3,5,10,12} \rvert$ (mm)	$\lvert A_{6,9} \rvert$ (mm)	A_{14} (mm)	$\lvert \alpha_{3,4,10,11} \rvert$ (degrees)	β_1 (degrees)	$N_{13,14}$	Aperture Stop Area on Grating (mm)	Y_o	Z_o
A	420.000	500.000	0	56.055	0	1.0000	100 x 180 Rectangle	2.000 5.000	1.000 1.000
B	420.000	500.000	0	56.115	0	1.0000	100 x 180 Rectangle	2.000 5.000	3.000 3.000
C	420.000	500.000	0	56.145	0	1.0000	100 x 180 Rectangle	2.000 5.000	4.000 4.000
D	420.000	500.000	0	56.055	0	1.0000	100 x 180 Rectangle	2.000 5.000	4.000 4.000
E	410.000	500.000	0	56.055	0	1.0000	100 x 180 Rectangle	2.000 5.000	4.000 4.000
F	420.000	500.000	0	56.055	0	1.0000	100 Dia. Circle	2.000 2.000	4.000 4.000
G	410.000	500.000	0	56.055	0	1.0000	100 Dia. Circle	2.000 2.000	4.000 4.000
H	410.000	499.918	-.250	56.055	-1.160	1.4460	100 x 180 Rectangle	2.000 3.500 5.000	4.000 3.954 3.880

Table 11. Differences Between Double Pass Monochromators A, B, C, D, E, F, G, and H

Grating Corner	X_3	Y_3	Z_3
1	0	50.0	-90.0
2	0	50.0	90.0
3	0	-50.0	90.0
4	0	-50.0	-90.0

Table 12. Coordinates on Grating Surface which Define Both Its Used Area and the Aperture Stop of the Double Pass Monochromator

$1/\lambda$ (cm^{-1})	$\lambda(\mu)$	$\frac{N\lambda K}{1000}$ (μ)
7223.12	1.38444	1.66133
7226.14	1.38386	1.66063
7229.09	1.38330	1.65996
7232.12	1.38272	1.65926
7234.85	1.38220	1.65864
7238.54	1.38149	1.65779
7213.57	1.38628	1.66354

Grating lines/mm, k = 1200 L/mm

Grating order N = 1

Table 13. The Wavelengths and Their Frequency Equivalents, and the $\frac{N\lambda k}{1000}$ Values Used in This Ray Trace Study

Tables 14 through 33 describe the spectral image characteristics for the eight double-pass monochromators for the same seven frequencies. The data in each table is for a single family of 100 rays starting from a point on the entrance slit. The terminology used for these tables is given in Tables 1 and 2. The A_{14} values for Tables 14 through 30 were obtained by letting the computer vary A_{14} until a best-spectral-image is obtained as represented by all one hundred Z_{14} values.

In Tables 31, 32, and 33, the value of A_{14} was fixed at 0.250 mm, which is the thickness of the quartz cover plate for the detectors. For monochromator H the entrance-slit plane tilt, $\beta_1 = 1.160°$, and the additional lateral tilt of the entrance slit in its plane, are designed to make the respective A_{14} and Z_{14} values equal to one another for the (H_2), $(H_{3.5})$, and (H_5) starting points and for the same frequencies.

Figure 3 is a composite plot of data from Tables 14 through 21 and shows the relative spectral image characteristics of monochromators A, B, C, and D. It can be seen from Figure 3 how important the location of the entrance slit is in determining those frequencies which have the best resolution.

Figure 4 is a plot of data from Tables 28, 29, and 30, showing the spectral image characteristics of monochromator H.

Figure 5 is the computer plot and equation for the best fit, second-degree curve for the seven frequency values versus their corresponding centroid Z_{14} values obtained from Table 32.

In the comparison of the eight different double-pass monochromators, not only their spectral image characteristics must be considered, but also where their rays actually intersect the two corner mirrors. Rays must not overlay or fall too near the corner between the two corner mirrors. Table 34 shows the maximum range of Z_6 values for each of the eight double-pass monochromators and for three frequencies. Two of these frequencies always come nearest the corner. The third frequency is always farthest from the corner. The Z_7 ranges on the second corner mirror have roughly the values of their Z_6 counterpart. It is

Ray Starting Point on Entrance Slit is (A_2): $X_o = 0$, $Y_o = 2.0$, $Z_o = 1.0$

Frequency cm-1	A_{14}	Not Used	Centroid Y14	ΔY_{14}	75% ΔY_{14}	Centroid Z_{14}	Not Used	ΔZ_{14}	75% ΔZ_{14}
7223.12	-.031		2.000	.040	.017	-5.012		.039	.022
7226.14	-.024		2.000	.0266	.0130	-3.727		.027	.015
7229.09	-.019		2.000	.0143	.0064	-2.503		.015	.0082
7232.12	-.016		2.000	.0016	.0008	-1.232		.0022	.0011
7234.85	-.014		2.000	.0115	.0059	-.113		.0101	.0059
7238.54	-.014		2.000	.0268	.0139	1.414		.025	.017
7213.57	-.068		2.000	.085	.038	-9.118		.076	.043

NOTE: All dimensions are in mm except as noted.

Table 14. Spectral Image Characteristics for Monochromator A

Ray Starting Point on Entrance Slit is (A_5): $X_o = 0$, $Y_o = 5.0$, $Z_o = 1.0$

Frequency cm^{-1}	A_{14}	Not Used	Centroid Y_{14}	ΔY_{14}	75% ΔY_{14}	Centroid Z_{14}	Z_{14} Comparison (A_2 - A_5)	ΔZ_{14}	75% ΔZ_{14}
7223.12	-.106		5.000	.036	.015	-5.139	.127	.040	.021
7226.14	-.098		5.000	.0245	.0091	-3.853	.126	.027	.016
7229.09	-.092		5.000	.0134	.0051	-2.629	.126	.014	.008
7232.12	-.087		5.000	.0122	.0053	-1.357	.125	.0042	.0017
7234.85	-.085		5.000	.0235	.0083	-.237	.124	.0132	.0079
7238.54	-.083		5.000	.0386	.0172	1.291	.123	.028	.018
7213.57	-.146		5.000	.077	.032	-9.247	.129	.079	.048

NOTE: All dimensions are in mm except as noted.

Table 15. Spectral Image Characteristics for Monochromator A

Ray Starting Point on Entrance Slit is (B_2): $X_o = 0$, $Y_o = 2.0$, $Z_o = 3.0$

Frequency cm^{-1}	A_{14}	Not Used	Centroid Y_{14}	Not Used	Centroid Z_{14}	Not Used	ΔZ_{14}	75% ΔZ_{14}
7223.12	-.045		2.000		-4.944		.0170	.0093
7226.14	-.037		2.000		-3.653		.0053	.0024
7229.09	-.030		2.000		-2.425		.0108	.0061
7232.12	-.025		2.000		-1.149		.0221	.0145
7234.85	-.023		2.000		-.024		.032	.019
7238.54	-.021		2.000		1.509		.047	.028
7213.57	-.088		2.000		-9.068		.053	.030

NOTE: All dimensions are in mm except as noted.

Table 16. Spectral Image Characteristics for Monochromator B

Ray Starting Point on Entrance Slit is (B_5): $X_o = 0$, $Y_o = 5.0$, $Z_o = 3.0$

Frequency cm^{-1}	A_{14}	Not Used	Centroid Y_{14}	Not Used	Centroid Z_{14}	Not Used	ΔZ_{14}	75% ΔZ_{14}
7223.12	-.121		5.000		-5.072		.0195	.0087
7226.14	-.111		5.000		-3.780		.0122	.0050
7229.09	-.103		5.000		-2.551		.0165	.0074
7232.12	-.097		5.000		-1.274		.027	.016
7234.85	-.094		5.000		-.149		.037	.026
7238.54	-.091		5.000		1.385		.050	.030
7213.57	-.167		4.999		-9.198		.058	.031

NOTE: All dimensions are in mm except as noted.

Table 17. Spectral Image Characteristics for Monochromator B

Ray Starting Point on Entrance Slit is (C_2): $X_o = 0$, $Y_o = 2.0$, $Z_o = 4.0$

Frequency cm^{-1}	A_{14}	Not Used	Centroid Y_{14}	Not Used	Centroid Z_{14}	Not Used	ΔZ_{14}	75% ΔZ_{14}
7223.12	-.056		2.000		-4.916		.0066	.0024
7226.14	-.046		2.000		-3.622		.0118	.0068
7229.09	-.039		2.000		-2.391		.0223	.0132
7232.12	-.033		2.000		-1.112		.034	.019
7234.85	-.030		2.000		.015		.044	.026
7238.54	-.028		2.000		1.551		.058	.035
7213.57	-.101		2.000		-9.049		.042	.023

NOTE: All dimensions are in mm except as noted.

Table 18. Spectral Image Characteristics for Monochromator C

Ray Starting Point on Entrance Slit is (C_5): $X_o = 0$, $Y_o = 5.0$, $Z_o = 4.0$

Frequency cm^{-1}	A_{14}	Not Used	Centroid Y_{14}	Not Used	Centroid Z_{14}	Not Used	ΔZ_{14}	75% ΔZ_{14}
7223.12	-.132		4.999		-5.044		.0164	.0055
7226.14	-.121		5.000		-3.749		.0190	.0079
7229.09	-.113		5.000		-2.518		.0286	.0146
7232.12	-.106		5.000		-1.238		.039	.023
7234.85	-.101		5.000		-.110		.049	.030
7238.54	-.098		5.000		1.427		.062	.037
7213.57	-.181		4.999		-9.180		.047	.023

NOTE: All dimensions are in mm except as noted.

Table 19. Spectral Image Characteristics for Monochromator C

Ray Starting Point on Entrance Slit is (D_2): $X_o = 0$, $Y_o = 2.0$, $Z_o = 4.0$

Frequency cm^{-1}	A_{14}	Not Used	Centroid Y_{14}	ΔY_{14}	75% ΔY_{14}	Centroid Z_{14}	Not Used	ΔZ_{14}	75% ΔZ_{14}
7223.12	-.090		2.000	.044	.016	-8.176		.035	.019
7226.14	-.074		2.000	.0299	.0110	-6.876		.023	.013
7229.09	-.062		2.000	.0165	.0062	-5.621		.0124	.0053
7232.12	-.051		2.000	.0051	.0027	-4.327		.0071	.0030
7234.85	-.043		2.000	.0129	.0061	-3.186		.0155	.0081
7238.54	-.035		2.000	.0275	.0121	-1.632		.029	.020
7213.57	-.155		2.000	.091	.038	-12.361		.069	.042

NOTE: All dimensions are in mm except as noted.

Table 20. Spectral Image Characteristics for Monochromator D

Ray Starting Point on Entrance Slit is (D_5): $X_o = 0$, $Y_o = 5.0$, $Z_o = 4.0$

Frequency cm^{-1}	A_{14}	Not Used	Centroid Y_{14}	ΔY_{14}	75% ΔY_{14}	Centroid Z_{14}	Z_{14} Comparison (D_2 - D_5)	ΔZ_{14}	75% ΔZ_{14}
7223.12	-.169		4.999	.037	.014	-8.306	.130	.039	.020
7226.14	-.152		4.999	.0244	.0089	-6.996	.129	.027	.0113
7229.09	-.139		4.999	.0119	.0057	-5.749	.128	.0181	.0094
7232.12	-.127		5.000	.0115	.0036	-4.454	.127	.0156	.0069
7234.85	-.118		5.000	.0219	.0089	-3.313	.127	.022	.012
7238.54	-.108		5.000	.0380	.0154	-1.758	.126	.035	.019
7213.57	-.239		4.999	.077	.030	-12.493	.132	.076	.041

NOTE: All dimensions are in mm except as noted.

Table 21. Spectral Image Characteristics for Monochromator D

Ray Starting Point on Entrance Slit is (E_2): $X_o = 0$, $Y_o = 2$, $Z_o = 4.0$

Frequency cm-1	A_{14}	Not Used	Centroid Y_{14}	ΔY_{14}	75% ΔY_{14}	Centroid Z_{14}	Not Used	ΔZ_{14}	75% ΔZ_{14}
7223.12	-.079		2.000	.046	.017	-8.176		.035	.019
7226.14	-.066		2.000	.031	.015	-6.867		.024	.012
7229.09	-.056		2.000	.0172	.0065	-5.621		.0157	.0058
7232.12	-.047		2.000	.0058	.0031	-4.327		.0073	.0031
7234.85	-.040		2.000	.0131	.0055	-3.186		.0156	.0098
7238.54	-.033		2.000	.0276	.0139	-1.632		.0291	.0187
7213.57	-.134		2.000	.094	.035	-12.360		.070	.041

NOTE: All dimensions are in mm except as noted.

Table 22. Spectral Image Characteristics for Monochromator E

Ray Starting Point on Entrance Slit is (E_5): $X_o = 0$, $Y_o = 5.0$, $Z_o = 4.0$

Frequency cm^{-1}	A_{14}	Not Used	Centroid Y_{14}	ΔY_{14}	75% ΔY_{14}	Centroid Z_{14}	Z_{14} Comparison (E_2 - E_5)	ΔZ_{14}	75% ΔZ_{14}
7223.12	-.156		4.999	.038	.015	-8.306	.130	.040	.017
7226.14	-.142		4.999	.0253	.0097	-6.996	.129	.0280	.0125
7229.09	-.130		4.999	.0127	.0064	-5.749	.128	.0189	.0079
7232.12	-.120		5.000	.0120	.0039	-4.454	.127	.0163	.0061
7234.85	-.113		5.000	.0223	.0087	-3.313	.127	.0228	.0099
7238.54	-.105		5.000	.0385	.0148	-1.758	.126	.035	.019
7213.57	-.215		4.999	.079	.041	-12.493	.133	.077	.044

NOTE: All dimensions are in mm except as noted.

Table 23. Spectral Image Characteristics for Monochromator E

Ray Starting Point on Entrance Slit is (F_2): $X_o = 0$, $Y_o = 2.0$, $Z_o = 4.0$

Frequency cm-1	A_{14}	Not Used	Centroid Y_{14}	ΔY_{14}	75% ΔY_{14}	Centroid Z_{14}	Not Used	ΔZ_{14}	75% ΔZ_{14}
7223.12	-.091		2.000	.0236	.0083	-8.172		.0203	.0113
7226.14	-.076		2.000	.0160	.0070	-6.864		.0132	.0071
7229.09	-.064		2.000	.0091	.0038	-5.620		.0063	.0037
7232.12	-.053		2.000	.0035	.0022	-4.327		.0042	.0024
7234.85	-.045		2.000	.0064	.0032	-3.188		.0098	.0049
7238.54	-.037		2.000	.0129	.0068	-1.636		.0189	.0098
7213.57	-.158		2.000	.0484	.0182	-12.352		.0412	.0237

NOTE: All dimensions are in mm except as noted.

Table 24. Spectral Image Characteristics for Monochromator F

Ray Starting Point on Entrance Slit is (F_5): $X_o = 0$, $Y_o = 5.0$, $Z_o = 4.0$

Frequency cm^{-1}	A_{14}	Not Used	Centroid Y_{14}	ΔY_{14}	75% ΔY_{14}	Centroid Z_{14}	Z_{14} Comparison (F_2 - F_5)	ΔZ_{14}	75% ΔZ_{14}
7223.12	-.171		5.000	.0183	.0076	-8.302	.130	.0221	.0119
7226.14	-.154		5.000	.0133	.0054	-6.993	.129	.0148	.0082
7229.09	-.142		5.000	.0084	.0035	-5.748	.128	.0102	.0056
7232.12	-.128		5.000	.0073	.0030	-4.455	.128	.0087	.0040
7234.85	-.119		5.000	.0117	.0054	-3.315	.127	.0121	.0071
7238.54	-.109		5.000	.0195	.0081	-1.762	.126	.0207	.0110
7213.57	-.243		5.000	.0395	.0170	-12.485	.133	.0440	.0226

NOTE: All dimensions are in mm except as noted.

Table 25. Spectral Image Characteristics for Monochromator F

Ray Starting Point on Entrance Slit is (G_2): $X_o = 0$, $Y_o = 2.0$, $Z_o = 4.0$

Frequency cm^{-1}	A_{14}	Not Used	Centroid Y_{14}	ΔY_{14}	75% ΔY_{14}	Centroid Z_{14}	Not Used	ΔZ_{14}	75% ΔZ_{14}
7223.12	-.080		2.000	.0246	.0091	-8.172		.0205	.0112
7226.14	-.068		2.000	.0167	.0074	-6.864		.0133	.0075
7229.09	-.056		2.000	.0098	.0046	-5.620		.0065	.0047
7232.12	-.046		2.000	.0042	.0027	-4.327		.0042	.0024
7234.85	-.041		2.000	.0067	.0033	-3.188		.0099	.0049
7238.54	-.034		2.000	.0130	.0070	-1.636		.0188	.0098
7213.57	-.136		2.000	.0506	.0212	-12.352		.0414	.0240

NOTE: All dimensions are in mm except as noted.

Table 26. Spectral Image Characteristics for Monochromator G

Ray Starting Point on Entrance Slit is (G_5): $X_o = 0$, $Y_o = 5.0$, $Z_o = 4.0$

Frequency cm^{-1}	A_{14}	Not Used	Centroid Y_{14}	ΔY_{14}	75% ΔY_{14}	Centroid Z_{14}	Z_{14} Comparison (G_2 - G_5)	ΔZ_{14}	75% ΔZ_{14}
7223.12	-.158		5.000	.0189	.0074	-8.302	.130	.0225	.0116
7226.14	-.144		5.000	.0140	.0061	-6.993	.129	.0151	.0112
7229.09	-.132		5.000	.0090	.0044	-5.748	.128	.0108	.0055
7232.12	-.122		5.000	.0078	.0034	-4.455	.128	.0092	.0044
7234.85	-.114		5.000	.0120	.0046	-3.315	.127	.0123	.0074
7238.54	-.105		5.000	.0199	.0079	-1.762	.126	.0208	.0110
7213.57	-.219		5.000	.0412	.0191	-12.485	.133	.0444	.0250

NOTE: All dimensions are in mm except as noted.

Table 27. Spectral Image Characteristics for Monochromator G

Ray Starting Point on Entrance Slit is (H_2): $X_o = 0$, $Y_o = 2.0$, $Z_o = 4.0$

Frequency cm^{-1}	A_{14} in Quartz	Not Used	Centroid Y_{14}	ΔY_{14}	75% ΔY_{14}	Centroid Z_{14}	Not Used	ΔZ_{14}	75% ΔZ_{14}
7223.12	-.305		1.999	.0441	.0189	-8.176		.0349	.0202
7226.14	-.285		1.999	.0297	.0120	-6.867		.0235	.0133
7229.09	-.268		1.999	.0162	.0059	-5.621		.0125	.0055
7232.12	-.253		1.999	.0048	.0026	-4.327		.0071	.0032
7234.85	-.242		1.999	.0129	.0050	-3.187		.0155	.0081
7238.54	-.231		2.000	.0274	.0137	-1.632		.0290	.0214
7213.57	-.394		1.999	.0911	.0375	-12.361		.0695	.0385

NOTE: All dimensions are in mm except as noted.

Table 28. Spectral Image Characteristics for Final Double Pass Monochromator, H

Ray Starting Point on Entrance Slit is ($H_{3.5}$): $X_o = 0$, $Y_o = 3.5$, $Z_o = 3.954$

Frequency cm^{-1}	A_{14} in Quartz	A_{14} Comparison (H_2-$H_{3.5}$)	Centroid Y_{14}	ΔY_{14}	75% ΔY_{14}	Centroid Z_{14}	Z_{14} Comparison (H_2-$H_{3.5}$)	ΔZ_{14}	75% ΔZ_{14}
7223.12	-.296	-.009	3.499	.0396	.0185	-8.178	.002	.0376	.0192
7226.14	-.276	-.009	3.499	.0268	.0100	-6.868	.001	.0260	.0129
7229.09	-.260	-.008	3.499	.0145	.0066	-5.623	.002	.0149	.0058
7232.12	-.245	-.008	3.499	.0065	.0032	-4.328	.001	.0114	.0049
7234.85	-.234	-.008	3.499	.0167	.0064	-3.188	.001	.0187	.0090
7238.54	-.224	-.007	3.499	.0308	.0140	-1.634	.002	.0317	.0197
7213.57	-.384	-.010	3.499	.0867	.0366	-12.362	.001	.0735	.0384

NOTE: All dimensions are in mm except as noted.

Table 29. Spectral Image Characteristics for Final Double Pass Monochromator, H

Ray Starting Point on Entrance Slit is (H_5): $X_o = 0$, $Y_o = 5.0$, $Z_o = 3.880$

Frequency cm^{-1}	A_{14} in Quartz	A_{14} Comparison (H_2 - H_5)	Centroid Y_{14}	ΔY_{14}	75% ΔY_{14}	Centroid Z_{14}	Z_{14} Comparison (H_2 - H_5)	ΔZ_{14}	75% ΔZ_{14}
7223.12	-.311	.006	4.998	.0386	.0141	-8.177	.001	.0402	.0177
7226.14	-.291	.006	4.998	.0255	.0130	-6.868	.001	.0283	.0126
7229.09	-.274	.006	4.998	.0128	.0060	-5.622	.001	.0190	.0074
7232.12	-.259	.006	4.998	.0119	.0039	-4.328	.001	.0160	.0069
7234.85	-.248	.006	4.998	.0219	.0087	-3.187	.000	.0224	.0108
7238.54	-.238	.007	4.999	.0380	.0148	-1.634	.002	.0348	.0196
7213.57	-.399	.005	4.998	.0793	.0352	-12.361	.000	.0769	.0447

NOTE: All dimensions are in mm except as noted.

Table 30. Spectral Image Characteristics for Final Double Pass Monochromator, H

Ray Starting Point on Entrance Slit is (H_2): $X_o = 0$, $Y_o = 2.0$, $Z_o = 4.0$

Frequency cm^{-1}	A_{14} in Quartz	Not Used	Centroid Y_{14}	ΔY_{14}	75% ΔY_{14}	Centroid Z_{14}	Not Used	ΔZ_{14}	75% ΔZ_{14}
7223.12	Fixed Value of -.250		1.999	.0517	.0176	-8.176		.0389	.0193
7226.14			1.999	.0345	.0114	-6.867		.0261	.0140
7229.09			1.999	.0186	.0071	-5.621		.0137	.0052
7232.12			1.999	.0052	.0027	-4.327		.0070	.0033
7234.85			1.999	.0129	.0052	-3.187		.0160	.0087
7238.54			2.000	.0284	.0129	-1.633		.0304	.0190
7213.57			1.999	.1109	.0381	-12.360		.0796	.0396

NOTE: All dimensions are in mm except as noted.

Table 31. Spectral Image Characteristics Without Computer Focus for Final Double Pass Monochromator, H

Ray Starting Point on Entrance Slit is ($H_{3.5}$): $X_o = 0$, $Y_o = 3.5$, $Z_o = 3.954$

Frequency cm^{-1}	A_{14} in Quartz	Not Used	Centroid Y_{14}	ΔY_{14}	75% ΔY_{14}	Centroid Z_{14}	Z_{14} Comparison (H_2-$H_{3.5}$)	ΔZ_{14}	75% ΔZ_{14}
7223.12	Fixed Value of -.250		3.499	.0460	.0174	-8.177	.001	.0409	.0203
7226.14			3.499	.0288	.0106	-6.868	.001	.0277	.0121
7229.09			3.499	.0145	.0058	-5.623	.002	.0154	.0054
7232.12			3.499	.0065	.0028	-4.328	.001	.0115	.0041
7234.85			3.499	.0166	.0060	-3.188	.001	.0197	.0092
7238.54			3.499	.0342	.0185	-1.634	.001	.0336	.0185
7213.57			3.498	.1052	.0349	-12.361	.001	.0828	.0404

NOTE: All dimensions are in mm except as noted.

Table 32. Spectral Image Characteristics Without Computer Focus for Final Double Pass Monochromator, H

Ray Starting Point on Entrance Slit is (H_5): $X_o = 0$, $Y_o = 5.0$, $Z_o = 3.880$

Frequency cm^{-1}	A_{14} in Quartz	Not Used	Centroid Y_{14}	ΔY_{14}	75% ΔY_{14}	Centroid Z_{14}	Z_{14} Comparison (H_2 - H_5)	ΔZ_{14}	75% ΔZ_{14}
7223.12	Fixed Value of -.250		4.998	.0405	.0158	-8.176	.000	.0442	.0173
7226.14			4.998	.0257	.0089	-6.867	.000	.0308	.0123
7229.09			4.998	.0129	.0048	-5.622	.001	.0197	.0064
7232.12			4.998	.0119	.0042	-4.328	.001	.0159	.0066
7234.85			4.999	.0221	.0082	-3.187	.000	.0225	.0105
7238.54			4.999	.0397	.0216	-1.634	.001	.0356	.0197
7213.57			4.997	.0997	.0331	-12.360	.000	.0873	.0474

NOTE: All dimensions are in mm except as noted.

Table 33. Spectral Image Characteristics Without Computer Focus for Final Double Pass Monochromator, H

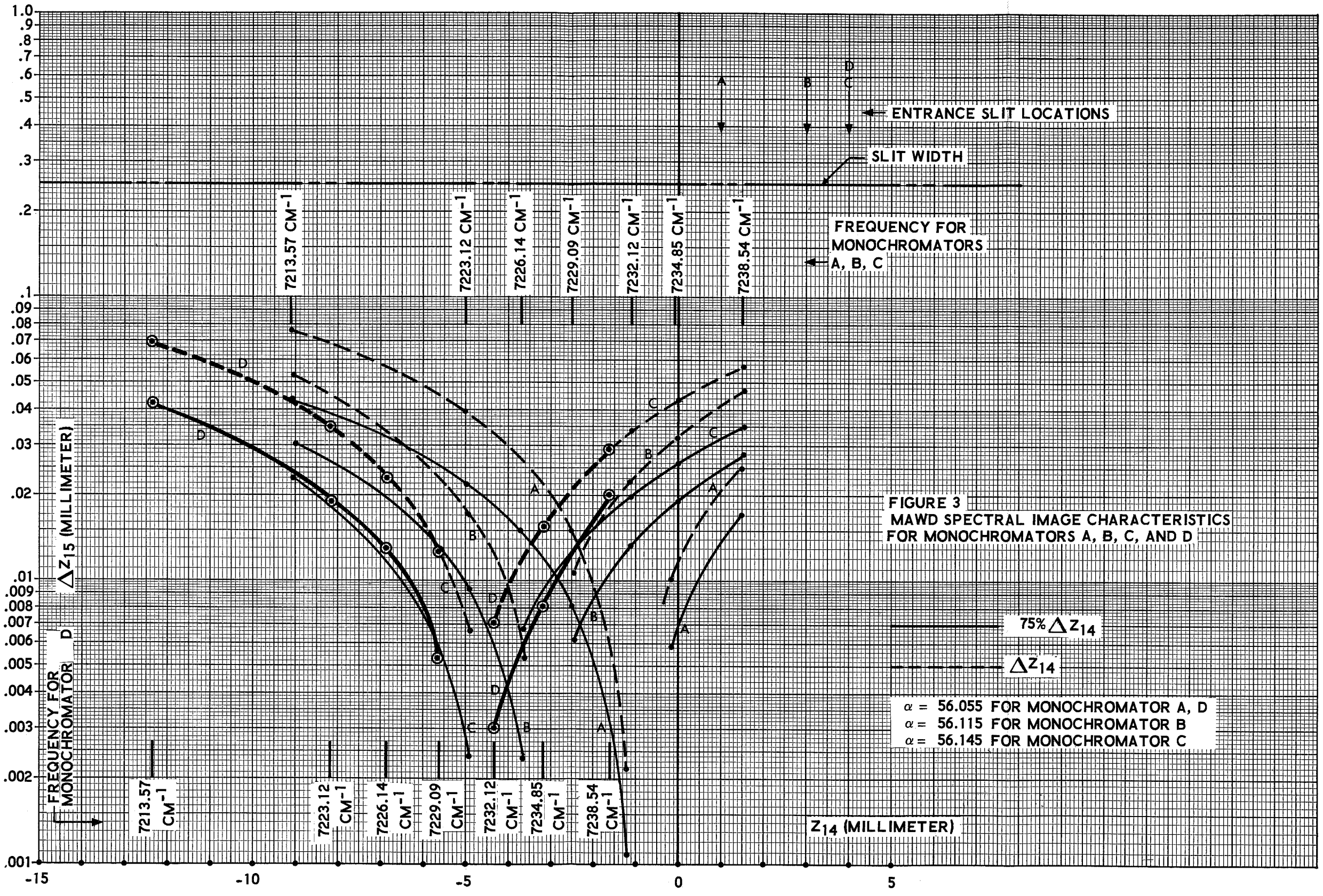

FIGURE 3
MAWD SPECTRAL IMAGE CHARACTERISTICS
FOR MONOCHROMATORS A, B, C, AND D

FIGURE 4 MAWD MONOCHROMATOR H SPECTRAL IMAGE CHARACTERISTICS

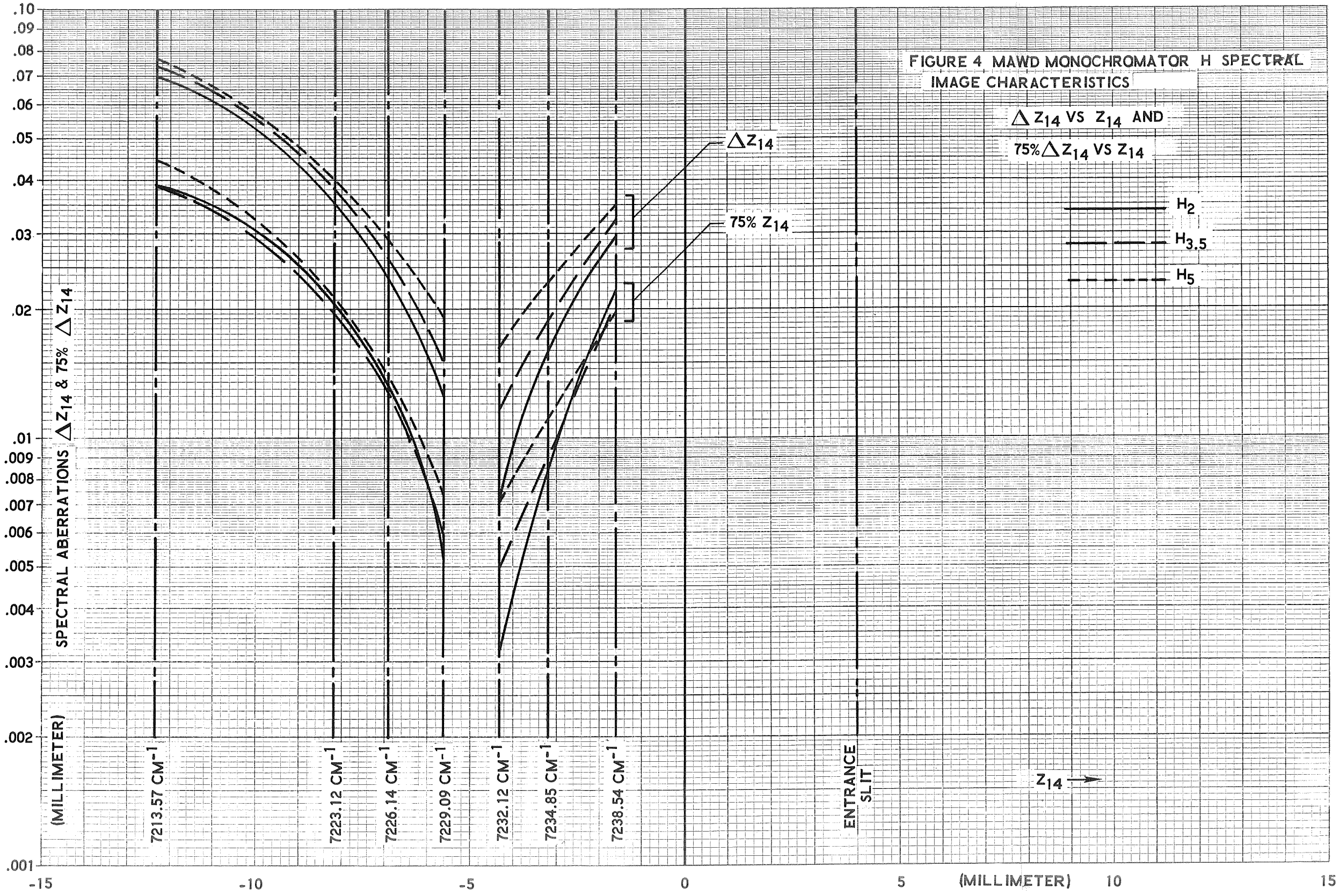

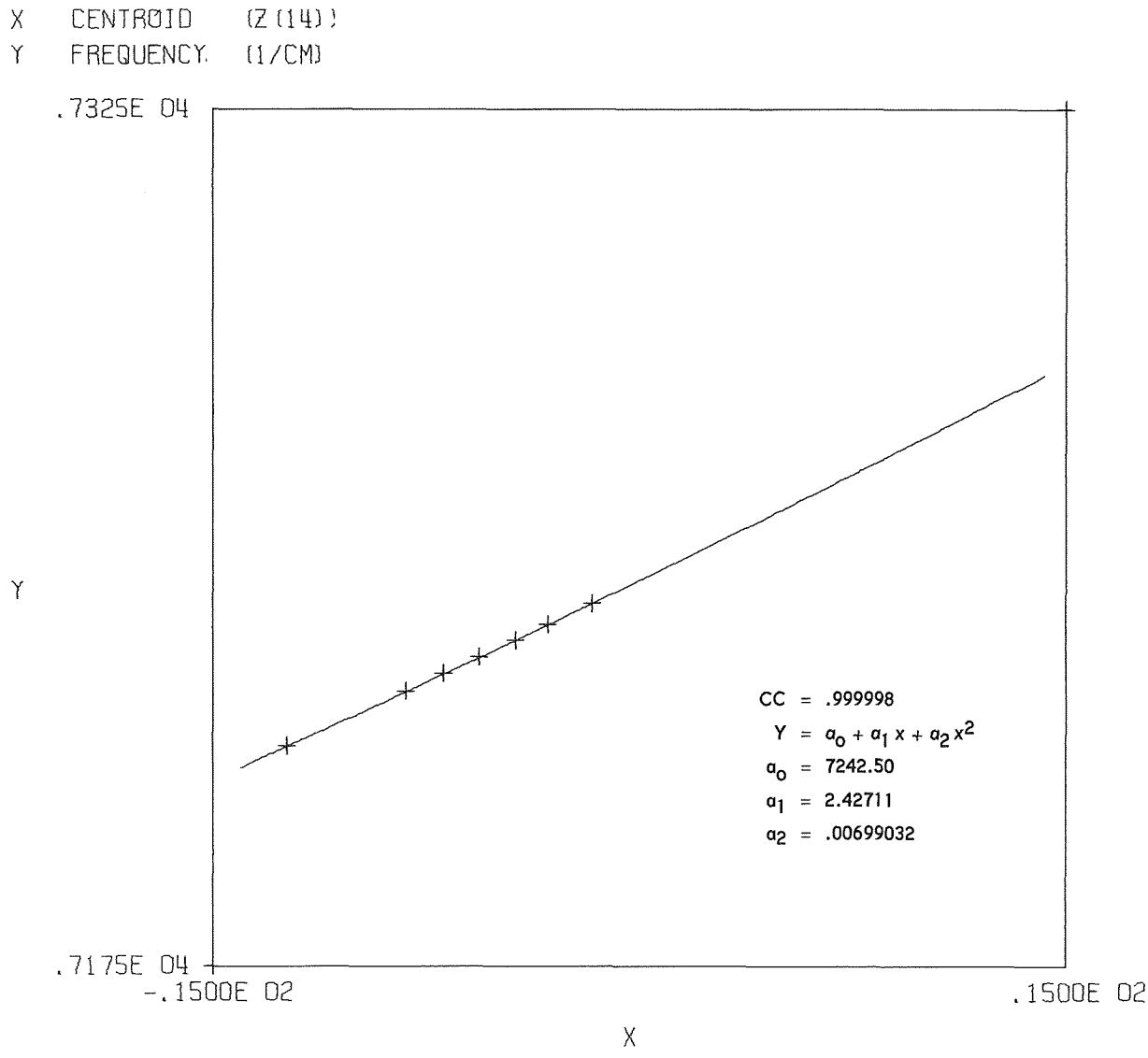

Figure 5. Monochromator H--Centroid Z_{14} vs Frequency

Monochromator	Range of Z_6 Values for Ray Filling Area on Surface #6			
	Freq.	7213.57 cm^{-1}	7234.85 cm^{-1}	7238.54 cm^{-1}
A	Min. Z_6	- 7.98	- .98	.20
	Max. Z_6	- 6.45	- .88	.34
B	Min. Z_6	- 9.50	- 2.47	-1.26
	Max. Z_6	- 7.70	- 1.94	- .94
C	Min. Z_6	-10.27	- 3.24	-2.02
	Max. Z_6	- 8.33	- 2.55	-1.56
D	Min. Z_6	-12.79	- 5.75	-4.53
	Max. Z_6	-10.40	- 4.61	-3.61
E	Min. Z_6	-12.78	- 5.75	-4.53
	Max. Z_6	-10.39	- 4.61	-3.61
F	Min. Z_6	-12.74	- 5.74	-4.53
	Max. Z_6	-10.40	- 4.62	-3.63
G	Min. Z_6	-12.73	- 5.73	-4.52
	Max. Z_6	-10.40	- 4.62	-3.63
H	Min. Z_6	-12.68	- 5.65	-4.43
	Max. Z_6	-10.31	- 4.53	-3.54

NOTE: All dimensions are in mm except as noted.

Table 34. Ray Locations on First Corner Mirror. This Table gives the maximum difference for all Z_6 values for two ray families with starting points (Y_o=2.0, Z_o=4.0), and(Y_o=5.0, Z_o=4.0). An exception is Monochromator H which has respective ray starting points (Y_o=2.0, Z_o=4.0) and (Y_o=5.0, Z_o=3.88).

seen from Table 34 that monochromator H has safe ray clearance--3.54 mm minimum, whereas monochromators A, B, and C have less clearance.

3.2 Single-Pass Monochromator

The design goal of this study at its beginning was to design an optimal double-pass monochromator, and monochromator H is the end result. At this stage of the study, JPL requested that in addition, an optical study be made of the front half of monochromator H used as a single-pass monochromator. Only one such single-pass monochromator has been studied, and it is referred to as monochromator J.

Figure 6 shows two views of the monochromator J optical system which are plotted directly by computer. The upper view is a ray trace using a family of ten rays with a single entrance-slit starting point ($X_o = 0$, $Y_o = 5.0$, $Z_o = 3.88$) which form a uniform line array on the grating face between points ($X_3 = 0$, $Y_3 = 50.0$, $Z_3 = 0$) and ($X_3 = 0$, $Y_3 = -50.0$, $Z_3 = 0$). This particular line array does not fill the full grating area which has been later outlined with phantom lines. The lower view uses a different family of ten rays which starts from the same entrance-slit point as for the upper view, but these ten rays form a uniform line array on the grating face between points ($X_3 = 0$, $Y_3 = 0$, $Z_3 = 90.0$) and ($X_3 = 0$, $Y_3 = 0$, $Z_3 = -90.0$). Both of these ray-trace plots are for a frequency of 7213.57 cm^{-1} for which the boundary rays have their greatest spread from the monochromator center line.

The monochromator J axis systems shown in Figure 6 are defined in Table 35, and the dimensional parameters for monochromator J are given in Table 36. The distortions in the spectral image of the entrance slit are only half as great as for monochromator H, so the entrance-slit plane tilt, β_1, is halved. Now $\beta_1 = 0.580°$, and the lateral tilt of the entrance slit in its plane is also halved.

Tables 37, 38, and 39 show the spectral image characteristics for monochromator J for three different entrance-slit starting points. In these three tables, A_7 is varied by the computer until a best-image is obtained for each family

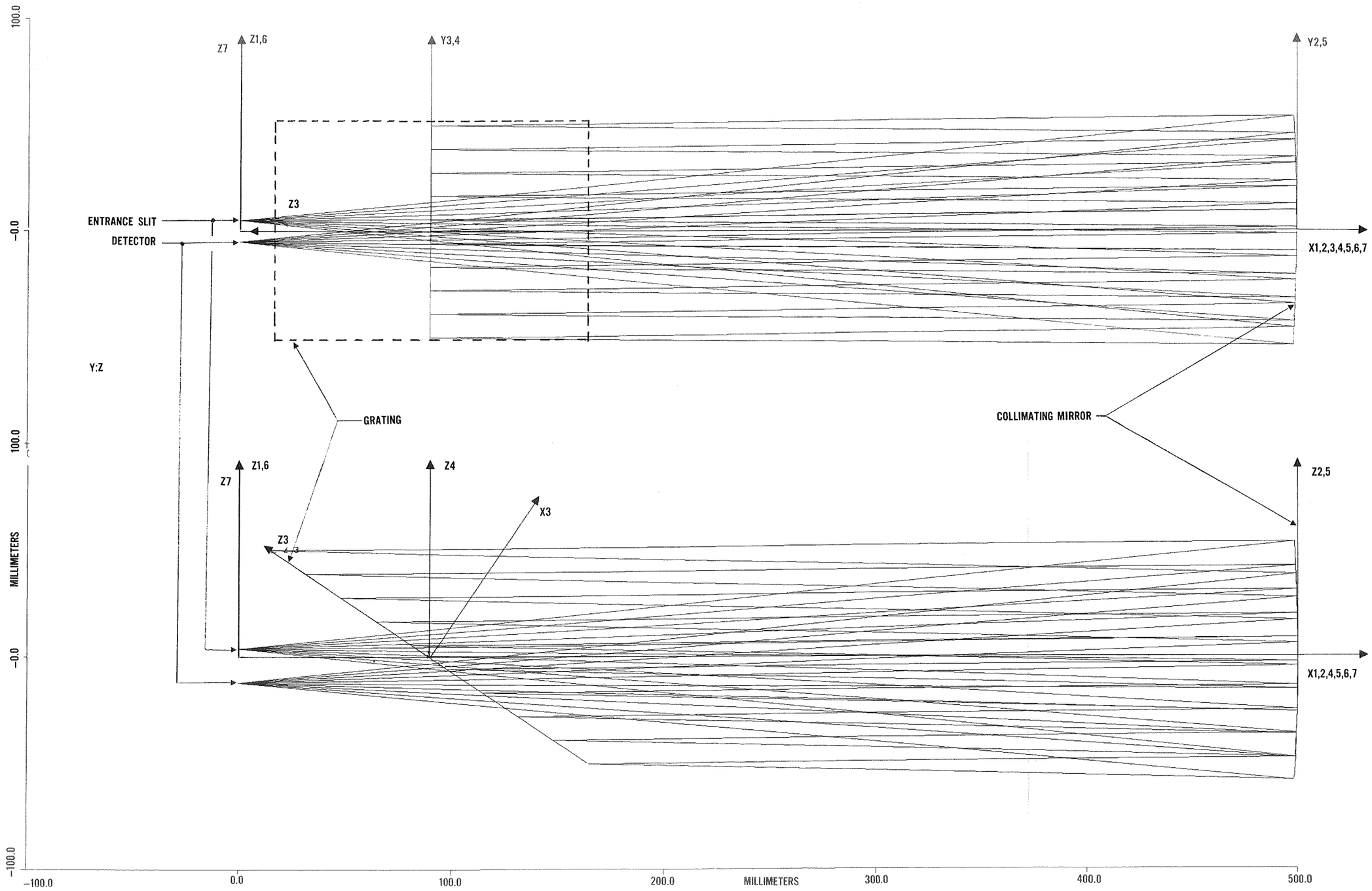

Figure 6. MAWD Fixed Single-Pass Littrow Mono, F/5, 1000 MM TFL, Paraboloid 7193.81 J

(X_o, Y_o, Z_o)	Entrance Slit--The entrance slit lies in the Y_o-Z_o plane, and each family of rays used to ray-trace the monochromator starts from a point on the entrance slit.
(X_1, Y_1, Z_1)	Mathematical Axis System.
(X_2, Y_2, Z_2) (X_5, Y_5, Z_5)	Paraboloid Collimating Mirror--These two axis systems are identical and may be referred to as the $(X_{2,5}, Y_{2,5}, Z_{2,5})$ axis system. The apex of this paraboloidal reflecting surface is at the origin of the $(X_{2,5}, Y_{2,5}, Z_{2,5})$ axis system, and the focus of the paraboloid is located on the negative $X_{2,5}$-axis.
(X_3, Y_3, Z_3)	Diffraction Grating--The ruled area of the grating is in the Y_3-Z_3 plane, and the grating rulings are parallel to the Y_3-axis.
(X_4, Y_4, Z_4)	Mathematical Axis System.
(X_6, Y_6, Z_6)	Front Face of Detector Cover Glass--This is a refracting surface in the Y_6-Z_6 plane.
(X_7, Y_7, Z_7)	Spectral Image Surface--The spectral images for the ray starting points on the entrance slit are formed on the Y_7-Z_7 plane.

Table 35. Description of Ray-Trace Axis Systems Used for Single-Pass Monochromator

Axis Sub-Script (n)	A_n (mm)	B_n (mm)	C_n (mm)	α_n (deg)	β_n (deg)	γ_n (deg)	Surface Shape	Optical Function of Surface	D_n (mm)	E_n (mm)	F_n (mm)	R_n (mm)	N_n
1					-.580		Plane	Transmit					1.0000
2	500.000						Paraboloid	Reflect	1.000	1.000		-1000.000	1.0000
3	-410.000			56.055			Plane	Diffract					1.0000
4				-56.055			Plane	Transmit					1.0000
5	410.000						Paraboloid	Reflect	1.000	1.000		-1000.000	1.0000
6	-499.750						Plane	Refract					1.4460
7	.250						Plane	Transmit					1.4460

Table 36. Dimensional Parameters for MAWD Single-Pass Monochromator, J

Ray Starting Point on Entrance Slit is (J_2): $X_o = 0$, $Y_o = 2.0$, $Z_o = 4.0$

Frequency cm^{-1}	A_7 in Quartz	Not Used	Centroid ΔY_7	ΔY_7	75% ΔY_7	Centroid Z_7	ΔZ_7	75% ΔZ_7
7223.12	-.259		-2.000	.0218	.0085	-6.051	.0185	.0111
7226.14	-.256		-2.000	.0150	.0063	-5.411	.0124	.0073
7229.09	-.253		-2.000	.0085	.0032	-4.799	.0066	.0032
7232.12	-.250		-2.000	.0033	.0018	-4.161	.0037	.0015
7234.85	-.249		-2.000	.0072	.0029	-3.597	.0082	.0052
7238.54	-.246		-2.000	.0145	.0071	-2.826	.0154	.0102
7213.57	-.271		-2.000	.0436	.0171	-8.080	.0375	.0213
Min.Freq. 7193.81	-.309		-2.000	.0901	.0378	-12.307	.0760	.0439
Max.Freq. 7308.16	-.298		-2.000	.1686	.0713	11.201	.1584	.1087

NOTE: All dimensions are in mm except as noted.

Table 37. Spectral Image Characteristics for Single-Pass Monochromator, J

Ray Starting Point on Entrance Slit is ($J_{3.5}$): $X_o = 0$, $Y_o = 3.5$, $Z_o = 3.976$

Frequency cm^{-1}	A_7 in Quartz	A_7 Comparison (J_2 - $J_{3.5}$)	Centroid Y_7	ΔY_{15}	75% ΔY_7	Centroid Z_7	Z_7 Comparison (J_2 - $J_{3.5}$)	ΔZ_7	75% ΔZ_7
7223.12	-.256	-.003	-3.499	.0201	.0094	-6.051	.000	.0196	.0109
7226.14	-.253	-.003	-3.499	.0136	.0051	-5.411	.000	.0134	.0069
7229.09	-.251	-.002	-3.499	.0075	.0026	-4.799	.000	.0077	.0033
7232.12	-.248	-.002	-3.499	.0036	.0021	-4.161	.000	.0059	.0023
7234.85	-.246	-.003	-3.499	.0090	.0033	-3.597	.000	.0100	.0045
7238.54	-.244	-.002	-3.499	.0164	.0065	-2.826	.000	.0170	.0099
7213.57	-.269	-.002	-3.499	.0412	.0169	-8.080	.000	.0389	.0211
Min.Freq. 7193.81	-.306	-.003	-3.500	.0878	.0472	-12.307	.000	.0779	.0438
Max.Freq. 7308.16	-.297	-.001	-3.500	.1685	.0756	11.201	.000	.1596	.1154

NOTE: All dimensions in mm except as noted.

Table 38. Spectral Image Characteristics for Single-Pass Monochromator, J

Ray Starting Point on Entrance Slit is (J_5): $X_o = 0$, $Y_o = 5.0$, $Z_o = 3.939$

Frequency cm^{-1}	A_7 in Quartz	A_7 Comparison (J_2 - J_5)	Centroid Y_7	ΔY_{15}	75% ΔY_7	Centroid Z_7	Z_7 Comparison (J_2 - J_5)	ΔZ_7	75% ΔZ_7
7223.12	-.261	.002	-4.999	.0194	.0080	-6.051	.000	.0205	.0107
7226.14	-.258	.002	-4.999	.0129	.0046	-5.411	.000	.0144	.0070
7229.09	-.256	.003	-4.999	.0067	.0034	-4.799	.000	.0095	.0038
7232.12	-.253	.003	-4.999	.0065	.0023	-4.161	.000	.0083	.0055
7234.85	-.251	.002	-4.999	.0118	.0043	-3.597	.000	.0121	.0053
7238.54	-.249	.003	-4.999	.0192	.0073	-2.826	.000	.0189	.0101
7213.57	-.274	.003	-4.999	.0399	.0167	-8.080	.000	.0399	.0239
Min.Freq. 7193.81	-.311	.002	-4.999	.0841	.0348	-12.307	.000	.0796	.0492
Max.Freq. 7308.16	-.302	.004	-5.001	.1684	.0748	11.201	.000	.1611	.1155

Table 39. Spectral Image Characteristics for Single-Pass Monochromator, J

of one hundred Z_7 values. Tables 40, 41, and 42 show the spectral image characteristics for monochromator J when A_7 has a fixed value of 0.250 mm. Tables 37 through 42 have two new frequencies added, which are not used with the double-pass monochromators. These represent the maximum and minimum frequencies which have just the same maximum utilization of the two corner mirrors as does monochromator H.

Figure 7 is the computer plot and equation for the best fit, second-degree curve for the nine frequency values versus their corresponding centroid Z_7 values obtained from Table 41.

3.3 Error Analysis for Monochromators H and J

The error analysis presented in this section determines the modifications to the monochromator spectral image characteristics due to component tolerances and instabilities. This analysis is performed in a fundamental manner in which only one dimensional parameter is modified at a time. Each dimensional parameter error has been actually varied through two full decades. As long as the dimensional parameter errors are relatively small, their individual changes to the monochromator spectral image characteristics may be added to give the overall spectral image characteristics for the monochromator with all its dimensional parameter errors.

Tables 43 through 49 give the results of single-ray error analyses. For the particular dimensional parameter errors presented in these tables, one axial ray is characteristic of a 100-ray family, since the monochromator focus will be unaffected. The same single ray is used for every dimensional parameter error change, and that ray has an entrance-slit starting point of (Y_o=5.0, Z_o=3.88), and a ray intercept at the origin of the (X_3,Y_3,Z_3) axis system.

If a dimensional parameter error modifies the monochromator focal length, then at least two rays are required for the spectral image analysis. Tables 50 and 51 show such 2-ray error analysis. These two rays have their entrance-slit starting points at (Y_o= 5.0, Z_o= 3.88) and they strike the grating at two points (Y_3 = 0, Z_3= 90.0) and (Y_3 = 0, Z_3 = -90.0). The computer then varies

Ray Starting Point on Entrance Slot is (J_2): $X_o = 0$, $Y_o = 2.0$, $Z_o = 4.0$

Frequency	A_7 in Quartz	Not Used	Centroid Y_7	ΔY_{15}	75% ΔY_7	Centroid Z_7	Not Used	ΔZ_7	75% ΔZ_7
7223.12	Fixed Value of -.250		-2.000	.0236	.0088	-6.051		.0195	.0113
7226.14			-2.000	.0161	.0064	-5.410		.0130	.0069
7229.09			-2.000	.0091	.0054	-4.799		.0069	.0037
7232.12			-2.000	.0034	.0019	-4.161		.0036	.0015
7234.85			-2.000	.0069	.0030	-3.597		.0083	.0048
7238.54			-2.000	.0144	.0069	-2.826		.0158	.0094
7213.57			-2.000	.0479	.0175	-8.080		.0399	.0251
Min.Freq. 7193.81			-2.000	.1020	.0369	-12.307		.0824	.0532
Max.Freq. 7308.16			-2.000	.1783	.0731	11.201		.1631	.1138

NOTE: All dimensions are in mm except as noted.

Table 40. Spectral Image Characteristics Without Computer Focus for Single-Pass Monochromator, J

Ray Starting Point on Entrance Slot is ($J_{3.5}$): $X_o = 0$, $Y_o = 3.5$, $Z_o = 3.976$

Frequency cm^{-1}	A_7 in Quartz	Not Used	Centroid Y_7	ΔY_{15}	75% ΔY_7	Centroid Y_u	Z_7 Comparison (J_2 - $J_{3.5}$)	ΔZ_7	75% ΔZ_7
7223.12	Fixed Value of -.250		-3.499	.0207	.0083	-6.051	.000	.0202	.0133
7226.14			-3.499	.0137	.0053	-5.411	.001	.0137	.0066
7229.09			-3.499	.0075	.0023	-4.799	.000	.0078	.0032
7232.12			-3.499	.0036	.0020	-4.161	.000	.0060	.0022
7234.85			-3.499	.0090	.0030	-3.597	.000	.0104	.0049
7238.54			-3.499	.0164	.0078	-2.826	.000	.0177	.0103
7213.57			-3.499	.0450	.0171	-8.080	.000	.0409	.0232
Min.Freq. 7193.81			-3.499	.0992	.0374	-12.307	.000	.0840	.0530
Max.Freq. 7308.16			-3.500	.1779	.0887	11.201	.000	.1635	.1135

NOTE: All dimensions are in mm except as noted.

Table 41. Spectral Image Characteristics Without Computer Focus for Single Monochromator, J

Ray Starting Point on Entrance Slit is (J_5): $X_o = 0$, $Y_o = 5.0$, $Z_o = 3.939$

Frequency cm^{-1}	A_7 in Quartz	Not Used	Centroid Y_7	ΔY_{15}	75% ΔY_7	Centroid Z_7	Z_7 Comparison (J_2 - J_5)	ΔZ_7	75% ΔZ_7
7223.12	Fixed Value of -.250		-4.999	.0195	.0077	-6.051	.000	.0216	.0104
7226.14			-4.999	.0130	.0050	-5.411	.001	.0151	.0063
7229.09			-4.999	.0067	.0037	-4.799	.000	.0098	.0036
7232.12			-4.999	.0065	.0026	-4.161	.000	.0083	.0034
7234.85			-4.999	.0018	.0044	-3.597	.000	.0120	.0057
7238.54			-4.999	.0192	.0077	-2.826	.000	.0190	.0101
7213.57			-4.999	.0423	.0170	-8.080	.000	.0425	.0242
Min.Freq. 7193.81			-4.999	.0964	.0373	-12.307	.000	.0861	.0459
Max.Freq. 7308.16			-5.001	.1788	.0800	11.201	.000	.1649	.1140

NOTE: All dimensions are in mm except as noted.

Table 42. Spectral Image Characteristics Without Computer Focus for Single Monochromator, J

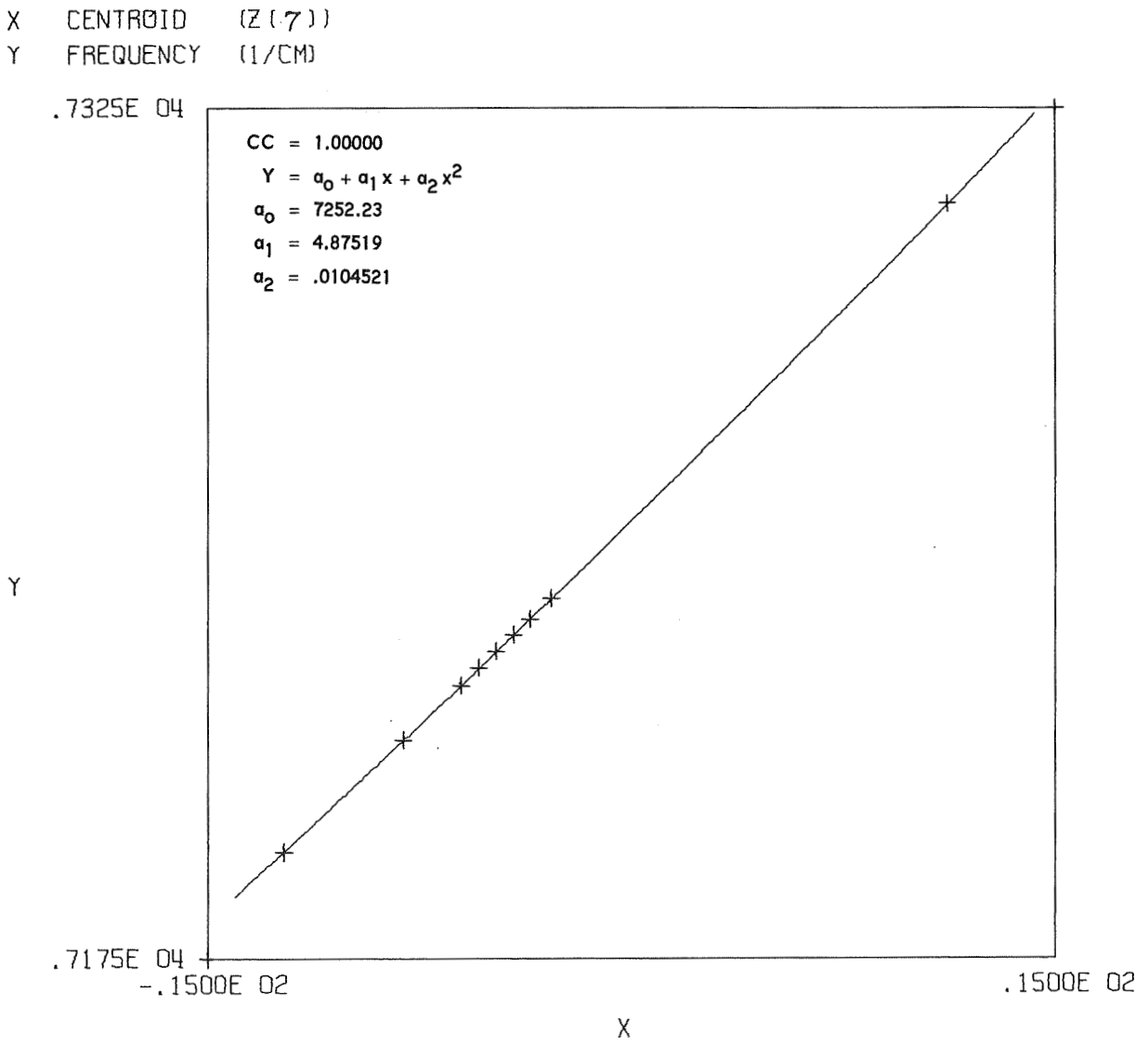

Figure 7. Monochromator J--Centroid Z_7 vs Frequency

A_{14} and A_7 for monochromator H and J, respectively, until the two rays have identical Z_{14} or Z_7 values.

Figure 8 is a composite plot of the single-ray errors from Tables 43 through 49. One interesting result of this error analysis is that the Y_{14} error displacement is zero, or substantially zero, for certain dimensional parameter errors, while the corresponding Y_7 error displacement is large. This is because these particular error displacements created in the first monochromator are cancelled by the second monochromator due to the vertical ray inversion at the corner mirror.

3.4 Component Dimensions for Monochromator H

This section presents a number of computer spot diagrams which show the maximum areas of each optical surface which are used by rays in Monochromator H. Figure 9 is a graph of the final entrance-slit shape in the Y_o-Z_o plane, with its final coordinates. Figure 10 is a composite view of surfaces 1, 6, 7, and 14 at a frequency of 7213.57 cm^{-1}. For this plot, nine families of nine rays each start from the nine entrance-slit starting points shown in Figure 9 for Monochromator H. The intercepts of these rays with the first corner mirror (the Y_6-Z_6 plane), the second corner mirror (the Y_7-Z_7 plane), and the exit-slit plane (the Y_{14}-Z_{14} plane) are accurately shown. Figure 11 is a similar plot, except the frequency is 7238.54 cm^{-1}. Figure 12 is also similar to Figures 10 and 11, and it is a composite plot of all seven frequencies listed in Table 13.

Figure 13 is a composite plot of surfaces 2, 5, 9, and 12 for the collimating mirror, at a frequency of 7213.59 cm^{-1}. A 100-ray family is used with an entrance-slit starting point of (Y_o - 5.0, Z_o= 3.88). Four 100-ray points are seen in Figure 13 since four 100-ray intercepts are shown at respective surfaces 2, 5, 9, and 12.

It has been necessary to develop a new ray-trace axis system in order to determine the hole location in the grating. This new ray-trace axis system

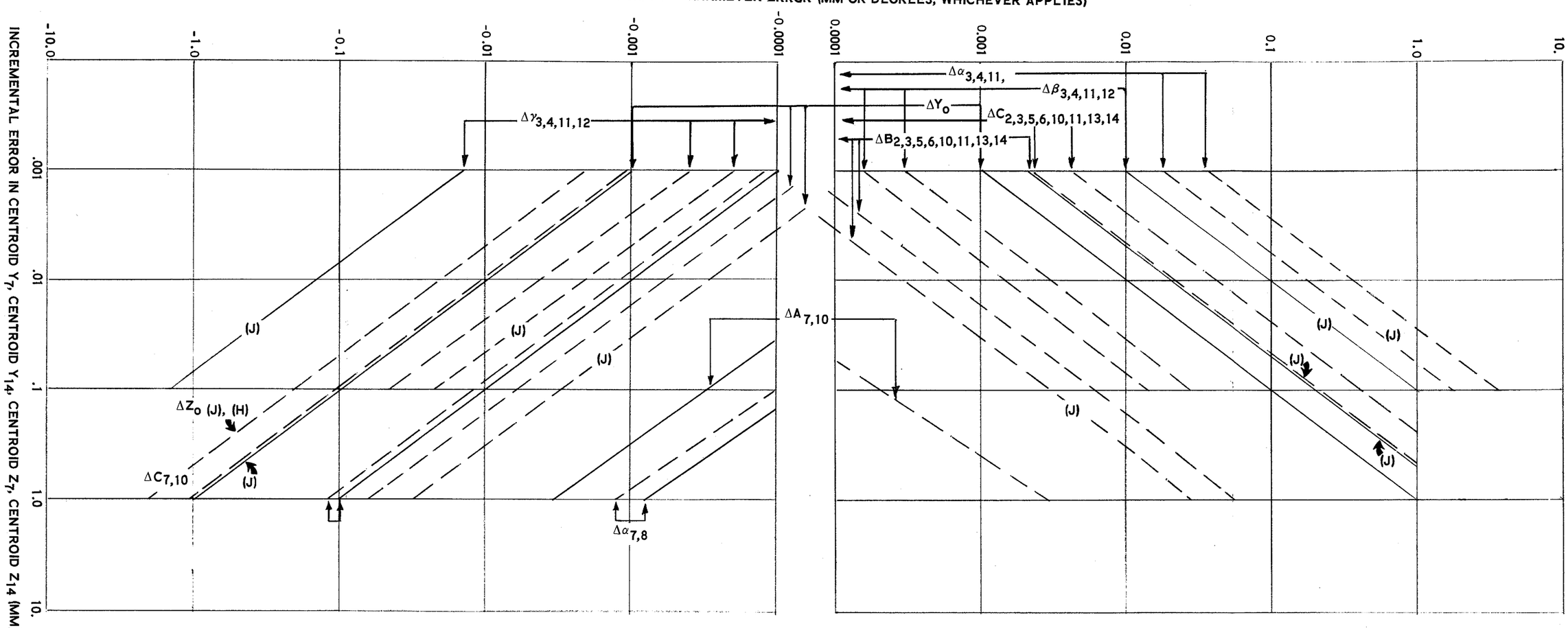

NOTES:

——— Incremental Errors in Centroid Y_7 or Centroid Y_{14}.

– – – Incremental Errors in Centroid Z_7 or Centroid Z_{14}.

All curves are for Monochromator H unless otherwise noted.

These image errors are smaller than 0.0001 inch:

$\Delta\alpha_{3,4,11,12}$(J) for Centroid Y_7
$\Delta\alpha_{3,4,11,12}$(H) for Centroid Y_{14}
$\Delta\beta_{3,4,11,12}$(H) for Centroid Y_{14}
$\Delta\gamma_{3,4,11,12}$(H) for Centroid Y_{14}
$\Delta B_{2,3,5,6,10,11,13,14}$(H) for Centroid Y_{14}
$\Delta C_{2,3,5,6,10,11,13,14}$(J) for Centroid Y_7
$\Delta C_{2,3,5,6,10,11,13,14}$(H) for Centroid Y_{14}
$\Delta C_{7,10}$(H) for Centroid Y_{14}
$\Delta\alpha_{7,9}$ (H) for Centroid Y_{14}
$\Delta\alpha_{7,9}$ (H) for Centroid Z_{14}
$\Delta\beta_{7,9}$ (H) for Centroid Y_{14}
$\Delta\beta_{7,9}$ (H) for Centroid Z_{14}
ΔZ_o (J) for Centroid Y_7
ΔZ_o (H) for Centroid Y_{14}

Figure 8. Result of Error Analyses from Tables 43 through 49

		Single Pass Monochromator J						Double Pass Monochromator H					
	Frequency	7213.57 cm^{-1}		7232.12 cm^{-1}		7238.54 cm^{-1}		7213.57 cm^{-1}		7232.12 cm^{-1}		7238.54 cm^{-1}	
	Error Description	Y_7	Z_7	Y_7	Z_7	Y_7	Z_7	Y_{14}	Z_{14}	Y_{14}	Z_{14}	Y_{14}	Z_{14}
(1)	Zero Error	-4.9988	-8.0045	-4.9987	-4.1017	-4.9986	-2.7718	4.9994	-12.3346	4.9993	-4.3296	4.9993	-1.6458
(2)	$\Delta\alpha_{3,11}$= .001° $\Delta\alpha_{4,12}$=-.001°	-4.9988	-7.9868	-4.9987	-4.0840	-4.9986	-2.7542	4.9994	-12.2977	4.9993	-4.2938	4.9993	-1.6103
	(2) - (1)	0	.0177	0	.0177	0	.0176	0	.0369	0	.0358	0	.0355
(3)	$\Delta\alpha_{3,11}$= .01° $\Delta\alpha_{4,12}$=-.01°	-4.9988	-7.8269	-4.9986	-3.9251	-4.9986	-2.5956	4.9994	-11.9659	4.9993	-3.9719	4.9993	-1.2917
	(3) - (1)	0	.1776	.0001	.1766	0	.1762	0	.3687	0	.3577	0	.3541
(4)	$\Delta\alpha_{3,11}$= .1° $\Delta\alpha_{4,12}$= -.1°	-4.9987	-6.2301	-4.9986	-2.3378	-4.9986	-1.0115	4.9993	- 8.6710	4.9993	- .7745	4.9993	1.8741
	(4) - (1)	.0001	1.7744	.0001	1.7639	0	1.7603	-.0001	3.6636	0	3.5551	0	3.5199
(5)	$\Delta\beta_{3,11}$= .001° $\Delta\beta_{4,12}$=-.001°	-4.9891	-8.0044	-4.9889	-4.1015	-4.9889	-2.7716	4.9994	-12.3343	4.9993	-4.3293	4.9993	-1.6455
	(5) - (1)	.0097	.0001	.0098	.0002	.0097	.0002	0	.0003	0	.0003	0	.0003
(6)	$\Delta\beta_{3,11}$= .01° $\Delta\beta_{4,12}$=-.01°	-4.9020	-8.0030	-4.9012	-4.1002	-4.9010	-2.7703	4.9994	-12.3315	4.9993	-4.3266	4.9993	-1.6429
	(6) - (1)	.0968	.0015	.0975	.0015	.0976	.0015	0	.0031	0	.0030	0	.0029
(7)	$\Delta\beta_{3,11}$= .1° $\Delta\beta_{4,12}$=-.1°	-4.0302	-7.9912	-4.0244	-4.0884	-4.0224	-2.7586	4.9991	-12.3070	4.9993	-4.3028	4.9993	-1.6193
	(7) - (1)	.9686	.0133	.9743	.0133	.9762	.0132	-.0003	.0276	0	.0268	0	.0265

NOTE: All dimensions are in mm except as noted.

Table 43. Single Ray Error Analysis for Single- and Double-Pass Monochromators: $\Delta\alpha_{3,4,11,12}$ and $\Delta\beta_{3,\ 4,\ 11,\ 12}$

		Single-Pass Monochromator J						Double-Pass Monochromator H					
	Frequency	7213.57 cm^{-1}		7232.12 cm^{-1}		7238.54 cm^{-1}		7213.57 cm^{-1}		7232.12 cm^{-1}		7238.54 cm^{-1}	
	Error Description	Y_7	Z_7	Y_7	Z_7	Y_7	Z_7	Y_{14}	Z_{14}	Y_{14}	Z_{14}	Y_{14}	Z_{14}
(1)	Zero Error	-4.9988	-8.0045	-4.9987	-4.1017	-4.9986	-2.7718	4.9994	-12.3346	4.9993	-4.3296	4.9993	-1.6458
(8)	$\Delta\gamma_{3,11} = .001°$ $\Delta\gamma_{4,12} = -.001°$	-5.0133	-8.0048	-5.0131	-4.1019	-5.0131	-2.7720	4.9994	-12.3350	4.9993	-4.3300	4.9993	-1.6462
	(8) - (1)	- .0145	- .0003	- .0144	- .0002	- .0145	- .0002	0	- .0004	0	- .0004	0	- .0004
(9)	$\Delta\gamma_{3,11} = .01°$ $\Delta\gamma_{4,12} = -.01°$	-5.1440	-8.0068	-5.1435	-4.1039	-5.1433	-2.7740	4.9994	-12.3392	4.9993	-4.3340	4.9993	-1.6501
	(9) - (1)	- .1452	- .0023	- .1448	- .0022	- .1447	- .0022	0	- .0046	0	- .0044	0	- .0043
(10)	$\Delta\gamma_{3,11} = .1°$ $\Delta\gamma_{4,12} = -.1°$	-6.4507	-8.0276	-6.4467	-4.1244	-6.4454	-2.7944	4.9993	-12.3822	4.9993	-4.3754	4.9993	-1.6910
	(10) - (1)	-1.4519	- .0231	-1.4480	- .0227	-1.4468	- .0226	-.0001	- .0476	0	- .0458	0	- .0452
(11)	$\Delta B_{2,5,10,13} = .01$ $\Delta B_{3,6,11,14} = -.01$	-4.9788	-8.0042	-4.9787	-4.1014	-4.9786	-2.7715	4.9994	-12.3339	4.9993	-4.3290	4.9993	-1.6452
	(11) - (1)	.0200	.0003	.0200	.0003	.0200	.0003	0	.0007	0	.0006	0	.0006
(12)	$\Delta B_{2,5,10,13} = .1$ $\Delta B_{3,6,11,14} = -.1$	-4.7988	-8.0015	-4.7987	-4.0987	-4.7986	-2.7688	4.9995	-12.3283	4.9993	-4.3235	4.9993	-1.6398
	(12) - (1)	.2000	.0030	.2000	.0030	.2000	.0030	.0001	.0063	0	.0061	0	.0060
(13)	$\Delta B_{2,5,10,13} = 1.0$ $\Delta B_{3,6,11,14} = -1.0$	-2.9990	-7.9771	-2.9988	-4.0746	-2.9987	-2.7448	4.9997	-12.2776	4.9992	-4.2747	4.9991	-1.5916
	(13) - (1)	1.9998	.0274	1.9999	.0271	1.9999	.0271	.0003	.0570	-.0001	.0549	-.0002	.0542

Note: All dimensions are in mm except as noted

Table 44. Single Ray Error Analysis for Single- and Double-Pass Monochromators: $\Delta\gamma_{3,4,11,12}$ and $\Delta B_{2,3,5,6,10,11,13,14}$

	Frequency	Single-Pass Monochromator J						Double-Pass Monochromator H					
		7213.57 cm^{-1}		7232.12 cm^{-1}		7238.54 cm^{-1}		7213.57 cm^{-1}		7232.12 cm^{-1}		7238.54 cm^{-1}	
	Error Description	Y_7	Z_7	Y_7	Z_7	Y_7	Z_7	Y_{14}	Z_{14}	Y_{14}	Z_{14}	Y_{14}	Z_{14}
(1)	Zero Error	-4.9988	-8.0045	-4.9987	-4.1017	-4.9986	-2.7718	4.9994	-12.3346	4.9993	-4.3296	4.9993	-1.6458
(14)	$\Delta C_{2,5,10,13} = .01$ $\Delta C_{3,6,11,14} = -.01$	-4.9988	-7.9842	-4.9987	-4.0814	-4.9986	-2.7516	4.9994	-12.2923	4.9993	-4.2886	4.9993	-1.6052
	(14) - (1)	0	.0203	0	.0203	0	.0202	0	.0423	0	.0410	0	.0406
(15)	$\Delta C_{2,5,10,13} = .1$ $\Delta C_{3,6,11,14} = -.1$	-4.9988	-7.8010	-4.9986	-3.8993	-4.9986	-2.5698	4.9994	-11.9122	4.9993	-3.9198	4.9993	-1.2401
	(15) - (1)	0	.2035	.0001	.2024	0	.2020	0	.4224	0	.4098	0	.4057
(16)	$\Delta C_{2,5,10,13} = 1.0$ $\Delta C_{3,6,11,14} = -1.0$	-4.9988	-5.9716	-4.9986	-2.0808	-4.9986	- .7550	4.9994	- 8.1407	4.9993	- .2596	4.9993	2.3839
	(16) - (1)	0	2.0329	.0001	2.0209	0	2.0168	0	4.1939	0	4.0700	0	4.0297
(17)	$\Delta A_7 = .01$ $\Delta A_{10} = -.01$	Do Not Apply	Do Not Apply	Do Not Apply	Do Not Apply	Do Not Apply	Do Not Apply	4.9994	-12.3345	4.9992	-4.3295	4.9992	-1.6457
	(17) - (1)							0	.0001	-.0001	.0001	-.0001	.0001
(18)	$\Delta A_7 = .1$ $\Delta A_{10} = -.1$							4.9991	-12.3340	4.9989	-4.3293	4.9989	-1.6455
	(18) - (1)							-.0003	- .0005	-.0003	.0002	-.0003	.0002
(19)	$\Delta A_7 = 1.0$ $\Delta A_{10} = -1.0$	"	"	"	"	"	"	4.9958	-12.3283	4.9957	-4.3264	4.9957	-1.6436
	(19) - (1)							-.0036	.0062	-.0035	.0031	-.0035	.0021

Note: All dimensions are in mm except as noted

Table 45. Single Ray Error Analysis for Single- and Double-Pass Monochromators: $\Delta C_{2,3,5,6,10,11,13,14}$ and $\Delta A_{7,10}$

	Frequency	Single-Pass Monochromator J						Double-Pass Monochromator H					
		7213.57 cm^{-1}		7232.12 cm^{-1}		7238.54 cm^{-1}		7213.57 cm^{-1}		7232.12 cm^{-1}		7238.54 cm^{-1}	
	Error Description	Y_7	Z_7	Y_7	Z_7	Y_7	Z_7	Y_{14}	Z_{14}	Y_{14}	Z_{14}	Y_{14}	Z_{14}
(1)	Zero Error							4.9994	-12.3346	4.9993	-4.3296	4.9993	-1.6458
(20)	$\Delta C_7 = .01$ $\Delta C_{10} = -.01$	Do Not Apply	Do Not Apply	Do Not Apply	Do Not Apply	Do Not Apply	Do Not Apply	4.9994	-12.3558	4.9993	-4.3501	4.9993	-1.6660
	(20) - (1)							0	- .0212	0	- .0205	0	- .0202
(21)	$\Delta C_7 = .1$ $\Delta C_{10} = -.1$							4.9994	-12.5473	4.9993	-4.5348	4.9993	-1.8485
	(21) - (1)	"	"	"	"	"	"	0	- .2127	0	- .2052	0	- .2027
(22)	$\Delta C_7 = 1.0$ $\Delta C_{10} = -1.0$							4.9993	-14.4736	4.9991	-6.3929	4.9992	-3.6845
	(22) - (1)							-.0001	- 2.1390	-.0002	-2.0633	-.0001	-2.0387
(23)	$\Delta\alpha_7 = .01°$ $\Delta\alpha_8 = -.01°$							4.9994	-12.3346	4.9993	-4.3296	4.9993	-1.6457
	(23) - (1)	"	"	"	"	"	"	0	0	0	0	0	.0001
(24)	$\Delta\alpha_7 = .1°$ $\Delta\alpha_8 = -.1°$							4.9992	-12.3347	4.9992	-4.3295	4.9992	-1.6456
	(24) - (1)							-.0002	- .0001	-.0001	.0001	-.0001	.0002
(25)	$\Delta\alpha_7 = 1.0°$ $\Delta\alpha_8 = -1.0°$							4.9973	-12.3426	4.9985	-4.3309	4.9990	-1.6449
	(25) - (1)							-.0021	- .0080	-.0008	- .0013	-.0003	.0009

Note: All dimensions are in mm except as noted

Table 46. Single Ray Error Analysis for Single- and Double-Pass Monochromators: $\Delta C_{7,10}$ and $\Delta\alpha_{7,8}$

	Frequency	Single-Pass Monochromator J						Double-Pass Monochromator H					
		7213.57 cm^{-1}		7232.12 cm^{-1}		7238.54 cm^{-1}		7213.57 cm^{-1}		7232.12 cm^{-1}		7238.54 cm^{-1}	
	Error Description	Y_7	Z_7	Y_7	Z_7	Y_7	Z_7	Y_{14}	Z_{14}	Y_{14}	Z_{14}	Y_{14}	Z_{14}
(1)	Zero Error							4.9994	-12.3346	4.9993	-4.3296	4.9993	-1.6458
(26)	$\Delta\alpha_7$ = .01° $\Delta\alpha_9$ = -.01°	Do Not Apply	Do Not Apply	Do Not Apply	Do Not Apply	Do Not Apply	Do Not Apply	4.9994	-12.3346	4.9993	-4.3296	4.9993	-1.6458
	(26) - (1)							0	0	0	0	0	0
(27)	$\Delta\alpha_7$ = .1° $\Delta\alpha_9$ = -.1°							4.9994	-12.3346	4.9993	-4.3296	4.9993	-1.6458
	(27) - (1)	"	"	"	"	"	"	0	0	0	0	0	0
(28)	$\Delta\alpha_7$ = 1.0° $\Delta\alpha_9$ = -1.0°							4.9994	-12.3346	4.9993	-4.3296	4.9993	-1.6458
	(28) - (1)							0	0	0	0	0	0
(29)	$\Delta\beta_7$ = .01° $\Delta\beta_8$ = -.01°							4.9975	-12.3358	4.9983	-4.3308	4.9986	-1.6470
	(29) - (1)	"	"	"	"	"	"	-.0019	- .0012	-.0010	- .0012	-.0007	- .0012
(30)	$\Delta\beta_7$ = .1° $\Delta\beta_8$ = -.1°							4.9799	-12.3469	4.9890	-4.3419	4.9923	-1.6580
	(30) - (1)							-.0195	- .0123	-.0103	- .0123	-.0070	- .0122
(31)	$\Delta\beta_7$ = 1.0° $\Delta\beta_8$ = -1.0°							4.8042	-12.4565	4.8969	-4.4513	4.9292	-1.7675
	(31) - (1)							-.1952	- .1219	-.1024	- .1217	-.0701	- .1217

Note: All dimensions are in mm except as noted

Table 47. Single Ray Error Analysis for Single- and Double-Pass Monochromators: $\Delta\alpha_{7,9}$ and $\Delta\beta_{7,8}$

	Frequency	Single-Pass Monochromator J						Double-Pass Monochromator H					
		7213.57 cm^{-1}		7232.12 cm^{-1}		7238.54 cm^{-1}		7213.57 cm^{-1}		7232.12 cm^{-1}		7238.54 cm^{-1}	
	Error Description	Y_7	Z_7	Y_7	Z_7	Y_7	Z_7	Y_{14}	Z_{14}	Y_{14}	Z_{14}	Y_{14}	Z_{14}
(1)	Zero Error	-4.9988	-8.0045	-4.9987	-4.1017	-4.9986	-2.7718	4.9994	-12.3346	4.9993	-4.3296	4.9993	-1.6458
(32)	$\Delta\beta_7$ = .01° $\Delta\beta_9$ = -.01°	Do Not Apply	Do Not Apply	Do Not Apply	Do Not Apply	Do Not Apply	Do Not Apply	4.9995	-12.3346	4.9993	-4.3296	4.9993	-1.6458
	(32) - (1)							.0001	0	0	0	0	0
(33)	$\Delta\beta_7$ = .1° $\Delta\beta_9$ = -.1°							4.9997	-12.3345	4.9992	-4.3295	4.9991	-1.6457
	(33) - (1)							.0003	.0001	-.0001	.0001	-.0002	.0001
(34)	$\Delta\beta_7$ = 1.0° $\Delta\beta_9$ = -1.0°	"	"	"	"	"	"	5.0032	-12.3339	4.9997	-4.3291	4.9992	-1.6454
	(34) - (1)							.0038	.0007	.0004	.0005	-.0001	.0004
(35)	ΔY_o = .01	-5.0088	-8.0049	-5.0086	-4.1020	-5.0086	-2.7721	5.0094	-12.3352	5.0093	-4.3302	5.0093	-1.6464
	(35) - (1)	- .0100	- .0004	- .0099	- .0003	- .0100	- .0003	.0100	- .0006	.0100	- .0006	.0100	- .0006
(36)	ΔY_o = .1	-5.0988	-8.0076	-5.0986	-4.1047	-5.0986	-2.7748	5.0994	-12.3410	5.0993	-4.3357	5.0992	-1.6518
	(36) - (1)	- .1000	- .0031	- .0999	- .0040	- .1000	- .0030	.1000	- .0064	.1000	- .0061	.0999	- .0060
(37)	ΔY_o = 1.0	-5.9986	-8.0380	-5.9983	-4.1347	-5.9983	-2.8047	5.9992	-12.4041	5.9990	-4.3965	5.9990	-1.7119
	(37) - (1)	- .9998	- .0335	- .9996	- .0330	- .9997	- .0329	.9998	- .0695	.9997	- .0669	.9997	- .0661

Note: All dimensions are in mm except as noted

Table 48. Single Ray Error Analysis for Single and Double Monochromators: $\Delta\beta_{7,9}$ and ΔY_o

	Frequency	Single-Pass Monochromator J						Double-Pass Monochromator H					
		7213.57 cm^{-1}		7232.12 cm^{-1}		7238.54 cm^{-1}		7213.57 cm^{-1}		7232.12 cm^{-1}		7238.54 cm^{-1}	
	Error Description	Y_7	Z_7	Y_7	Z_7	Y_7	Z_7	Y_{14}	Z_{14}	Y_{14}	Z_{14}	Y_{14}	Z_{14}
(1)	Zero Error	-4.9988	-8.0045	-4.9987	-4.1017	-4.9986	-2.7718	4.9994	-12.3346	4.9993	-4.3296	4.9993	-1.6458
(38)	ΔZ_o = .01	-4.9988	-8.0149	-4.9987	-4.1119	-4.9986	-2.7820	4.9994	-12.3456	4.9993	-4.3401	4.9993	-1.6561
	(38) - (1)	0	- .0104	0	- .0102	0	- .0102	0	- .0110	0	- .0105	0	- .0103
(39)	ΔZ_o = .1	-4.9988	-8.1082	-4.9987	-4.2041	-4.9986	-2.8738	4.9994	-12.4448	4.9993	-4.4346	4.9993	-1.7492
	(39) - (1)	0	- .1037	0	- .1024	0	- .1020	0	- .1102	0	- .1050	0	- .1034
(40)	ΔZ_o = 1.0	-4.9989	-9.0439	-4.9987	-5.1287	-4.9986	-3.7947	4.9994	-13.4429	4.9992	-5.3860	4.9992	-2.6854
	(40) - (1)	- .0001	-1.0394	0	-1.0270	0	-1.0229	0	- 1.1083	-.0001	-1.0564	-.0001	-1.0396

Note: All dimensions are in mm except as noted

Table 49. Single Ray Error Analysis for Single and Double Pass Monochromators: ΔZ_o.

Figure 9. The Nine-Ray Starting Points Used to Define the Respective Entrance Slits for Monochromators H and J.

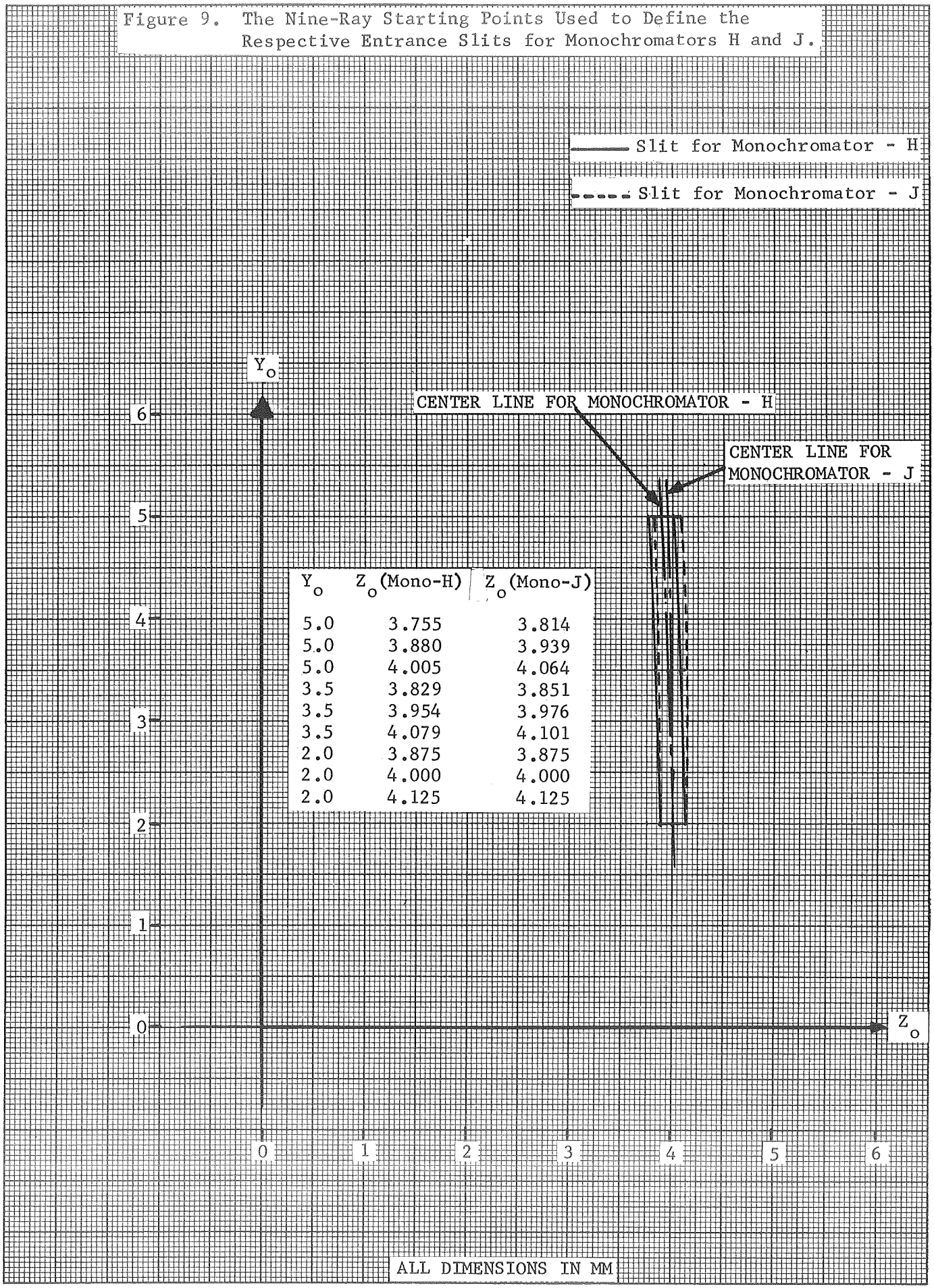

Y_o	Z_o (Mono-H)	Z_o (Mono-J)
5.0	3.755	3.814
5.0	3.880	3.939
5.0	4.005	4.064
3.5	3.829	3.851
3.5	3.954	3.976
3.5	4.079	4.101
2.0	3.875	3.875
2.0	4.000	4.000
2.0	4.125	4.125

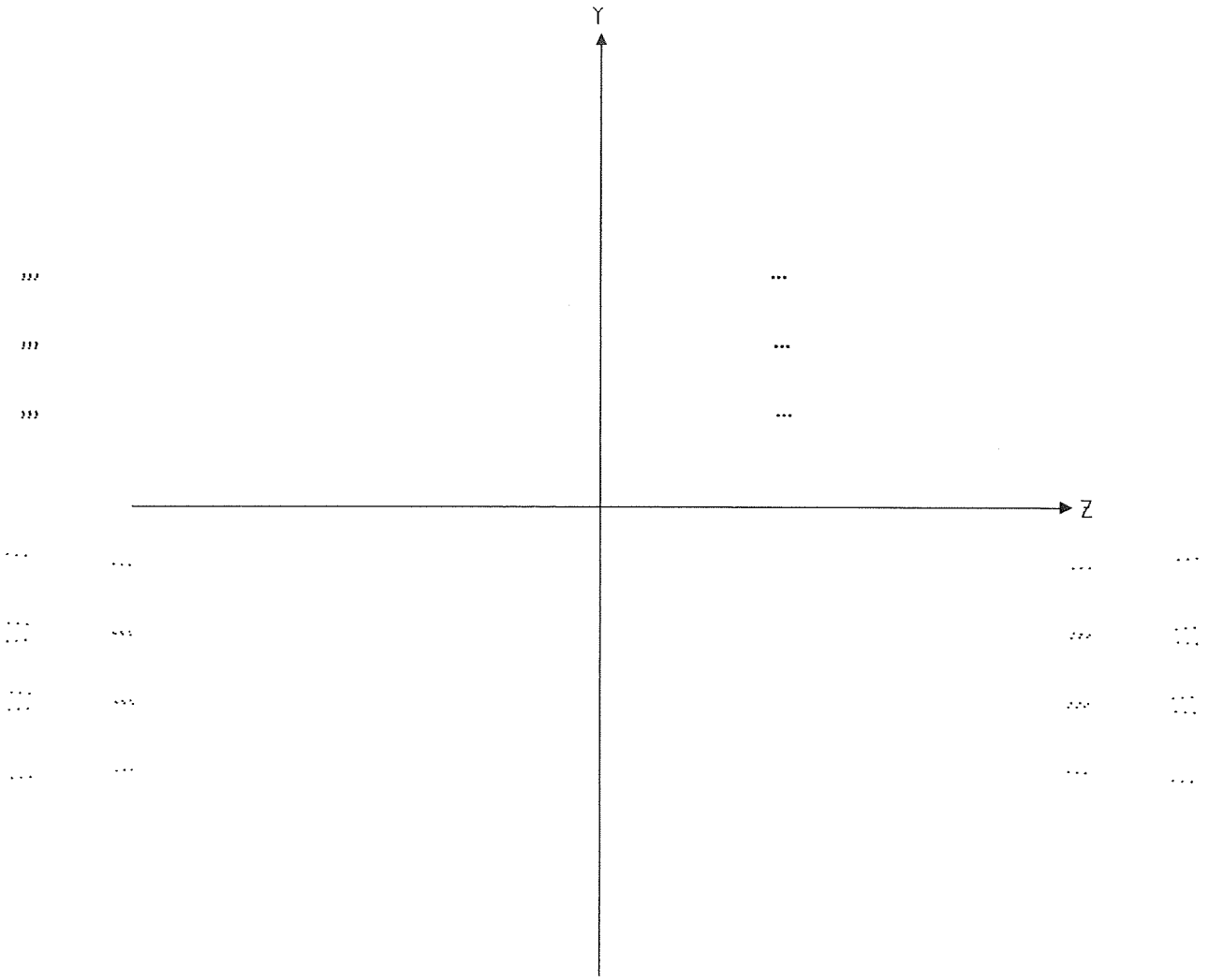

				MAX	MIN	
Z	HALF AXIS LENGTH 10.160	Z	=	12.944	-12.883	SURFACE NO.
Y	HALF AXIS LENGTH 10.160	Y	=	5.038	-5.927	1 6 7 14

Figure 10. MAWD Fixed Double-Pass Littrow Mono--F/5, 1000 mm TFL, Paraboloid--7213.57 H

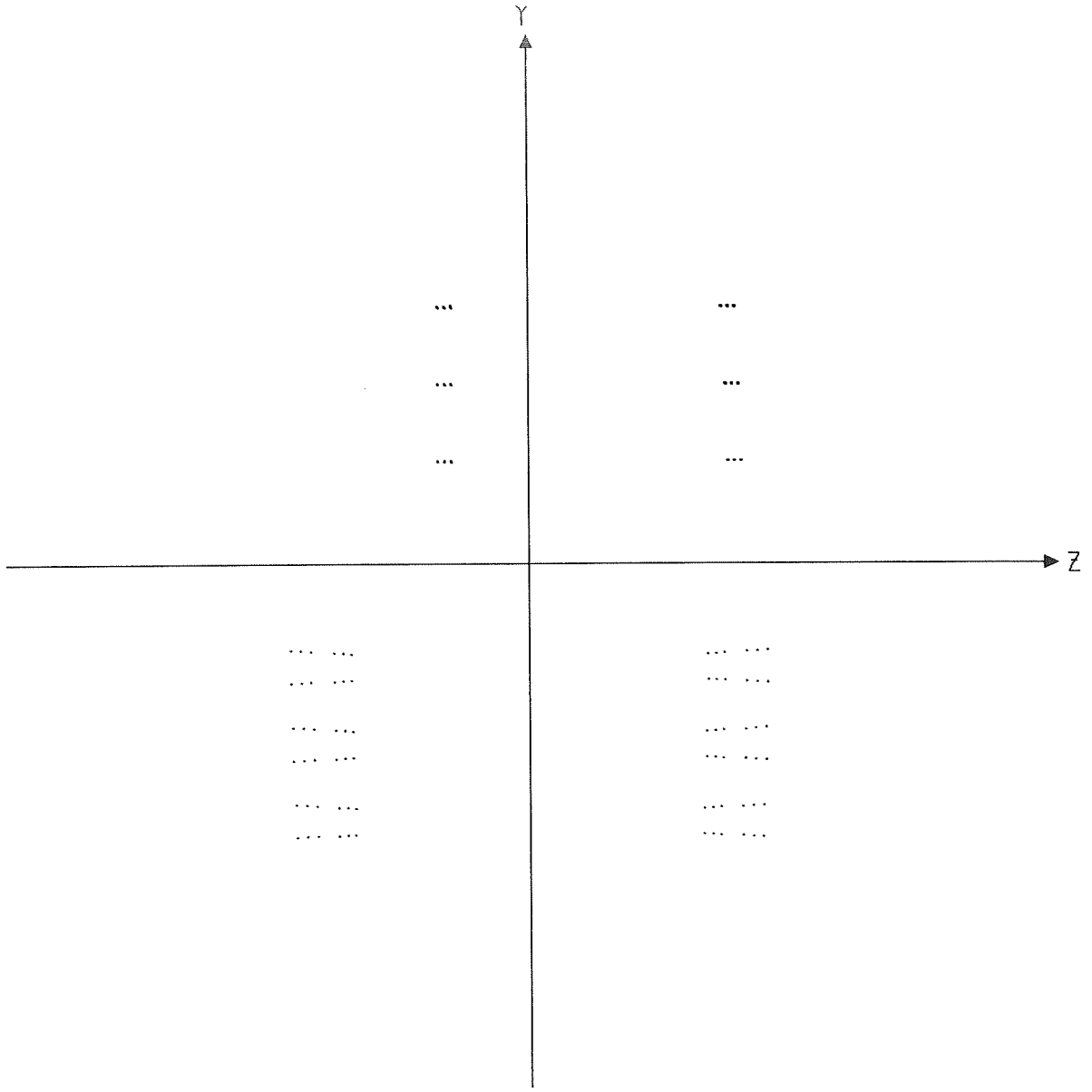

				MAX	MIN	
Z	HALF AXIS LENGTH 10.160	Z	=	4.625	-4.634	SURFACE NO.
Y	HALF AXIS LENGTH 10.160	Y	=	5.017	-5.312	1 6 7 14

Figure 11. MAWD Fixed Double-Pass Littrow Mono--F/5, 1000 mm TFL, Paraboloid--7238.54 H

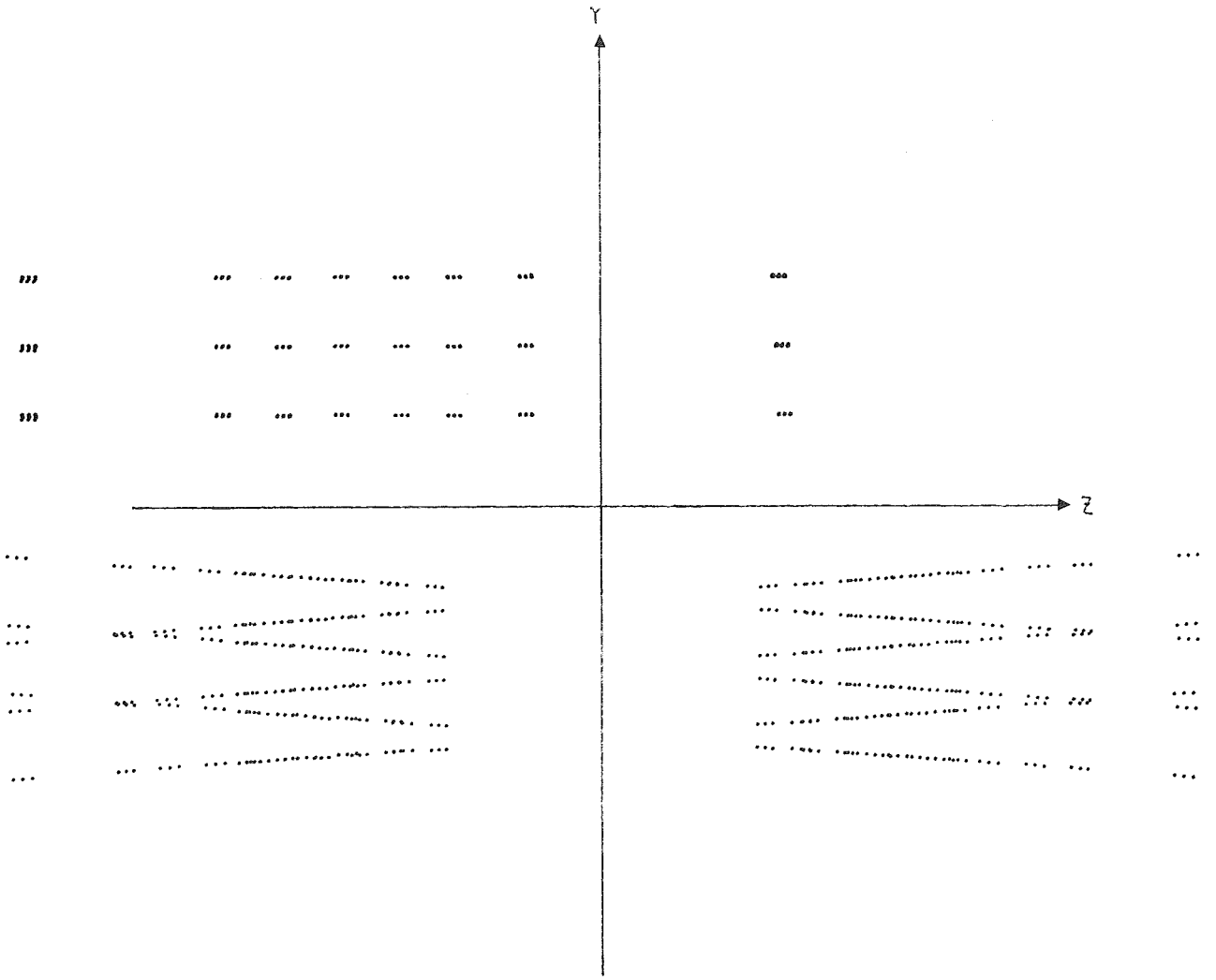

				MAX	MIN	
Z	HALF AXIS LENGTH 10.160	Z	=	12.944	-12.883	SURFACE NO.
Y	HALF AXIS LENGTH 10.160	Y	=	5.038	-5.927	1 6 7 14

Figure 12. MAWD Fixed Double-Pass Littrow Mono--F/5, 1000 mm TFL, Paraboloid--7 frequencies

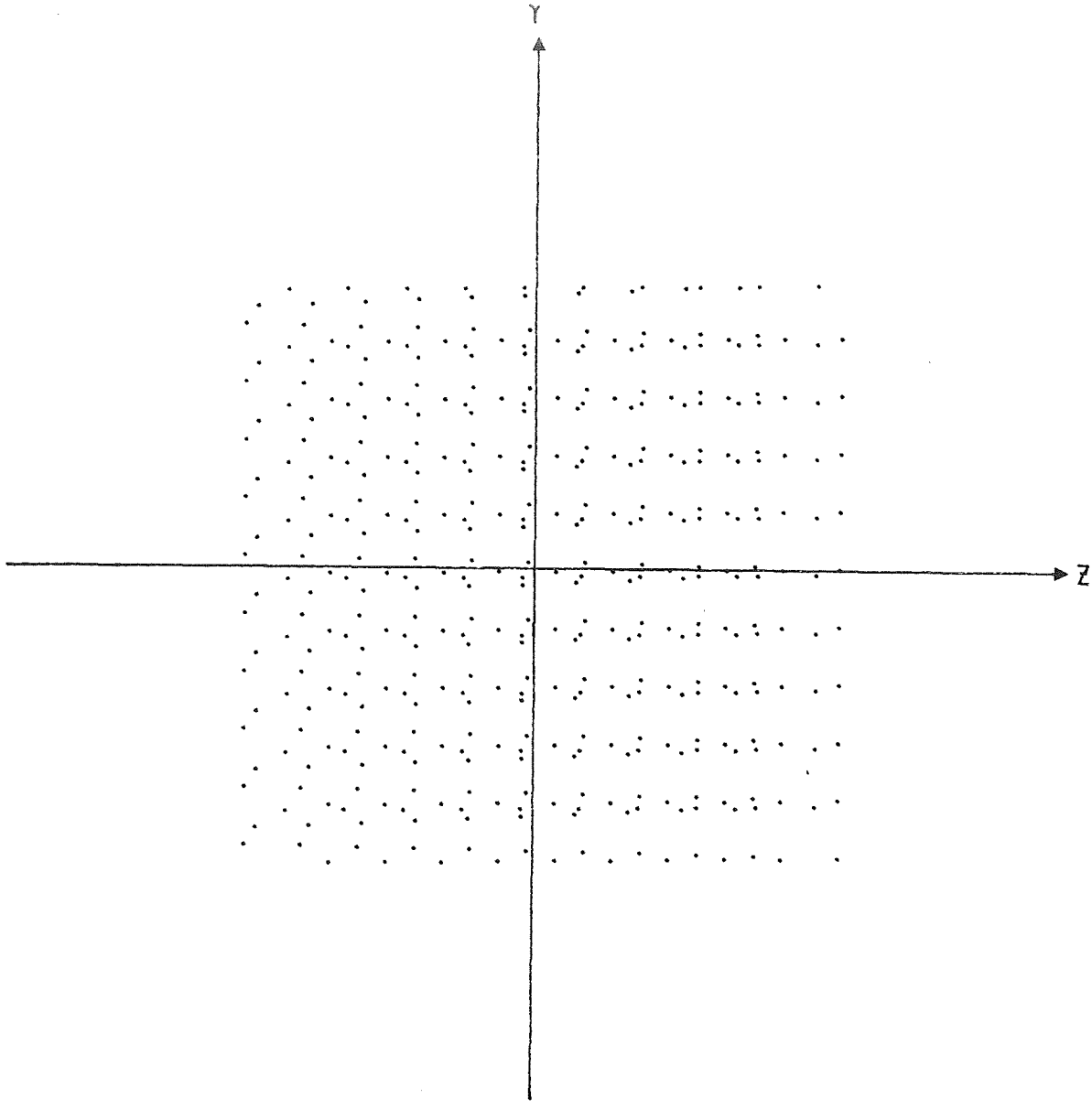

				MAX	MIN	
Z	HALF AXIS LENGTH 101.600	Z	=	58.709	-55.660	SURFACE NO.
Y	HALF AXIS LENGTH 101.600	Y	=	54.755	-56.656	2 5 9 12

Figure 13. MAWD Fixed Double-Pass Littrow Mono--F/5, 1000 mm TFL, Paraboloid--7213.57 H

inserts the grating surface into the ray trace each time the rays pass through its hole. This ray-trace axis system is called monochromator HA, and is described in Table 52, and its dimensional parameters are defined in Table 53. Figure 14 is a composite plot of the intercepts for a 100-ray family with surfaces 2, 5, 8, 13, 16, and 19. For this particular monochromator HA ray-trace 2, 8, 13, and 19 represent the one hundred rays passing through the grating face and surfaces 5 and 16 represent the rays filling the full grating face. Any holes cut through the grating must, of course, include the four groups of one hundred ray points which represent surfaces 2, 8, 13, and 19.

Figure 15 is Figure 14 with an ellipsoidal ring of points and a second axis system superimposed. This elliptical ring of points represents the projection on the grating face of a 45-mm-diameter hole cut through the grating parallel to the monochromator axis, X_1-axis. The X-axis of this bored hole is located at Z_5= -10.0 mm, wherein the grating face is in the (X_5, Y_5, Z_5) axis system.

Figure 16 shows a family of computer-generated holes for the grating. Each elliptical ring is the intercept of 40 equally-spaced rays, forming a cylinder about the X_1-axis, of the monochromator. Figure 16 shows bored holes through the grating having 38-mm through 60-mm diameters.

Figure 17 shows the required hole size and location in the collimating mirror. This hole dimension was developed by ray-tracing those rays which started from two entrance-slit starting points (Y_o = 2.0, Z_o = 4.0) and (Y_o = 5.0, Z_o = 3.88), and intercept the 45-mm-diameter bored hole through the grating shown in Figure 16. The intercepts of these rays with the collimating mirror determine this hole size. Figure 17 is given in terms of the monochromator H axis system.

	Frequency	Single Pass Monochromator J						Double Pass Monochromator H					
		7213.57 cm^{-1}		7232.12 cm^{-1}		7238.54 cm^{-1}		7213.57 cm^{-1}		7232.12 cm^{-1}		7238.54 cm^{-1}	
	Error Description	A_7	Z_7	A_7	Z_7	A_7	Z_7	A_{14}	Z_{14}	A_{14}	Z_{14}	A_{14}	Z_{14}
1	Zero Error	-.2191	-8.0302	-.1998	-4.1001	-.1963	-2.7606	-.2743	-12.3794	-.1790	-4.3263	-.1632	-1.6243
2	$\Delta A_{2,10}$ = .01 $\Delta A_{6,14}$ = -.01	-.1984	-8.0302	-.1793	-4.1001	-.1759	-2.7606	-.2296	-12.3791	-.1370	-4.3261	-.1221	-1.6242
	2 - 1	.0207	0	.0205	0	.0204	0	.0447	.0003	.0420	.0002	.0411	.0001
3	$\Delta A_{2,10}$ = .1 $\Delta A_{6,14}$ = -.1	-.0118	-8.0298	.0050	-4.0998	.0076	-2.7604	.1721	-12.3763	.2411	-4.3249	.2485	-1.6235
	3 - 1	.2073	.0004	.2048	.0003	.2039	.0002	.4464	.0031	.4201	.0014	.4117	.0008
4	$\Delta A_{2,10}$ = 1.0 $\Delta A_{6,14}$ = -1.0	1.8530	-8.0255	1.8473	-4.0970	1.8426	-2.7581	4.1815	-12.3492	4.0145	-4.3139	3.9474	-1.6174
	4 - 1	2.0721	.0047	2.0471	.0031	2.0389	.0025	4.4558	.0302	4.1935	.0124	4.1106	.0069
5	ΔA_6 = .01 ΔA_{10} = -.01	Do Not Apply	Do Not Apply	Do Not Apply	Do Not Apply	Do Not Apply	Do Not Apply	-.2517	-12.3792	-.1580	-4.3262	-.1427	-1.6243
	5 - 1							.0226	.0002	.0210	.0001	.0205	0
6	ΔA_6 = .1 ΔA_{10} = -.1	"	"	"	"	"	"	-.0489	-12.3777	.0310	-4.3256	.0418	-1.6240
	6 - 1							.2254	.0017	.2100	.0007	.2050	.0003
7	ΔA_6 = 1.0 ΔA_{10} = -1.0	"	"	"	"	"	"	1.9767	-12.3629	1.9180	-4.3201	1.8849	-1.6213
	7 - 1							2.2510	.0165	2.0970	.0062	2.0481	.0040

Note: All dimensions are in mm except as noted

Table 50. Two-Ray Error Analysis for Single- and Double-Pass Monochromators: $\Delta A_{2,6,10,14}$ and $\Delta A_{6,10}$

	Frequency	Single Pass Monochromator J						Double Pass Monochromator H					
		7213.57 cm^{-1}		7232.12 cm^{-1}		7238.54 cm^{-1}		7213.57 cm^{-1}		7232.12 cm^{-1}		7238.54 cm^{-1}	
	Error Description	A_7	Z_7	A_7	Z_7	A_7	Z_7	A_{14}	Z_{14}	A_{14}	Z_{14}	A_{14}	Z_{14}
1	Zero Error	- .2191	-8.0302	- .1998	-4.1001	- .1963	-2.7606	- .2743	-12.3794	- .1790	-4.3263	- .1632	-1.6243
8	$\Delta R_{2,5,10,13}$= .01	- .2295	-8.0303	- .2100	-4.1001	- .2065	-2.7606	- .2966	-12.3796	- .2000	-4.3263	- .1838	-1.6243
	8 - 1	- .0104	- .0001	- .0102	0	- .0102	0	- .0223	- .0002	- .0210	0	- .0206	0
9	$\Delta R_{2,5,10,13}$= .1	- .3227	-8.0309	- .3022	-4.1002	- .2983	-2.7606	- .4974	-12.3817	- .3891	-4.3269	- .3692	-1.6244
	9 - 1	- .1036	- .0007	- .1024	- .0001	- .1020	0	- .2231	- .0023	- .2101	- .0006	- .2060	- .0001
10	$\Delta R_{2,5,10,13}$=1.0	-1.2555	-8.0365	-1.2238	-4.1017	-1.2162	-2.7606	-2.5076	-12.4031	-2.2813	-4.3332	-2.2241	-1.6258
	10 - 1	-1.0364	- .0063	-1.0240	- .0016	-1.0199	0	-2.2333	- .0237	-2.1023	- .0069	-2.0609	- .0015
11	ΔX_o = .01	- .2298	-8.0303	- .2103	-4.1001	- .2067	-2.7607	- .2864	-12.3796	- .1900	-4.3264	- .1739	-1.6244
	11 - 1	- .0107	- .0001	- .0105	0	- .0104	- .0001	- .0121	- .0002	- .0110	- .0001	- .0107	- .0001
12	ΔX_o = .1	- .3264	-8.0308	- .3046	-4.1005	- .3003	-2.7609	- .3954	-12.3810	- .2892	-4.3271	- .2700	-1.6249
	12 - 1	- .1073	- .0006	- .1048	- .0004	- .1040	- .0003	- .1211	- .0016	- .1102	- .0008	- .1068	- .0006
13	ΔX_o = 1.0	-1.2930	-8.0358	-1.2487	-4.1040	-1.2370	-2.7640	-1.4872	-12.3952	-1.2827	-4.3345	-1.2328	-1.6302
	13 - 1	-1.0739	- .0056	-1.0489	- .0039	-1.0407	- .0034	-1.2129	- .0158	-1.1037	- .0082	-1.0696	- .0049

Note: All dimensions are in mm except as noted

Table 51. Two-Ray Error Analysis for Single- and Double-Pass Monochromators: $\Delta R_{2,5,10,13}$ and ΔX_o

(X_o,Y_o,Z_o)	Entrance Slit--The entrance slit lies in the Y_o-Z_o plane, and each family of rays used to ray-trace the monochromator starts from a point on the entrance slit.
(X_1,Y_1,Z_1)	Mathematical Axis System.
(X_4,Y_4,Z_4) (X_7,Y_7,Z_7) (X_{15},Y_{15},Z_{15}) (X_{18},Y_{18},Z_{18})	Paraboloid Collimating Mirror--These four axis systems are identical and may be referred to as the $(X_{4,7,15,18}, Y_{4,7,15,18}, Z_{4,7,15,18})$ axis system. The apex of this paraboloidal reflecting surface is at the origin of the $(X_{4,7,15,18}, Y_{4,7,15,18}, Z_{4,7,15,18})$ axis system, and the focus of the paraboloid is located on the negative $X_{4,7,15,18}$-axis.
(X_2,Y_2,Z_2) (X_5,Y_5,Z_5) (X_8,Y_8,Z_8) (X_{13},Y_{13},Z_{13}) (X_{16},Y_{16},Z_{16}) (X_{19},Y_{19},Z_{19})	Diffraction Grating--These six axis systems are identical and may be referred to as the $(X_{2,5,8,13,16,19}, Y_{2,5,8,13,16,19}, Z_{2,5,8,13,16,19})$ axis system. The ruled area of the grating is in the $Y_{2,5,8,13,16,19}$-$Z_{2,5,8,13,16,19}$ plane, and the grating rulings are parallel to the $Y_{2,5,8,13,16,19}$-axis.
(X_3,Y_3,Z_3) (X_6,Y_6,Z_6) (X_9,Y_9,Z_9) (X_{14},Y_{14},Z_{14}) (X_{17},Y_{17},Z_{17}) (X_{20},Y_{20},Z_{20})	Mathematical Axis Systems--These six axis systems are identical and may be referred to as the $(X_{3,6,9,14,17,20}, Y_{3,6,9,14,17,20}, Z_{3,6,9,14,17,20})$ axis system.
(X_{10},Y_{10},Z_{10})	First surface of Corner Mirror--This is a plane-reflecting surface in the Y_{10}-Z_{10} plane.
(X_{11},Y_{11},Z_{11})	Second Surface of Corner Mirror--This is a plane-reflecting surface in the Y_{11}-Z_{11} plane.

Table 52 (Sheet 1 of 2). Description of Special Ray-Trace Axis Systems Used to Define the Hole Size in the Grating for the Double-Pass Monochromator, HA

(X_{12},Y_{12},Z_{12})	Mathematical Axis System.
(X_{21},Y_{21},Z_{21})	Front Face of Detector Cover Glass--This is a refracting surface in the Y_{21}-Z_{21} plane.
(X_{22},Y_{22},Z_{22})	Spectral Image Surface--The spectral images for the ray starting points on the entrance slit are formed on the Y_{22}-Z_{22} plane.

Table 52 (Sheet 2 of 2). Description of Special Ray-Trace Axis Systems Used to Define the Hole Size in the Grating for the Double-Pass Monochromator, HA

Axis Sub-Script (n)	A_n (mm)	B_n (mm)	C_n (mm)	α_n (deg)	β_n (deg)	γ_n (deg)	Surface Shape	Optical Function of Surface	D_n (mm)	E_n (mm)	F_n (mm)	R_n (mm)	N_n
1					-1.160		Plane	Transmit					1.0000
2	90.000			56.055			Plane	Transmit					1.0000
3				-56.055			Plane	Transmit					1.0000
4	410.000						Paraboloid	Reflect	1.000	1.000		-1000.000	1.0000
5	-410.000			56.055			Plane	Diffract					1.0000
6				-56.055			Plane	Transmit					1.0000
7	410.000						Paraboloid	Reflect	1.000	1.000		-1000.000	1.0000
8	-410.000			56.055			Plane	Transmit					1.0000
9				-56.055			Plane	Transmit					1.0000
10	- 89.918			45.000			Plane	Reflect					1.0000
11				-90.000			Plane	Reflect					1.0000
12				45.000			Plane	Transmit					1.0000
13	89.918			56.055			Plane	Transmit					1.0000
14				-56.055			Plane	Transmit					1.0000
15	410.000						Paraboloid	Reflect	1.000	1.000		-1000.000	1.0000
16	-410.000			56.055			Plane	Diffract					1.0000
17				-56.055			Plane	Transmit					1.0000
18	410.000						Paraboloid	Reflect	1.000	1.000		-1000.000	1.0000
19	-410.000			56.055			Plane	Transmit					1.0000
20				-56.055			Plane	Transmit					1.0000
21	- 90.000						Plane	Transmit					1.4560
22	- .250						Plane	Transmit					1.0000

NOTE: All dimensions are in mm except as noted.

Table 53. Dimensional Parameters for MAWD Monochromator, HA

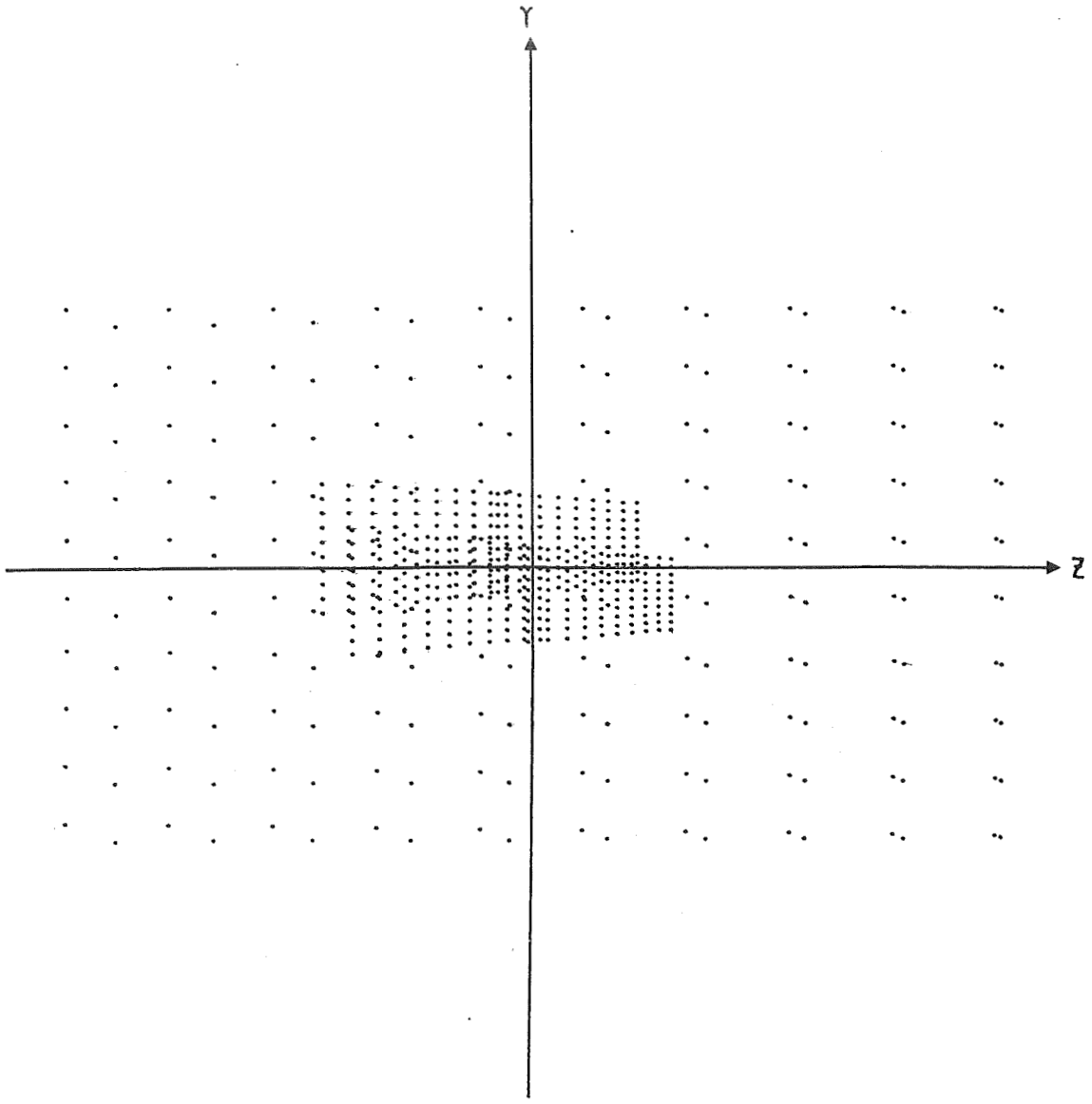

Z HALF AXIS LENGTH 101.600
Y HALF AXIS LENGTH 101.600

SURFACE NO.
2 5 8 131619

Figure 14. MAWD Fixed Double-Pass Littrow Mono--F/5, 1000 mm TFL, Paraboloid--7213.57 H_A

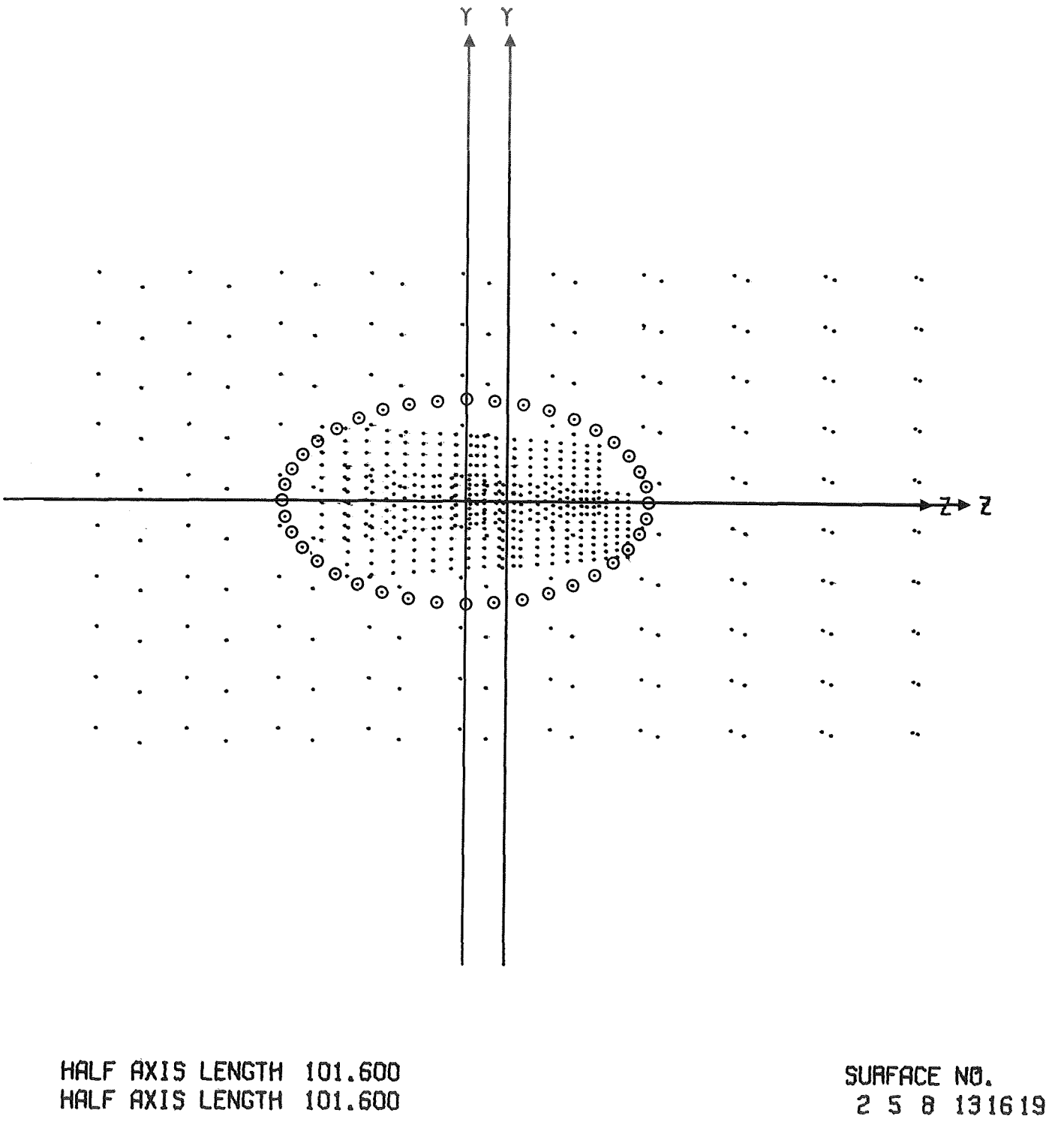

Figure 15. MAWD Grating Hole Size and Location for Double-Pass Monochromator H_A

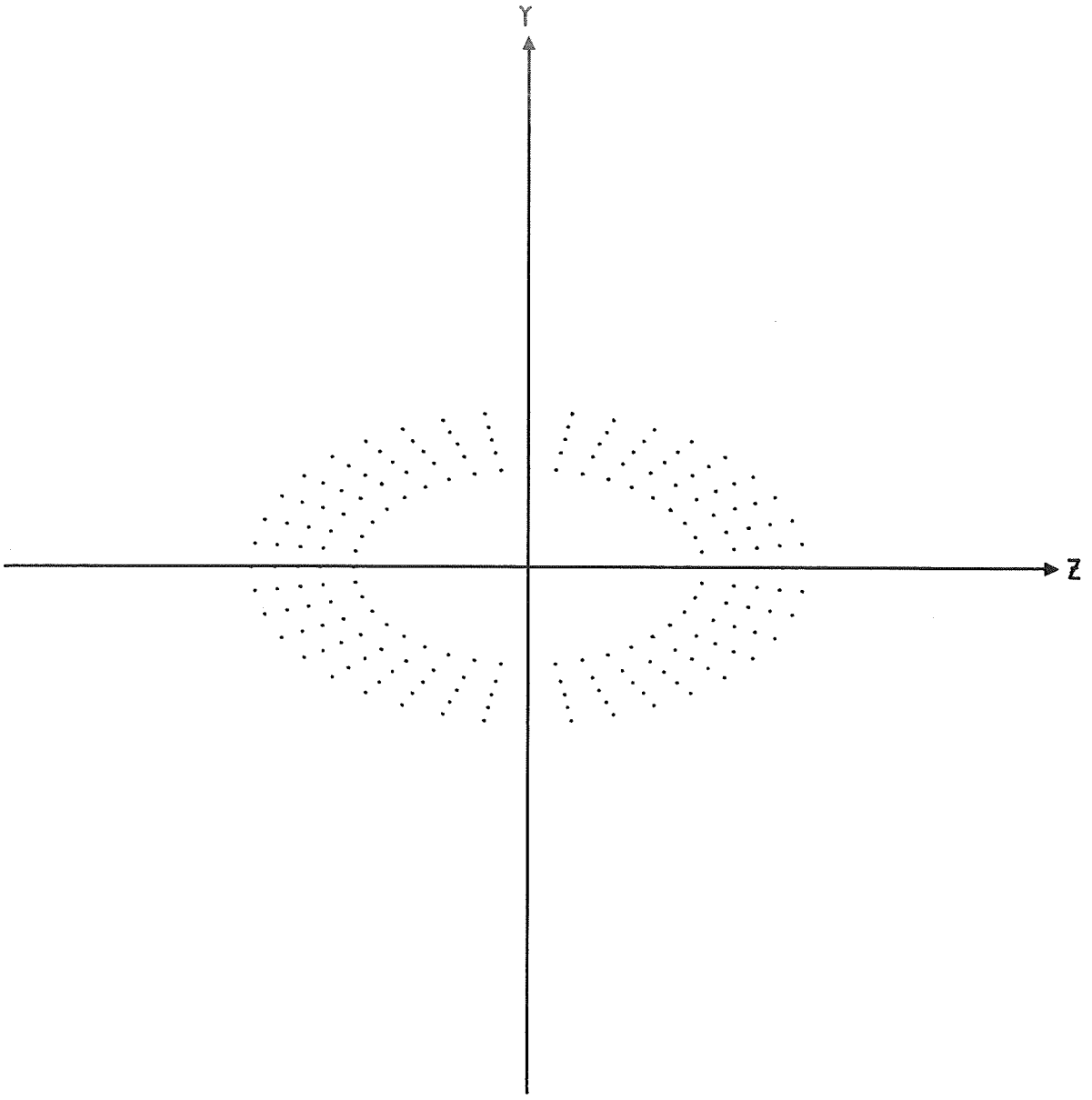

Z HALF AXIS LENGTH 101.600
Y HALF AXIS LENGTH 101.600

SURFACE NO.
1.

Figure 16. MAWD Grating Hole Projection. Grating Angle--56.055 Degrees. 38,45,50, and 60 MM Dia Holes

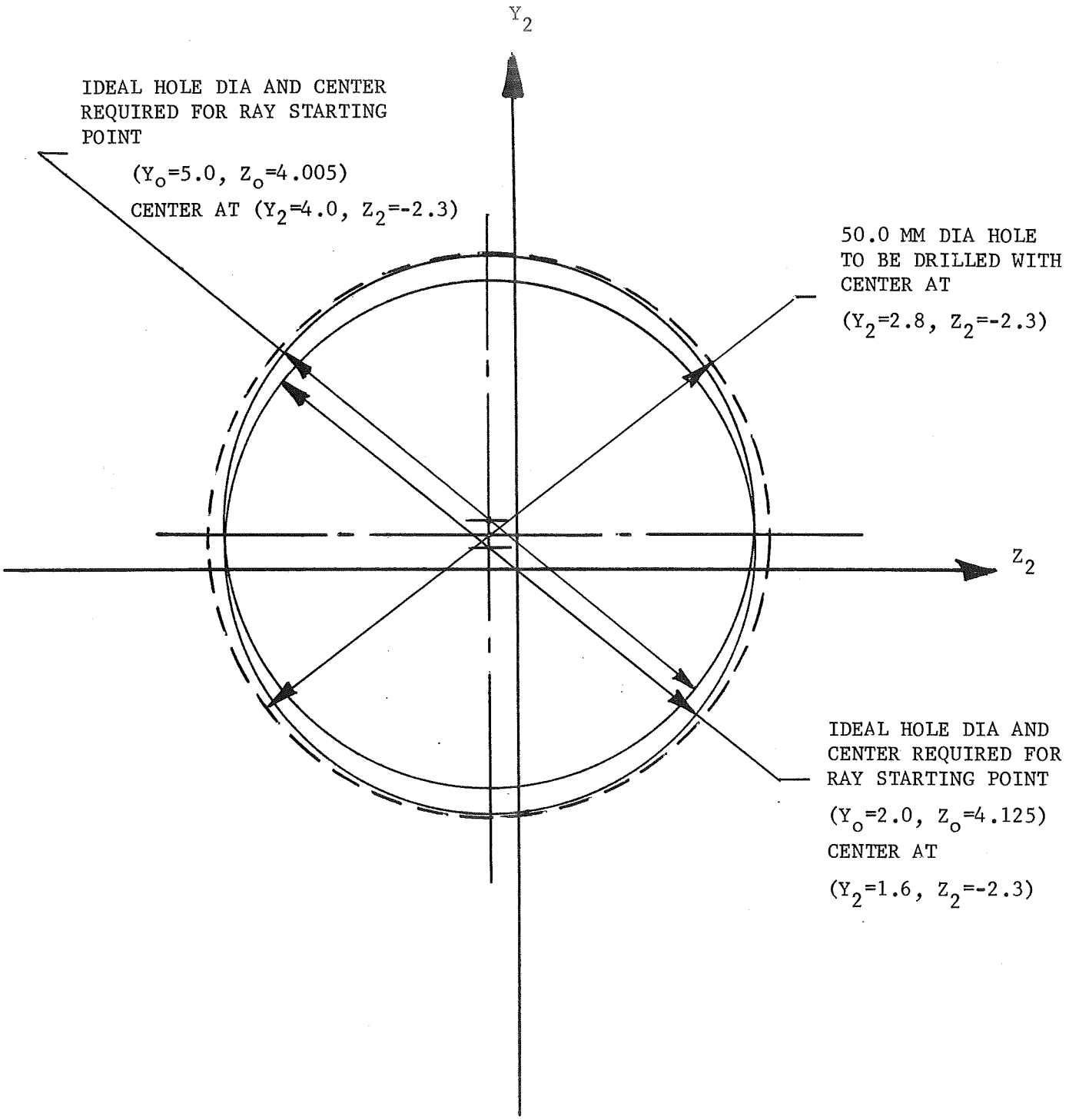

Figure 17. MAWD Collimating Mirror Hole Size and Location for Double-Pass Monochromator, H

4.0 TELESCOPE

The telescope must be reflective and have an effective focal length of roughly 125 mm. JPL requested further that several different beam deviation angles be studied for the telescope. Since the beam deviation angle affects both the image quality of the telescope as well as its compactness, three different beam deviation angles of 45°, 67.5° and 90° were eventually ray traced, and the 45° beam deviation was selected as the final design.

Figure 18 is a computer plot of the 45° telescope. Table 54 describes its axis systems and these axis systems apply as well as for the 67.5° and 90° telescopes. Table 55 gives the dimensional parameters for the 45° telescope. Figure 19 is an angular image spot diagram for the nine starting points on the monochromator H entrance slit shown in Figure 9. The one hundred ray families which are used from each of these nine starting points were used to ray trace the monochromator.

Figure 20 is a computer plot of the 67.5° telescope. Its dimensional parameters are given in Table 56, and its angular image spot diagram is given in Figure 21.

Figure 22 is a computer plot of the 90° telescope. Its dimensional parameters are given in Table 57, and its angular image spot diagram is given in Figure 23.

Figure 24 shows an angular image spot diagram for the 90° telescope when the paraboloid primary mirror is changed to a spherical mirror with a 250.0 mm radius while all other things remain unchanged.

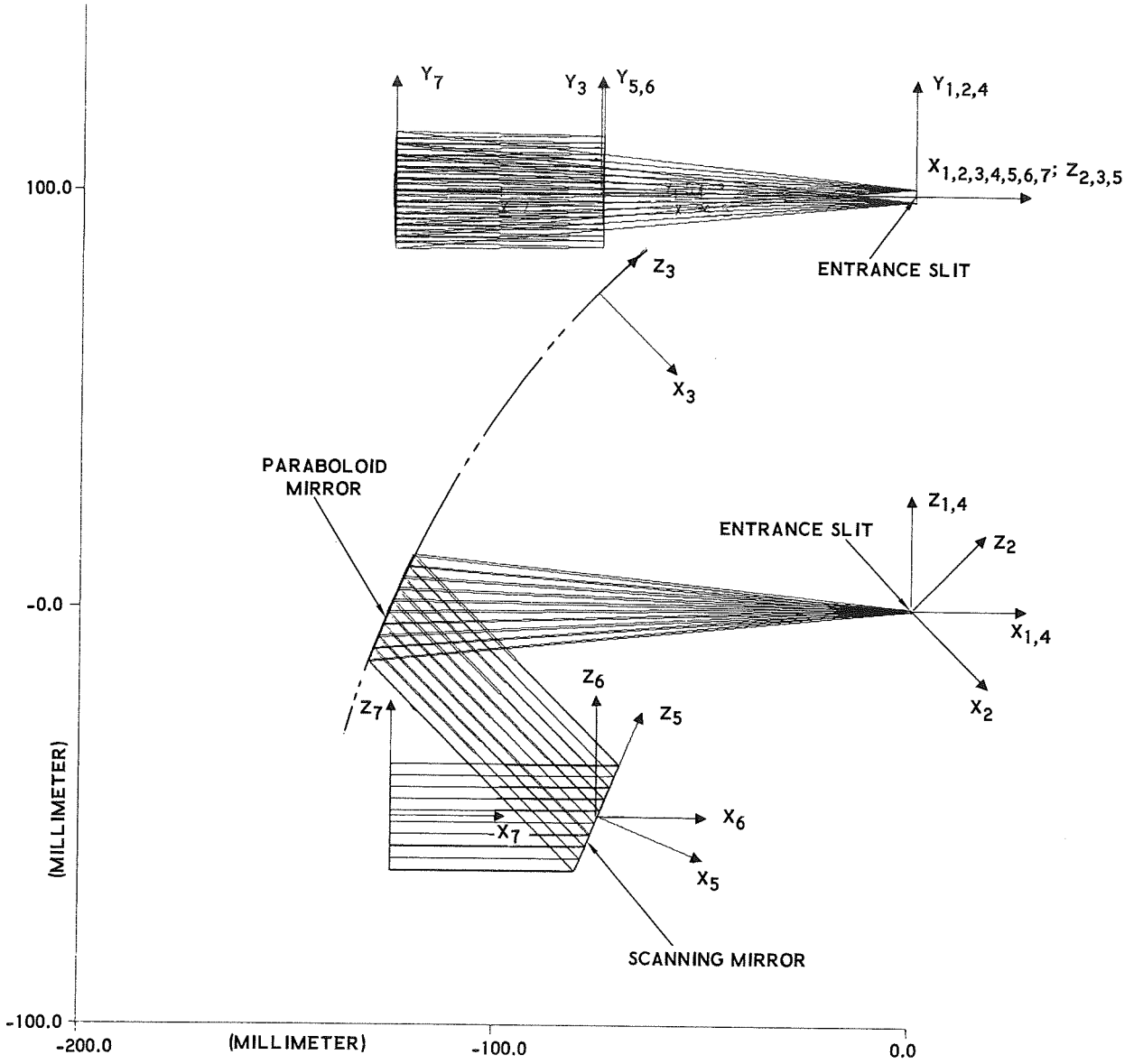

Figure 18. MAWD Telescope--45° with Paraboloid Mirror and Scan Mirror

(X_o, Y_o, Z_o)	Monochromator Entrance Slit--The monochromator entrance slit lies in the Y_o-Z_o plane, and each family of rays used to ray-trace the telescope starts from a point on the monochromator entrance slit. All rays have been traced through the telescope to object space. In this manner, the telescope is ray-traced using precisely the same ray families that are used for the monochromator.
(X_1, Y_1, Z_1)	Telescope Optical Axis--The telescope optical axis at the monochromator entrance slit is defined by the telescope's X_1-axis which is parallel to the monochromator's X_1-axis, but laterally off-set to the center of the entrance-slit area.
(X_2, Y_2, Z_2)	Mathematical Axis System.
(X_3, Y_3, Z_3)	Paraboloid Primary Mirror--This mirror has a paraboloid reflecting surface with its apex at the origin of the (X_3, Y_3, Z_3) axis system, and its focus on the positive X_3-axis.
(X_4, Y_4, Z_4)	Mathematical Axis System.
(X_5, Y_5, Z_5)	Scanning Mirror--This is a reflecting plane surface in the X_5-Z_5 plane.
(X_6, Y_6, Z_6)	Mathematical Axis System.
(X_7, Y_7, Z_7)	Image Surface--This is a plane transmitting surface in object space which is in the Y_7-Z_7 plane.

Table 54. Description of Ray-Trace Axis Systems Used for Telescopes

Axis Sub-Script (n)	A_n (mm)	B_n (mm)	C_n (mm)	α_n (deg)	β_n (deg)	γ_n (deg)	Surface Shape	Optical Function of Surface	D_n (mm)	E_n (mm)	F_n (mm)	R_n (mm)	N_n
1		3.500	3.954		-1.160		Plane	Transmit					1.0000
2				-45.000			Plane	Transmit					1.0000
3	-107.000						Paraboloid	Reflect	1.000	1.000		214.000	1.0000
4	107.000			45.000			Plane	Transmit					1.0000
5	- 75.000		-50.000	-22.500			Plane	Reflect					1.0000
6				22.500			Plane	Transmit					1.0000
7	- 50.000						Plane	Transmit					1.0000

NOTE: All dimensions are in mm except as noted.

Table 55. Dimensional Parameters for MAWD Telescope With 45° Beam Deviation

Axis Sub-Script (n)	A_n (mm)	B_n (mm)	C_n (mm)	α_n (deg)	β_n (deg)	γ_n (deg)	Surface Shape	Optical Function of Surface	D_n (mm)	E_n (mm)	F_n (mm)	R_n (mm)	N_n
1		3.500	3.954		-1.160		Plane	Transmit					1.0000
2				-67.500			Plane	Transmit					1.0000
3	- 87.500						Paraboloid	Reflect	1.000	1.000		175.000	1.0000
4	87.500			67.500			Plane	Transmit					1.0000
5	-104.810		-50.000	-33.750			Plane	Reflect					1.0000
6				33.750			Plane	Transmit					1.0000
7	- 75.000						Plane	Transmit					1.0000

NOTE: All dimensions are in mm except as noted

Table 56. Dimensional Parameters for MAWD Telescope With 67.5° Beam Deviation

Axis Sub-Script (n)	A_n (mm)	B_n (mm)	C_n (mm)	α_n (deg)	β_n (deg)	γ_n (deg)	Surface Shape	Optical Function of Surface	D_n (mm)	E_n (mm)	F_n (mm)	R_n (mm)	N_n
1		3.500	3.954		-1.160		Plane	Transmit					1.0000
2				-90.000			Plane	Transmit					1.0000
3	-62.500						Paraboloid	Reflect	1.000	1.000		125.000	1.0000
4	62.500		-125.000				Plane	Transmit					1.0000
5	50.000			45.000			Plane	Reflect					1.0000
6				45.000			Plane	Transmit					1.0000
7	-50.000						Plane	Transmit					1.0000

NOTE: All dimensions are in mm except as noted

Table 57. Dimensional Parameters for MAWD Telescope With 90° Beam Deviation

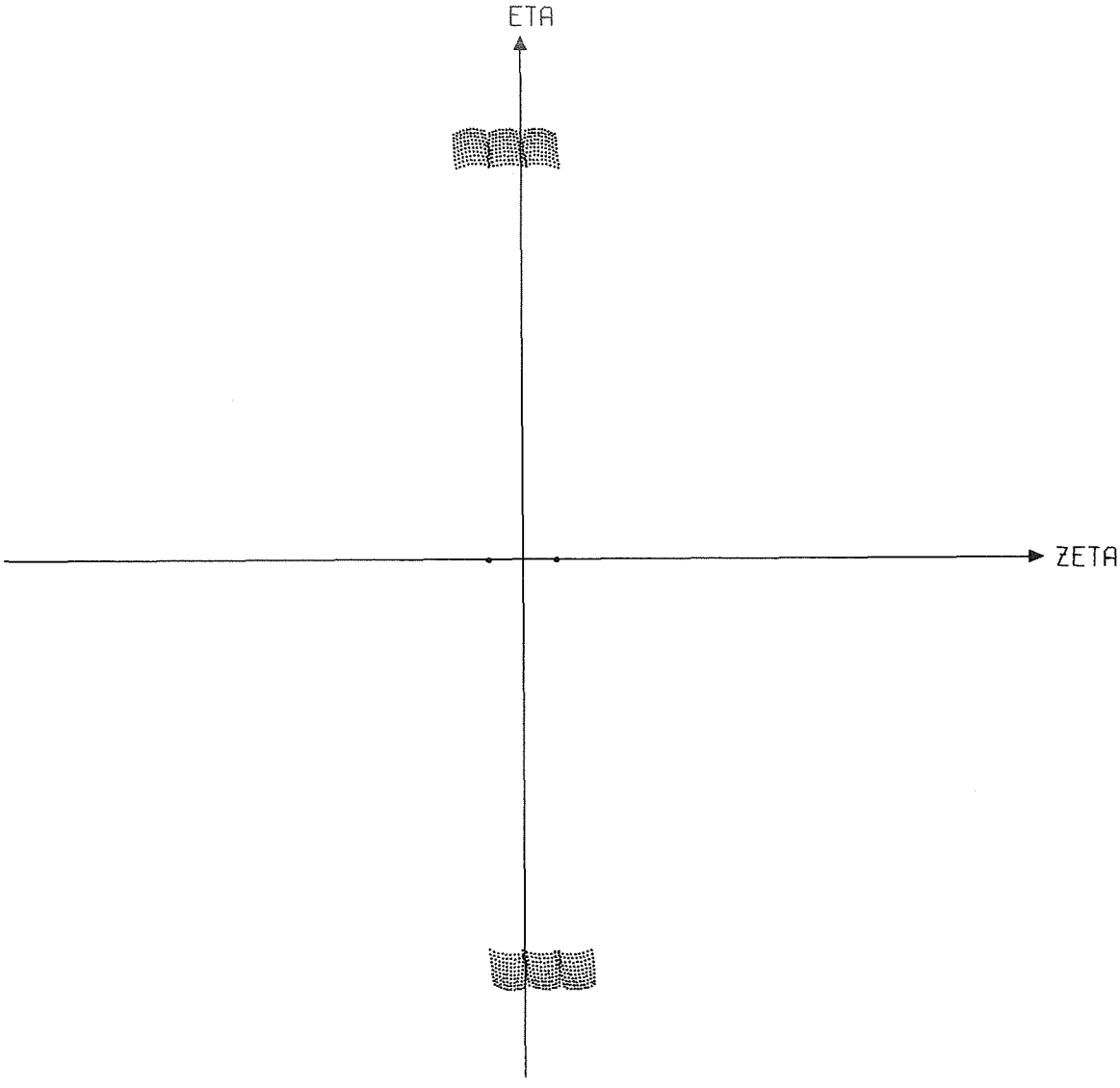

					MAX	MIN	
ZETA	HALF AXIS LENGTH	0.015	ZETA	=	0.002	-0.002	SURFACE NO.
ETA	HALF AXIS LENGTH	0.015	ETA	=	0.012	-0.012	3

Figure 19. MAWD Telescope--45-Degree with Paraboloid Mirror

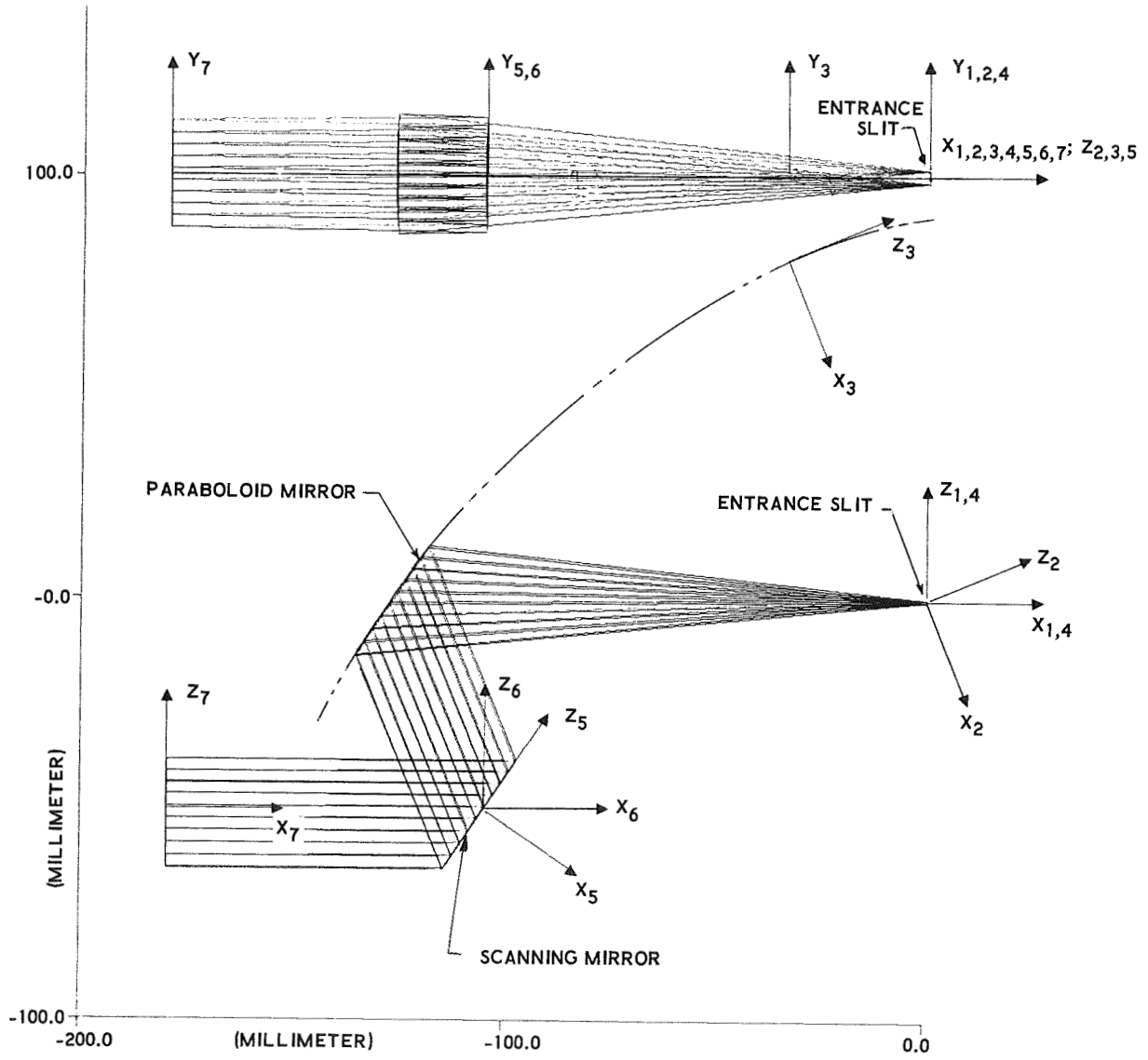

Figure 20. MAWD Telescope--67.50° with Paraboloid Mirror and Scan Mirror

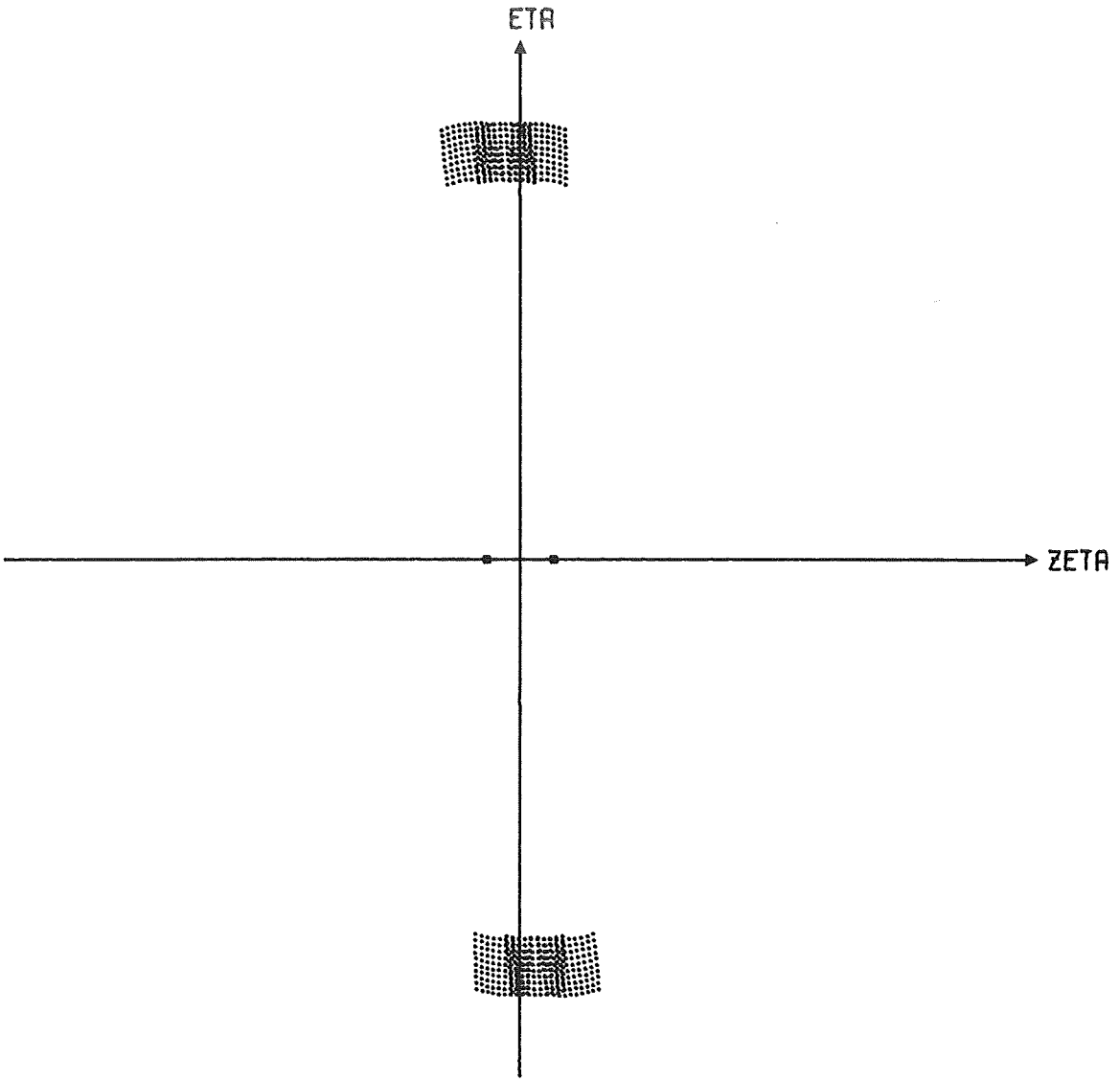

					MAX	MIN	
ZETA	HALF AXIS LENGTH	0.015	ZETA	=	0.002	-0.002	SURFACE NO.
ETA	HALF AXIS LENGTH	0.015	ETA	=	0.013	-0.013	3

Figure 21. MAWD Telescope--67.5-Degree with Paraboloid Mirror

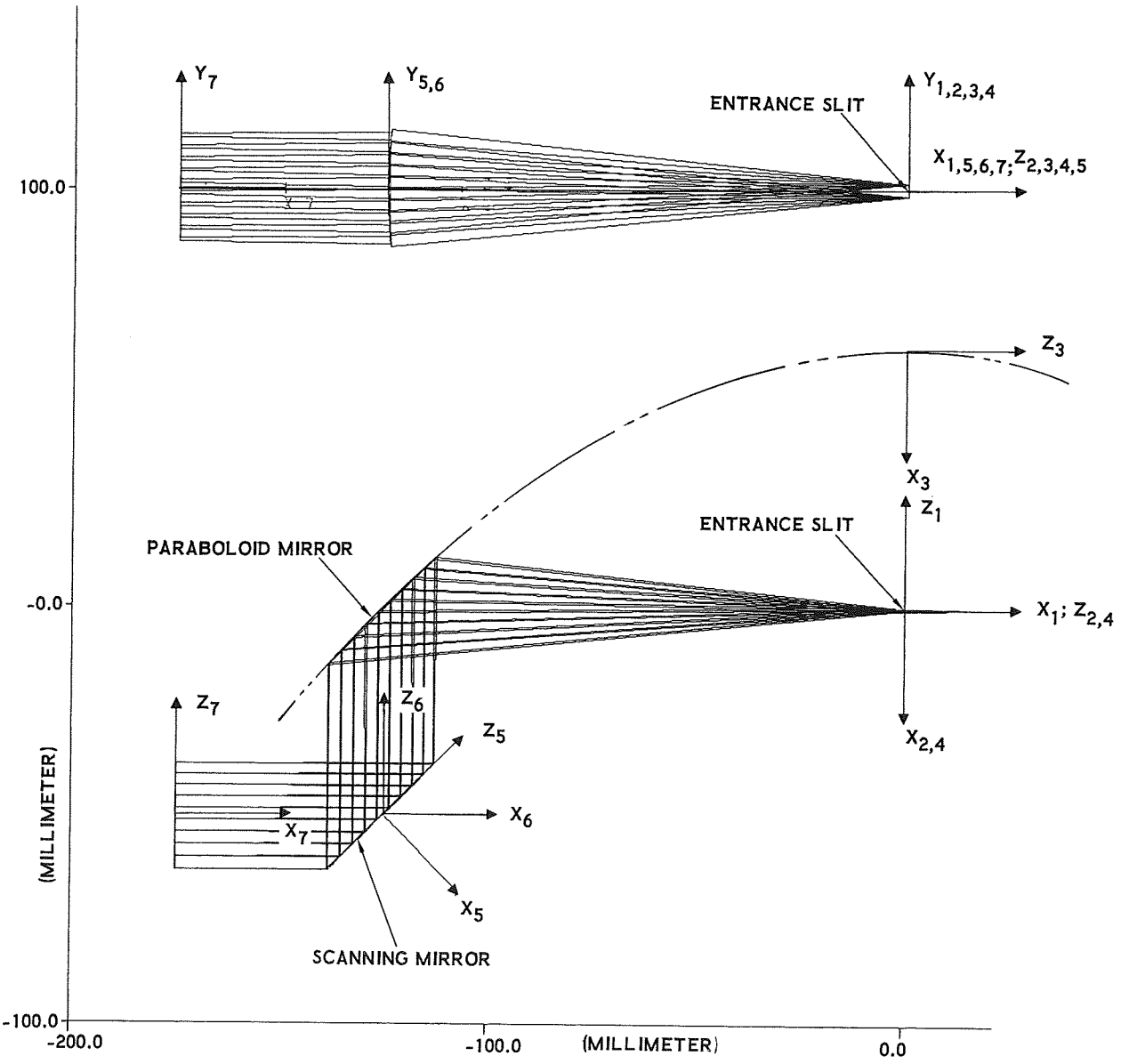

Figure 22. MAWD Telescope--90° with Paraboloid Mirror and Scan Mirror

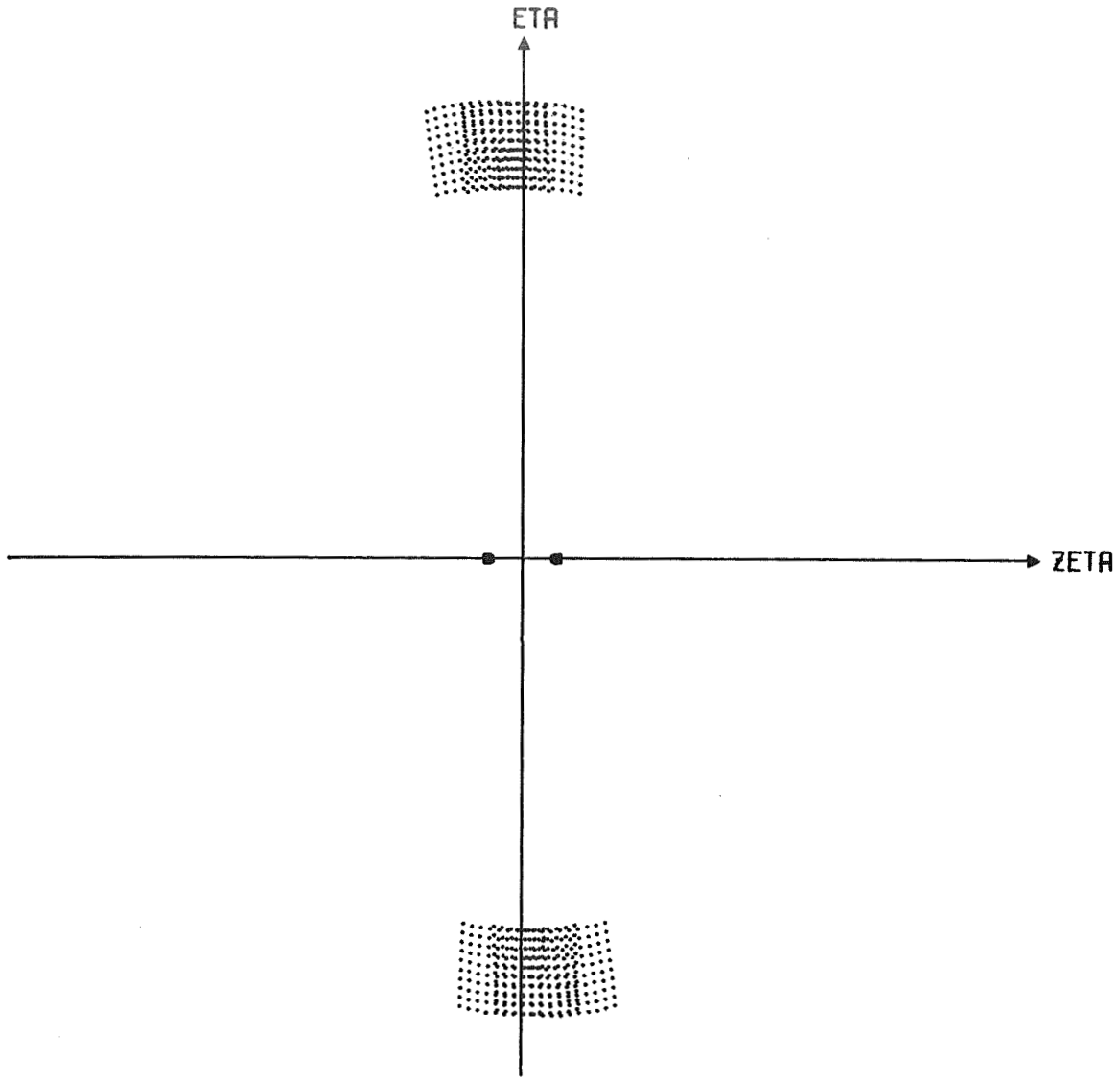

				MAX	MIN	
ZETA	HALF AXIS LENGTH	0.015	ZETA =	0.003	-0.003	SURFACE NO.
ETA	HALF AXIS LENGTH	0.015	ETA =	0.013	-0.013	3

Figure 23. MAWD Telescope--90-Degree with Paraboloid Mirror

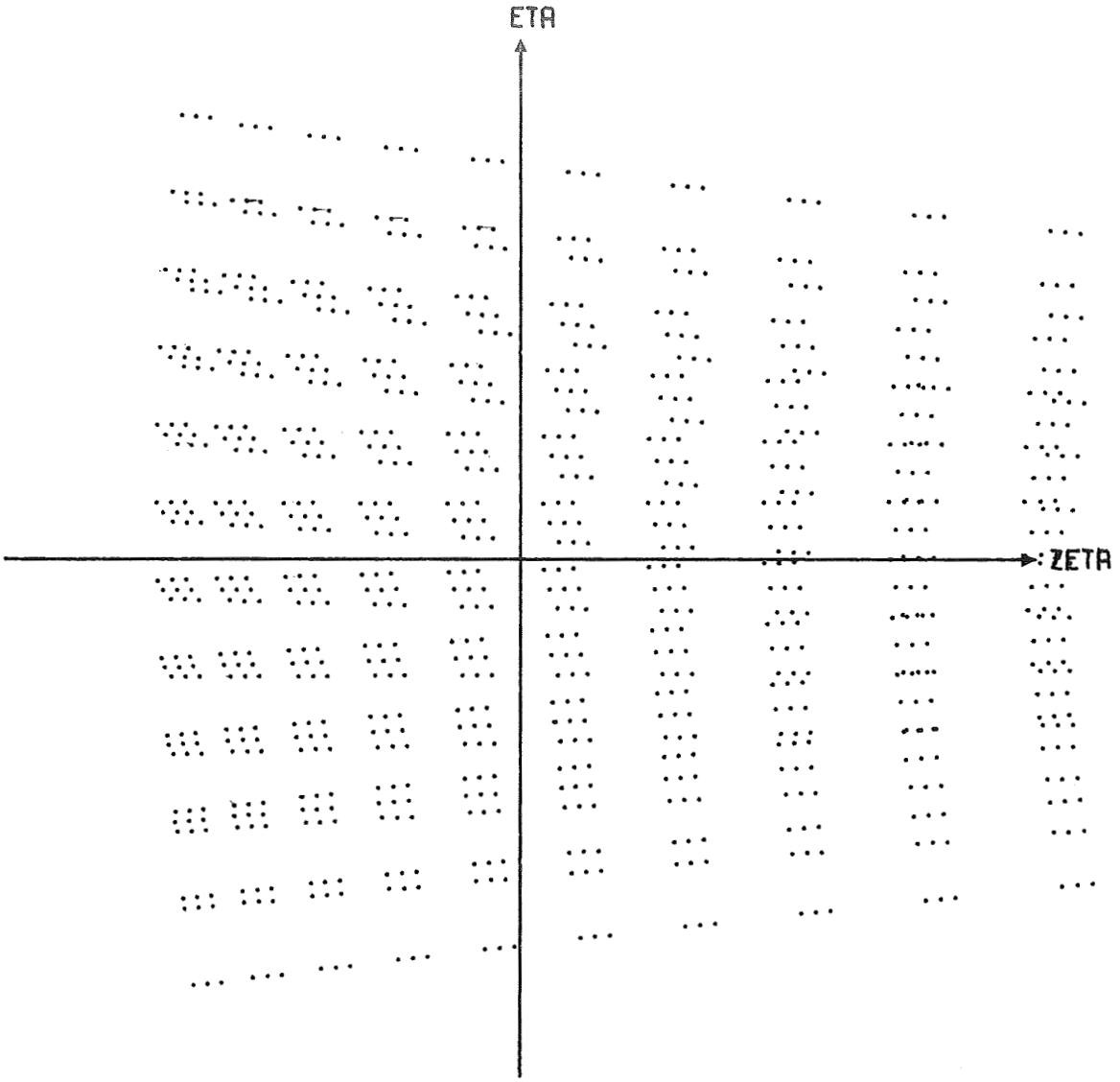

				MAX	MIN	
ZETA	HALF AXIS LENGTH	0.050	ZETA =	0.055	-0.035	SURFACE NO.
ETA	HALF AXIS LENGTH	0.050	ETA =	0.043	-0.041	3

Figure 24. MAWD Telescope--90 Degree with Spherical Mirror

5.0 OPTICS FOR NEON CALIBRATION SOURCE

The optical system which has been designed for neon calibration sources is able to image the arcs of two in-series neon sources into the monochromator. Figure 25 is a computer plot of this optical system without including a beam-splitter. Table 58 is a description of the axis systems used for the ray trace, and Table 59 is a definition of the dimensional parameters used.

For the ray trace shown in Figure 25, three families of 4-rays each start from the following three points on the monochromator H entrance slit:

(1) $Y_o = 2.0$, $Z_o = 4.000$

(2) $Y_o = 3.5$, $Z_o = 3.954$

(3) $Y_o = 5.0$, $Z_o = 3.880$

Each of the three families of four rays are such that they will intercept the four corners of the monochromator grating.

The two neon sources are at the origins of the (X_4, Y_4, Z_4) and (X_7, Y_7, Z_7) axis systems, respectively. Only an X-Y view is seen in Figure 25, but the maximum spread of all Z_4 or Z_7 values are never greater than ± 1.5 mm from the center-line. Therefore, the neon arc need be no greater than 3 mm in diameter about the Y_4 or Y_7-axis.

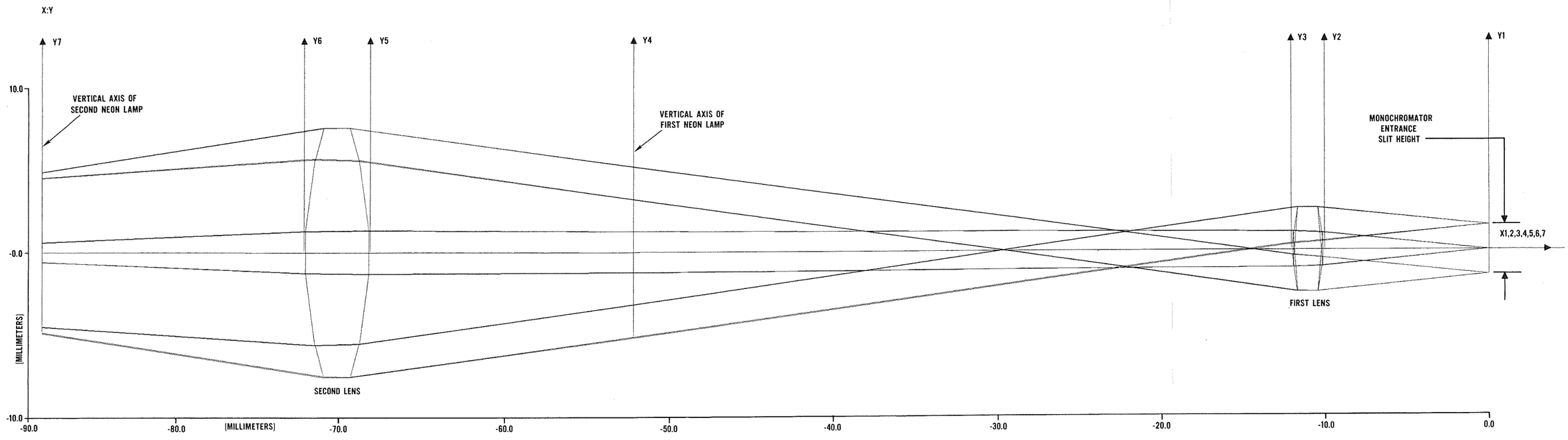

Figure 25. MAWD Neon Calibration Lens System

(X_o, Y_o, Z_o)	Monochromator Entrance Slit--The monochromator entrance slit lies in the Y_o-Z_o plane, and each family of rays used to ray-trace the neon source optical system starts from a point on the monochromator entrance slit. All rays have been traced through the neon source optical system to two neon sources in series. In this manner, the neon source optical system is ray-traced, using precisely the same ray families that are used for the monochromator.
(X_1, Y_1, Z_1)	Optical Axis of Neon Source Optics--The optical axis of the neon source optics at the monochromator entrance slit is defined by this X_1-axis, which is parallel to the monochromator's X_1-axis, but laterally offset to the center of the entrance-slit area.
(X_2, Y_2, Z_2)	First Surface of First Lens--This is a spherical refracting surface with its apex at the origin of the (X_2, Y_2, Z_2) axis system, and its center is on the negative X_2-axis.
(X_3, Y_3, Z_3)	Second Surface of First Lens--This is a spherical refracting surface with its apex at the origin of the (X_3, Y_3, Z_3) axis system, and its center is on the positive X_3-axis.
(X_4, Y_4, Z_4)	First Neon Source--The origin of the (X_4, Y_4, Z_4) axis system is at the center of the neon arc. The ray-trace image formed in this arc is defined on the transmitting Y_4-Z_4 plane.
(X_5, Y_5, Z_5)	First Surface of Second Lens--This is a spherical refracting surface with its apex at the origin of the $(X5, Y5, Z5)$ axis system, and its center is on the negative X_5-axis.
(X_6, Y_6, Z_6)	Second Surface of Second Lens--This is a spherical refracting surface with its apex at the origin of the (X_6, Y_6, Z_6) axis system, and its center is on the positive X_6-axis.
(X_7, Y_7, Z_7)	Second Neon Source--The origin of the (X_7, Y_7, Z_7) axis system is at the center of the neon arc. The ray-trace image formed in this arc is defined on the transmitting Y_4-Z_4 plane.

Table 58. Description of Ray-Trace Axis Systems Used for Neon Source Optical System

Axis Sub-Script (n)	A_n (mm)	B_n (mm)	C_n (mm)	α_n (deg)	β_n (deg)	γ_n (deg)	Surface Shape	Optical Function of Surface	D_n (mm)	E_n (mm)	F_n (mm)	R_n (mm)	N_n
1		3.500	3.954		-1.160								1.0000
2	-10.000								1.000	1.000	1.000	-10.000	1.4460
3	- 2.000								1.000	1.000	1.000	10.000	1.0000
4	-40.000												1.0000
5	-16.000								1.000	1.000	1.000	-25.000	1.4460
6	- 4.000								1.000	1.000	1.000	25.000	1.0000
7	-16.000												1.0000

NOTE: All dimensions are in mm except as noted.

Table 59. Dimensional Parameters for Neon Source Optical System

6.0 INTENSITY CALIBRATION SOURCE

The intensity calibration source is to be a small reflective integrating sphere containing several small tungsten lamps. The monochromator is to view uniformly illuminated walls within this integrating sphere during intensity calibration cycles. This integrating sphere is viewed by the monochromator whenever a small paraboloid mirror is moved into the telescope field of view at a location beyond the scanning mirror.

Figure 26 is a computer plot of the intensity calibration optical system. Figure 26 includes the 45° paraboloid telescope mirror and the scan mirror, and is precisely the same as Figure 18 up through the (X_6, Y_6, Z_6) axis system. Table 60 describes the ray trace axis systems used for the intensity calibration optical system, and Table 61 defines its dimensional parameters.

The upper view of Figure 26 uses two families of ten rays starting from entrance slit points (Y_o = 2.00, Z_o = 4.00) and (Y_o = 5.00, Z_o = 3.88). The ten rays of each family will strike the grating in a line array between the points (Y_3 = 50.0, Z_3 = 0) and (Y_3 = -50.0, Z_3 = 0).

The lower view of Figure 26 uses two families of nine rays each having the same two entrance slit starting points, but which will intercept the gratings full 100 mm x 180 mm rectangular area.

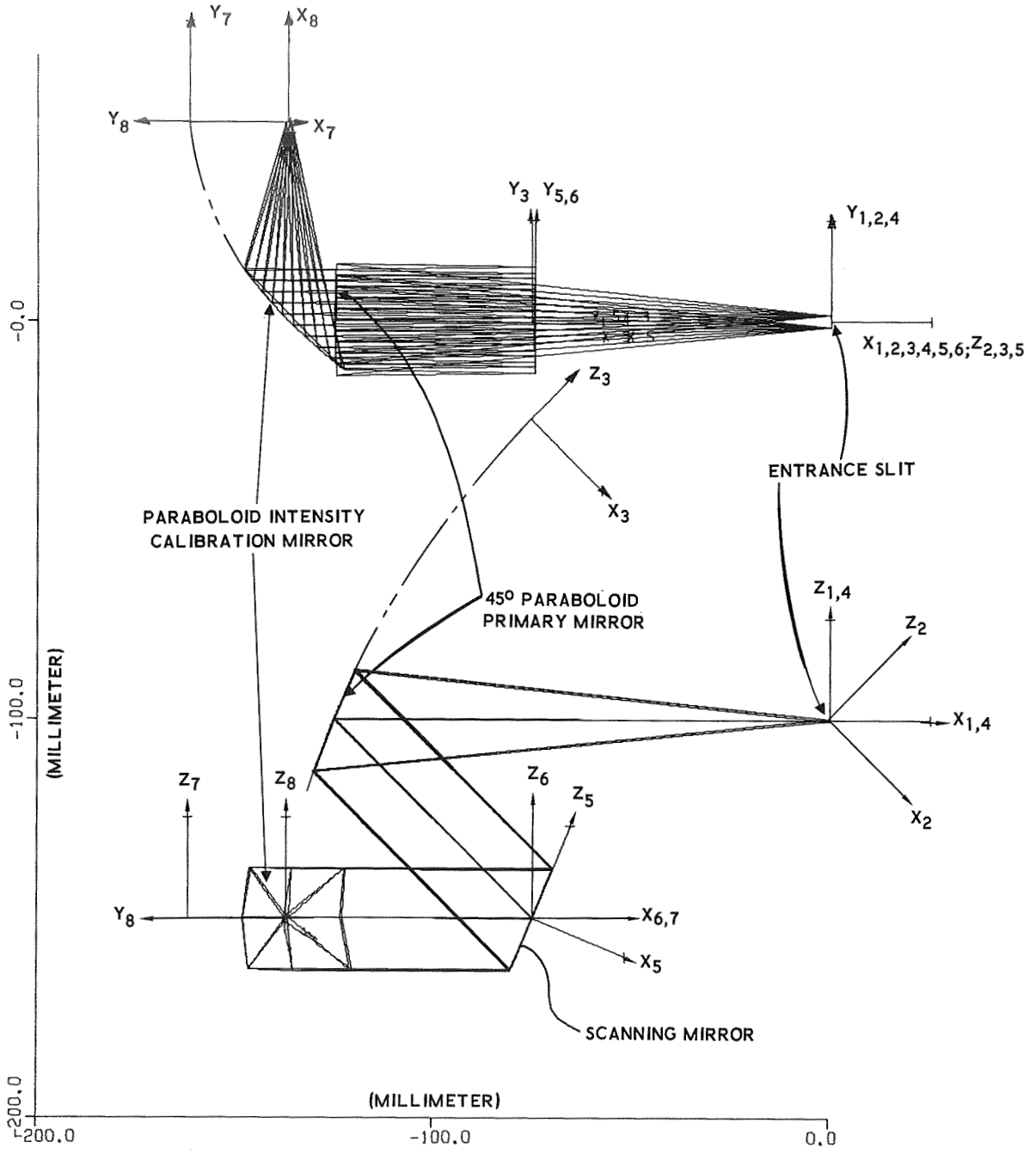

Figure 26. MAWD 45° Paraboloid Telescope Mirror, Scanning Mirror, and Paraboloid Intensity Calibration Mirror

(X_o, Y_o, Z_o)	Monochromator Entrance Slit--The monochromator entrance slit lies in the Y_o-Z_o plane, and each family of rays used to ray-trace the telescope starts from a point on the monochromator entrance slit. All rays have been traced through the telescope to object space. In this manner, the telescope is ray-traced using precisely the same ray families that are used for the monochromator.
(X_1, Y_1, Z_1)	Telescope Optical Axis--The telescope optical axis at the monochromator entrance slit is defined by the telescope's X_1-axis which is parallel to the monochromator's X_1-axis, but laterally off-set to the center of the entrance-slit area.
(X_2, Y_2, Z_2)	Mathematical Axis System.
(X_3, Y_3, Z_3)	Paraboloid Primary Mirror--This mirror has a paraboloid reflecting surface with its apex at the origin of the (X_3, Y_3, Z_3) axis system, and its focus on the positive X_3-axis.
(X_4, Y_4, Z_4)	Mathematical Axis System.
(X_5, Y_5, Z_5)	Scanning Mirror--This is a reflecting plane surface in the Y_5-Z_5 plane.
(X_6, Y_6, Z_6)	Mathematical Axis System.
(X_7, Y_7, Z_7)	Paraboloid Calibration Mirror--This mirror has a paraboloid reflecting surface with its apex at the origin of the (X_7, Y_7, Z_7) axis system, and its focus on the positive X_7-axis.
(X_8, Y_8, Z_8)	Image Surface--This is a plane transmitting surface in the Y_8-Z_8 plane.

Table 60. Description of Ray-Trace Axis Systems Used for 45° Telescope and Calibration Source Optical Systems

Axis Sub-Script (n)	A_n (mm)	B_n (mm)	C_n (mm)	α_n (deg)	β_n (deg)	γ_n (deg)	Surface Shape	Optical Function of Surface	D_n (mm)	E_n (mm)	F_n (mm)	R_n (mm)	N_n
1		3.500	3.954		- 1.160		Plane	Transmit					1.0000
2				-45.000			Plane	Transmit					1.0000
3	-107.000						Paraboloid	Reflect	1.000	1.000		214.000	1.0000
4	107.000			45.000			Plane	Transmit					1.0000
5	- 75.000		-50.000	-22.500			Plane	Reflect					1.0000
6				22.500			Plane	Transmit					1.0000
7	- 87.000	50.000					Paraboloid	Reflect				50.000	1.0000
8	25.000				90.000		Plane	Transmit					1.0000

NOTE: All dimensions are in mm except as noted.

Table 61. Dimensional Parameters for MAWD 45° Telescope with Calibration Source Optical System

7.0 SPECTRAL RADIANT FLUX TRANSFER

The spectral radiant flux transferred from a uniform extended source through the MAWD telescope, scanning mirror, and monochromator and imaged on each detector is given by:

$$P_\nu = \frac{N_\nu(\Delta\nu)\ T_\nu A_s A_g\ (\cos i)\ \tau}{(F)^2} \quad \text{(watts)}$$

where:

N_ν = spectral radiancy of a uniform extended source in watt/cm^2/cm^{-1}-str.

$(\Delta\nu)$ = the monochromator spectral bandpass in cm^{-1}

= 1.21 cm^{-1} for monochromator J

= .599 cm^{-1} for monochromator H

T_ν = the spectral transmittance of all the optics from the source to the detector sensitive surface

A_s = effective area of the entrance slit in cm^2

= .0025 cm^2

A_g = area of the grating ruled area in cm^2

= 180 cm^2

i = grating incident angle in degrees

= 56.055°, and cos i = .558

F = focal length of monochromator collimator mirror in cm

= 50 cm

τ = fractional chopper dwell time

= .5

The spectral transmittance of all optics T_ν can be expressed as follows:

$T_\nu = (R^m_\nu)^8\ (E^g_\nu)^2\ T^d_\nu$, for monochromator H

$= (R^m_\nu)^4\ E^g_\nu\ T^d_\nu$, for monochromator J

where: R_ν^m = the spectral reflectance of each mirror surface

= .98

E_ν^g = the spectral efficiency of the grating

= .65

T_ν^d = the spectral transmittance of the detector cover plate

= .94

so: $T_\nu = (.98)^8 \times (.65)^2 \times .94$

= .338 for monochromator H

and: $T_\nu = (.98)^4 \times .65 \times .94$

= .563 for monochromator J

Finally, for monochromator H

$$P_\nu = \frac{N_\nu\ (.599 \times .338 \times .0025 \times 180 \times .558 \times .5)}{(50)^2}$$

$$= 10.2 \times 10^{-6}\ N_\nu,\ \text{(watts)}$$

and for monochromator J

$$P_\nu = \frac{N_\nu\ (1.21 \times .563 \times .0025 \times 180 \times .558 \times .5)}{(50)^2}$$

$$= 34.1 \times 10^{-6}\ N_\nu,\ \text{(watts)}$$

8.0 CONSTRUCTION TECHNIQUES FOR COLLIMATING MIRROR AND GRATING

When component weight is not a problem, the ideal material from which to construct both the grating blank and the collimating mirror is generally one of the low expansion glasses such as Cer-Vit of Owens-Illinois, #7971 glass of Corning Glass Works, or Zerosil by Amersil, Inc., etc. These low expansion glasses already have a low specific gravity which is roughly equal to that of aluminum. The low expansion glasses also are easy to cut, figure, and polish, and they can provide super high quality reflective surfaces. They are also very stable materials, usually holding their surface shape for life. They also have been used successfully in many long duration space flights through high radiation in space.

In recent years, the need to build special light weight optics have created many design studies and new approaches to manufacturing optical mirrors. Some of the new approaches have been:

(1) Polished Beryllium
(2) Nickel coated Beryllium
(3) Nickel coated aluminum
(4) Thin electroformed parts
(5) Cored glass
(6) Built up glass
(7) Special thinned shapes of glass or nickel coated metal

Beryllium metal has about 73 percent the density of the low expansion glasses. It has good thermal conductivity and high strength, and high stability which make it a good candidate for the light weight grating blank and collimating mirror. Beryllium mirrors have been used successfully both with a nickel overcoat and uncoated[3],[4],[5],[6]. Beryllium does have a major disadvantage

when used as a grating blank. Its thermal coefficient of expansion is similar in magnitude to optical glass, so thermal changes will cause wavelength errors produced by changes in the groove spacing of the grating on the substrate. This error can be several decades greater than for a near-zero expansion glass substrate.

Light weight aluminum structures with nickel coating are finding many applications[5],[6],[7],[8]. The aluminum mirror approach is economical for massive optics, but its density, thermal expansion, and long term stability characteristics are inferior to those of beryllium.

Electroforming of the optical surfaces in thin nickel sheets[9] is still another possible approach. It would, however, be necessary to prove first that one could manufacture parts to the required accuracy, and second that the parts are mechanically stable to fractions of a fringe of light. Nickel also has too high a thermal expansion coefficient for the grating blank.

The best approach to a light weight collimating mirror and grating seems to be the cored or built up structures of low-expansion glass[10],[11],[12],[13]. These structures are now being manufactured with only 25 percent to 30 percent of the weight of the solid blank, with apparently the same high optical quality obtained with the solid blank.

BIBLIOGRAPHY

(1) B. D. Henderson, Study to Determine the Optimal Optical Design for a Mars Atmospheric Water Detection Spectrophotometer, Preliminary Report, JPL Contract No. 952552, May 23, 1969.

(2) B. D. Henderson, The Detailed Optical Design of a Double-pass Littrow Monochromator for a Mars Atmospheric Water Detection Spectrophotometer, Final Report, JPL Contract No. 952552, June 1969.

(3) W. P. Barnes, Jr., Some Effects of Aerospace Thermal Environments on High-Acuity Optical Systems, Appl. Opt. 5, 701-711 (1966).

(4) W. P. Barnes, Jr., Considerations in the Use of Beryllium Mirrors, Appl. Opt. 5, 1883-1886 (1966).

(5) J. T. Bloxsom and J. B. Schroeder, Preparations of Optical Surfaces on Beryllium, Appl. Opt. 9, 539-543 (1970).

(6) J. Espiard and G. Pienchard, Etude Therique sur le choix du materiau constitutif des miroirs d'un telescope embarque a bord d'um satellite, Sciences et Industries Spatiales 7/8, 25-28 (1969).

(7) F. F. Forbes, A 40-cm Welded-Segment Lightweight Aluminum Alloy Telescope Mirror, Appl. Opt. 8, 1361-1363 (1969).

(8) F. F. Forbes, Large Aperture Aluminum Alloy Telescope Mirrors, Appl. Opt. 7, 1407-1408 (1968).

(9) F. J. Schmidt, Electroforming of Large Mirrors, Appl. Opt. 5, 719-725 (1966).

(10) H. E. Mohn, Hanau Quartz Glass for Optical Components of High Precision for Use in Measurement Technology, Astronomy, and Space Research, Appl. Opt. 7, 368-371 (1968).

(11) W. P. Barnes, Jr., Optimal Design of Cored Mirror Structures, Appl. Opt. 8, 1191-1196 (1969).

(12) E. Y. Loytty, Mirror Blanks for Orbiting, Optical Spectra, 57-59 (January 1970).

(13) G. A. Simmons, Lightweight Mirror Blanks for Space, Optical Spectra, 47-51 (June 1970).